Bone Morphogenetic Protein 9 and Bone Morphogenetic Protein 10 are Vital Factors in Maintaining Adult Vascular Homeostasis and Cardiac Function

INAUGURAL-DISSERTATION

zur Erlangung des Doktorgrades der Naturwissenschaften

- Doctor rerum naturalium -

(Dr. rer. nat.)

vorgelegt dem

Fachbereich Biologie (FB 17)

der Philipps-Universität Marburg

eingereicht von

Megan Rice, Dublin

Marburg, 2017

Die vorliegende Arbeit wurde am Max-Plank-Institut für Herz- und Lungenforschung (W.G. Kerckhoff Institut), 61231 Bad Nauheim angefertigt.

Dekan:

Prof. Dr. Diethart Matthies

Institut für Pflanzenökologie und Geobotanik

Karl-von-Frisch-Straße 8

35043 Marburg

Erstgutachter:

Prof. Dr. rer. nat. Renate Renkawitz-Pohl

Institut für Entwicklungsbiologie der Tiere

Karl-von-Frisch-Straße 8

35043 Marburg

Zweitgutachter:

Prof. Dr. Dr. Thomas Braun

Abteilung Entwicklung und Umbau des Herzens

Max-Planck-Institut für Herz- und Lungenforschung

Ludwigstraße 43

61231 Bad Nauheim

Eidesstattliche Erklärung

"Ich versichere hiermit an Eides statt, dass ich die vorliegende Arbeit selbstständig verfasst, ganz oder in Teilen noch nicht als Prüfungsleistung vorgelegt und keine anderen als die angegebenen Hilfsmittel benutzt habe. Sämtliche Stellen der Arbeit, die benutzten Werken im Wortlaut oder dem Sinn nach entnommen sind, habe ich durch Quellenangaben kenntlich gemacht. Dies gilt auch für Zeichnungen, Skizzen, bildliche Darstellungen und dergleichen sowie für Quellen aus dem Internet. Mir ist bewusst, dass es sich bei Plagiarismus um akademisches Fehlverhalten handelt, das sanktioniert werden kann."

Ort, Datum Megan Rice

“Ever tried. Ever failed. No matter. Try Again. Fail again. Fail better.”

Samuel Beckett

Table of Contents

1 Table of Abbreviations

Abbrevation	Meaning
%	Percent
°C	Degrees celcius
µCT	Micro computed tomography
AB	Aortic banding
ABCC6	ATP-binding cassette sub-family C member 6
ACE	Angiotensin-converting enzyme
ActR	Activin type receptors
ALK	Activin receptor-like kinase
ANF/ANP	Atrial natriuretic peptide
ANG	Angiopoietin
APJ/ APLNR	Apelin receptor
APLN	Apelin
A-V	Arterial-venous
AVM	Arteriovenous malformation
BAC	Bacterial artificial chromosome
BF	Blood flow
BMP	Bone morphogenetic proteins
BMPR	Bone morphogenetic protein receptor
BNP	Brain natriuretic peptide
BP	Blood pressure
BSA	Bovine serum albumin
BV	Blood velocity
cAMP	Cyclic adenosine monophosphate
CCV	Common cardinal vein
cDNA	Complementary DNA
ChIP	Chromatin immunoprecipitation
cKO	Conditional single knockout
cm	Centimetre
CM	Cardiomyocyte
Co-SMAD	Co-mediated SMAD
cT	Cycle threshold
CVD	Cardiovascular disease
Cy2	Carbocyanin
Cy3	Indocarbocyanin
DA	Dorsal aorta
DAG	Diacylglycerol
DAPI	4',6-diamidino-2-phenylindole
ddH_2O	Double distilled water
DEPC	Diethylpyrocarbonate
DKO	Double knockout
Dll	Delta-like
DMEM	Dulbecco’s modified Eagle's medium
DNA	Deoxyribonucleic acid
dNTP	Deoxyribonucleotides
DTA	Diphtheria toxin A
DTT	Dithiothreitol
E	Embryonic day
EC	Endothelial cell
ECM	Extracellular matrix

EDN-1	Endothelin-1
EDTA	Ethylenediaminetetraacetic acid
EdU	5-ethynyl-2´-deoxyuridine
EDV	End diastolic volume
EF	Ejection fraction
EFN	Ephrin
EGTA	Ethylene glycol-bis(β-aminoethyl ether)-N,N,N',N'-tetraacetic acid
ELA	Elabela
ENG	Endoglin
eNOS	Endothelial nitric oxide synthase
ERK	Extracellular-regulated kinases
ESC	Embryonic stem cell
ESV	End systolic volume
EtOH	Ethanol
FBS	Fetal bovine serum
FCS	Fetal calf serum
FGF	Fibroblast growth factor
FIH	Factor inhibiting HIF
FLK	Fetal liver kinase
FRT	Short flippase recognition target sites
g	Gram
GAPDH	Glyceraldehyde-3-phosphate dehydrogenase
GDF	Growth differentiation factor
GDP	Guanosine diphosphate
GI	Gastrointestinal
G_i	Inhibitory G protein
GOF	Gain of function
GPCR	G-protein coupled receptor
GSEA	Gene Set Enrichment Analysis
GTP	Guanosine-5'-triphosphate
h	Hour
H&E	Hematoxylin and eosin staining
Hb	Hemoglobin
HB-EGF	Heparin-binding egf-like growth factor
HBSS	Hank's balanced salt solution
HCL	Hydrochloric acid
HEPES	4-(2-hydroxyethyl)-1-piperazineethanesulfonic acid
HF	Heart failure
HGF	Hepatocyte growth factor
HHT	Hereditary haemorrhagic telangiectasia
HIF	Hypoxia-inducible factor
HMVEC-d	Human dermal microvascular endothelial cell
HR	Heart rate
HRP	Horse-radish-peroxidase
HUVEC	Human umbilical vein endothelial cell
i.p	Intraperitoneal
IP3	Inositol 1, 4, 5-triphosphate
i-SMAD	Inhibitory SMAD
JAG	Jagged
JNK	c-jun N-terminal kinase
JP	Juvenile polyposis
KD	Knock down
KLF	Kruppel-like factor
KO	Knockout
L	Litre

LAD	Left anterior descending artery
L-NAME	NG-nitro-L-arginine methyl ester
LOS	Loss of function
loxP	Locus of cross-over (x) of the bacteriophage P1
LVM	Left ventricular mass
M	Molar
MAPK	Mitogen-activated protein kinase
MCP	Monocyte chemoattractant protein
MEF	Myocyte enhancer factor
MES	2-(N-morpholino)ethanesulfonic acid
mg	Milligram
MHz	Megahertz
MI	Myocardial infarction
min	Minute
mL	Millilitre
mM	Millimolar
mm	Millimetre
mmHg	Millimetre of mercury
MMP	Matrix metalloproteinases
MRI	Magnetic resonance imaging
mSMC	Mouse smooth muscle cell
mT/m	Millitesla per meter
neg	Negative
ng	Nanogram
nm	Manometers
NO	Nitric oxide
NOS	Nitric oxide synthase
NRP	Neuropilin
O/N	Overnight
O_2	Oxygen
P	Postnatal day
P/S	Penicillin/ streptomycin
PA	Plasminogen activator
PAH	Pulmonary arterial hypertension
PAI	Plasminogen activator inhibitor
PBS	Phosphate-buffered saline
PCA	Phase contrast angiography
PCR	Polymerase chain reaction
PDGF	Platelet-derived growth factor
PECAM	Platelet-endothelial cell adhesion molecule
PFA	Paraformaldehyde
PH	Pulmonary hypertension
PHD	Prolyl Hydroxylase Domain
PI3K	Phosphatidylinositol 3'-kinase
PKC	Protein kinase C
PLC	Phospholipase C
PlGF	Placental Growth Factor
pos	Positive
PP	Pulse pressure
PTX	Pertussis toxin
PXE	Pseudoxanthoma elasticum
qRT-PCR	Quantitative reverse transcription PCR
RNA	Ribonucleic acid
R-SMAD	Receptor-regulated SMAD
rSMC	Rat smooth muscles cell

RT	Room temperature
RV	Right ventricle
RVH	Right ventricle hypertrophy
s	Seconds
SC	Stem cell
SDS	Sodium dodecyl sulfate
SDS-PAGE	Sodium dodecyl sulfate-polyacrylamide gel electrophoresis
shRNA	Short hairpin RNA
SKO	Single knockout
SMA	Smooth muscle actin
SMAD	Mothers against DPP homolog
SMC	Smooth muscle cell
SMURF	Smad-mediated ubiquitin regulatory factor
STAT	Signal Transducer And Activator Of Transcription
SV	Stroke volume
T	Tesla
TAC	Thoracic aortic constriction
TBST	Tris buffered saline / tween-20
TE	Tris-EDTA
TEM	Transmission electron microscope
TEMED	Tetramethylethylenediamine
TGF	Transforming growth factor
TIE	TEK receptor tyrosine kinase
TIMP	Tissue inhibitors of metalloproteinase
TKO	Triple knockout
TMX	Tamoxifen
TOF	Time of flight
V	Volts
VE	Vascular endothelial
VEGF	Vascular endothelial growth factor
vSMC	Vascular smooth muscle cell
WT	Wild type
x g	Times gravity
ZFN	Zinc-finger nuclease
αSMA	Alpha smooth muscle actin
µg	Microgram
µl	Microliter

2 List of Tables

3 List of Figures

4 Summary

Bone Morphogenetic Proteins (BMPs) are members of the well-known Transforming Growth Factor (TGF) superfamily, consisting of TGFβ proteins, Activins and Growth Differentiation Factors (GDFs). These factors play an essential role in numerous different aspects of embryonic development and physiological organ function. BMP9 and BMP10 are members of this superfamily; however their role, especially in the cardiovascular system, is still poorly characterised.

BMP9 is produced by and is secreted from the liver and is proposed to act as a major circulating vascular quiescence factor. BMP10, however, has a more limited expression where it is expressed during embryonic development in the ventricles from embryonic day (E) 9.0 to 13.5. After E14.5, expression of BMP10 declines in the ventricles, but is maintained in the right atria of postnatal and adult hearts. BMP9 and BMP10 bind with high affinity to ALK1, an endothelial specific receptor as well as to endoglin (ENG), a TGFβ co-receptor.

Since both of these ligands bind with very high affinity to the ALK1 receptor and soluble ENG receptor, it was suggested that BMP9 and BMP10 are important mediators of cardiovascular development and homeostasis. So far it has been shown that mutations in ALK1, ENG and SMAD4 genes can result in hereditary haemorrhagic telangiectasias (HHT), which is a disease that results in vascular abnormalities. BMP10 along with ENG has been shown to be involved in pre-eclampsia, a disease resulting in high blood pressure (BP), thus strengthening the argument that these BMP family members are involved in cardiovascular homeostasis.

The aim of this project was to elucidate the role of BMP9 and BMP10 in the adult heart and their role in cardiovascular homeostasis. Constitutive BMP9 knockout mice were generated, with a conditional heart-specific BMP10 deletion under the control of ANF Cre. Results demonstrated that the loss of BMP9 and BMP10 leads to vessel defects which caused disruption in vascular tone and altered cardiac function. In summary, these results have identified an essential role for BMP9 and BMP10 in postnatal cardiac remodelling and vascular homeostasis.

5 Zusammenfassung

Die knochenmorphogenetischen Proteine (engl.: bone morphogenic proteins, BMPs) sind Bestandteil der intensiv erforschten TGF-β Superfamilie (engl.: Transforming Growth Factor), hierzu zählen TGF-β Proteine, Activine, Wachstums- und Differenzierungsgene (engl.: Growth and differentiation factors, GDFs). Diese Proteine spielen eine essenzielle Rolle in zahlreichen Aspekten der Embryonalentwicklung und in physiologischen Organfunktionen. BMP9 und BMP10 sind Teil dieser Familie, deren Rolle im kardiovaskulären System weitgehend unbekannt.

BMP9 wird in der Leber produziert und über das Blut im Organismus verteilt, wo es als zirkulierender Faktor an der vaskulären Ruhe beteiligt ist. Im Vergleich dazu ist die Expression von BMP10 strenger reguliert. Während der Embryonalentwicklung wird BMP10 ab Tag 9 (E9) in den Ventrikeln exprimiert. Ab E14.5 verlagert sich die Expression in die Atrien, wobei BMP10 im adulten Organismus nur noch im rechten Atrium exprimiert wird.

BMP9 und BMP10 binden mit hoher Affinität an ALK1, einem endothelspezifischen Rezeptor, als auch an Endoglin (ENG), einem TGF-β-Korezeptor. Diese gemeinsamen Bindeeigenschaften sind ein Anzeichen dafür, dass BMP9 und BMP10 wichtige Mediatoren der kardiovaskulären Entwicklung als auch der vaskulären Homöostase sind. Bisher konnte gezeigt werden, dass Mutationen in den Genen für ALK1, ENG bzw. Smad4 verantwortlich für die Entstehung der sogenannten hereditären hämorrhagischen Teleangiektasie (HHT) sein können, eine Krankheit, die durch eine Erweiterung des Gefäßsystems gekennzeichnet ist. Des weiteren wurde gezeigt, dass BMP10, zusammen mit ENG, an der Entstehung der Präeklampsie beteiligt ist, was noch einmal zusätzlich darauf hindeutet, dass BMP9 und BMP10 in der vaskulären Homöostase involviert sind.

Das Ziel dieses Projektes ist es, die Rolle von BMP9 und BMP10 im adulten Herzen und deren Funktion in der vaskulären Homöostase näher zu untersuchen und besser zu verstehen. Dazu wurde eine konstitutive BMP9-*Knockout*maus generiert, in welcher BMP10 mittels einer konditionellen Cre-Rekombinase herzspezifisch (ANF-Cre) deletiert werden kann. Unsere Versuche zeigten, dass der Verlust von BMP9 und BMP10 zu Gefäßveränderungen führt, welche die vaskuläre Homöostase negativ beeinflussen und die Herzfunktion beeinträchtigen. Darüber hinaus konnte gezeigt werden, dass BMP9 und BMP10 eine essentielle Funktion im postnatalen Herzumbau und der vaskulären Homöostase haben.

6 Introduction

To this day, cardiovascular disease (CVD) is still the most common cause of death, with approximately 15.6 million people affected worldwide [1]. Even though over the last two years previous statistics and publications have shown a decrease in CVD mortality [2,3], more than 4 million Europeans still die annually as a result of CVD. Although CVD is the most prominent killer worldwide, treatment of these diseases is lacking and current treatments only delay the onset of CVD rather than curing or reversing its affects. Obviously, further intensive research in this area is critical [4]. CVDs cover a range of heart conditions from blood vessel diseases like coronary artery disease; heart rhythm problems, also known as arrhythmias; and heart defects from birth (congenital heart defects), to name but a few [5]. With such a wide range of differing diseases, herein lies the problem and difficulty of finding specific biomarkers as well as preventing and treating each individual condition. Ultimately, any untreated CVD will result in death simply due to the fact that, in the end stages, the flow of blood to or away from the heart is blocked or hindered resulting in insufficient oxygen availability whereby the cardiac tissue will begin to die and all cardiac function will be lost. The fact that it is very difficult to treat CVD long term or to cure these conditions due to the hearts inability to repair or regenerate itself, it is essential to focus on improving diagnosis and early detection methods to combat against further cardiac deterioration, which is characteristic of CVD.

Throughout my thesis I will outline the role of two understudied proteins, BMP9 and BMP10, and their function in maintaining vascular homeostasis and therefore in turn, cardiac function. These proteins could have the potential to be used therapeutically as well as being possible biomarkers for cardiac dysfunction.

6.1 Outline of cardiovascular diseases, their causes and current therapies

There are many different types of heart disease that are covered by the term CVD as shown in Table 1. They result from electrical problems, such as arrhythmias, or problems with the heart structure itself including cardiomyopathies and congenital heart defects. Additionally, many of these diseases result from disruption to the circulatory system, where vascular homeostasis is essential for normal cardiac function, as is the case with elevated BP or coronary artery disease.

As seen in Table 1, many of these CVDs can only be treated by either alleviating the condition, via medication or changes in lifestyle, or by assisting the heart, via implantable devices, but never curing or removing the primary defect. Due to the fact that most CVD mechanisms are unknown and that the symptoms are detected when irreversible damage already exists, it is therefore essential to fully understand the underlying mechanisms involved to be able to fully reverse or cure these diseases, as well as establishing early detection methods to act as a preventive measure. As mentioned previously, all CVDs will eventually lead to heart failure (HF) and sudden death, whereby the heart loses its ability to pump blood and ceases to function. The consequence of CVD is the loss and death of cardiomyocytes (CMs) [4]. Loss of CMs due to a myocardial infarction (MI) results in a decrease in the overall function of the heart. As CMs cannot replace themselves [6], there is an invasion of immune cells accompanied by myofibroblasts, which causes scar formation further impairing the hearts ability to pump [7]. Over the past decade many different groups have focused on CMs and their proliferative capacity [8], cardiac stem cell therapy [4], reduction of scar formation and survival of CMs in damaged areas [7] and the importance of the epicardium in cardiac repair [9]. Current focus is based not only on cardiac repair but also on the possibility of cardiac regeneration, where the heart can return back to its normal, full function. However, none of these treatments will be of significant benefit or even possible unless vascular homeostasis is maintained. If this is not the case the heart will again be put under huge strain, cardiac function will again diminish over time leading to severe cardiac disease [9]. In the following section the development, maintenance and function of the vascular system as well as its significance and role in CVD development, and its prevention and treatment of such diseases will be discussed.

Table 1: Cardiovascular diseases and description

Condition	Damage	Caused by	Treatment
Rheumatic Heart Disease (results from attacks of rheumatic fever which causes damage to the heart, particularly the heart valves)			
Rheumatic Heart Disease	Heart valves	Streptococcal bacteria	Surgical replacement of damaged valves
Stenosis	Narrow valves	Birth defect, rheumatic fever, medication	Valvuloplasty, surgical replacement
Regurgitation	Leaky valves	Birth defect, rheumatic fever, medication	Intra-aortic balloon pump, surgical replacement
Prolapse	Valves won't close properly	Birth defect, rheumatic fever, medication	Medication, surgical replacement in extreme cases
Hypertensive Heart Disease (result of high BP that strains the heart and blood vessels)			
Aneurysm	Bulge in blood vessel wall, can grow and rupture	Hypertension, Atherosclerosis	Graft is added to strengthen wall, surgical removal
Atherosclerosis	Artery walls become thick and stiff due to fatty deposits (plaques) which restricts BF	High BP, high cholesterol, smoking	Healthy lifestyle, medication, surgical removal, angioplasty and stent placement
High BP (hypertension)	Excessive force of blood pumping through your blood vessels	Smoking, weight, high salt diet, stress, age, genetics, kidney disease, thyroid disorders	Healthy lifestyle, medication
Peripheral arterial disease (PAD)	Narrowing and / or blockage of the blood vessels in the legs	High BP, high cholesterol, high sugar intake, smoking	Healthy lifestyle, medication, surgical removal, angioplasty and stent placement
Ischemic Heart Disease (result due to narrowing of coronary arteries which decreases blood supply to the heart)			
Angina	Reduced blood supply to the heart	Atherosclerosis, coronary heart disease	Healthy lifestyle, medication, angioplasty, coronary artery bypass grafting
Atherosclerosis	Artery walls become thick and stiff due to fatty deposits (plaques) which restricts BF	High BP, high cholesterol, smoking	Healthy lifestyle, medication, surgical removal, angioplasty and stent placement
Coronary artery disease	Narrowing/blockage of blood vessels that supply heart	High BP, high cholesterol, high sugar intake, smoking, blood vessel inflammation	Healthy lifestyle, medication, angioplasty, coronary artery bypass grafting

Condition	Damage	Caused by	Treatment
Coronary heart disease	Disease of the arteries to the heart	High BP, high cholesterol, high sugar intake, smoking, blood vessel inflammation	Healthy lifestyle, medication, angioplasty, coronary artery bypass grafting
Heart attack (MI)	Heart's supply of blood is stopped	Coronary heart disease, atherosclerosis	Healthy lifestyle, medication, coronary artery bypass grafting
Sudden death (cardiac arrest)	Abrupt loss of the heart's ability to pump blood	Heart attack, abnormal heart rhythm	None
Cerebrovascular Heart Disease (result of vascular problems, usually impeded blood supply, within the brain)			
Atherosclerosis	Artery walls become thick and stiff due to fatty deposits that restricts BF	High BP, high cholesterol, smoking	Healthy lifestyle, medication, surgical removal, angioplasty, stents
Cerebral vascular disease	Effects BF to vessels in the brain	Atherosclerosis	Healthy lifestyle, medication, carotid stent placement
Stroke	When BF to the brain the hindered or reduced	Atherosclerosis, atrial fibrillation, coronary artery disease	Healthy lifestyle, medication, angioplasty, arteriovenous malformation repair, surgery
Transient ischemic attacks	Due to a temporary blot clot or small amount of haemorrhaging	Vascular injury, age, smoking, diabetes, high cholesterol, atrial fibrillation	Healthy lifestyle, medication, surgery
Inflammatory Heart Disease (due to inflammation within the different layers of the heart tissue)			
Atherosclerosis	Artery walls become thick and stiff due to fatty deposits (plaques) which restricts BF	High BP, high cholesterol, smoking	Healthy lifestyle, medication, surgical removal, angioplasty and stent placement
Idiopathic dilated cardiomyopathy	Heart enlargement and dilation (thinning) of ventricle walls	Unknown	Healthy lifestyle, medication, heart transplant [10]
Ischemic dilated cardiomyopathy	Heart enlargement, weakening and dilation (thinning) of ventricle walls	Coronary artery disease, heart attack, mainly due to lack of blood supply	Healthy lifestyle, medication, implantable devices, angioplasty, stents, bypass surgery, transplant
Dilated cardiomyopathy	Decreased ability to pump blood and the left ventricle (LV) becomes enlarged and weakened	Coronary heart disease, heart attack, high BP, diabetes, thyroid disease, infections	Medication, implantable devices, transplant
Hypertrophic cardiomyopathy	Thickening of the heart muscle, making it difficult for the heart to pump blood	Genetic, secondary effect due to BF impediment	Medication, surgery, implantable devices
Pericardial disease	Abnormal amount of blood between the heart and the sac surrounding the heart, the pericardium	Viral infections, autoimmune disorder, heart attack	Medication, removal of excess fluid, removal of pericardium

Condition	Damage	Caused by	Treatment
Arrhythmias (results from problems in the electrical system of the heart)			
Bradyarrythmia	When the HR is too slow and not enough blood is being circulated	Heart attack, underactive thyroid, chemical imbalance that effects the electrical system	Medication, pacemaker, surgery
Tachyarrhythmia (tachycardia)	When the HR exceeds the normal resting rate, problems with electrical connections	Heart attack, high BP, coronary heart disease, HF, rheumatic heart disease	Medication, pacemaker, surgery
Atrial Fibrillation	An irregular HR that leads to atrial contraction that is too fast and irregular	High BP, coronary heart disease, age, inflammation	Medication, pacemaker,
Ventricular Fibrillation	Disorganized electrical signals that make the ventricles quiver instead of pump blood	Heart attack	Defibrillation
Other			
Congenital heart disease	Defects with the heart's structure from birth	Genetic, smoking during pregnancy, most reasons unknown	Surgery
Heart failure	Heart's inability to pump enough blood for the whole body	Coronary heart disease, diabetes, high BP, other heart diseases, alcohol abuse	Healthy lifestyle, medication, surgery, implantable devices, transplant

6.2 The network and function of the cardiovascular system

In the vertebrate, the cardiovascular system is a closed system that is comprised of the heart, blood and blood vessels. This system is the first organ to function during embryogenesis, with numerous vital functions that are needed for embryogenesis and postnatal survival. The cardiovascular system is used to transport oxygenated blood throughout the whole organism along with essential metabolites and nutrients for normal cellular function and is also important for removal of waste products. Furthermore, the system facilitates hormonal communications between distant organs and also allows for the development of the organisms immune response. For a fully functioning closed circulatory system, that continually re-circulates blood to and from peripheral tissues, a system with two distinct networks is needed. Although these two vascular networks are separate from each other in structure and function they need to be interconnected and interlaced with each other to be to fully operational. Arteries, veins and capillaries are the blood vessel structures that make up this very complex system and differ in structure to deal with the different pressure systems and functions involved as shown in Table 2.

Table 2: Comparison of arteries, capillaries and veins

	Artery	Capillary	Vein
Function	Carry blood away from the heart	Delivers needed products and removes waste products	Carry blood to the heart
Wall structure	Thick, strong with muscles, elastic fibres and fibrous tissue	Thin, only one cell thick	Thin, mainly fibrous tissue with less muscle and elastic tissue
Lumen diameter	Narrow	Very narrow	Wide
Valves	None	None	Present
Why structure needed for function	Strength and elasticity needed to deal with pulsing blood, prevent rupturing, maintain high BP High BP ensures no back flow of blood	Thick walls not needed due to low BP Thin walls and narrow lumen bring blood close to tissue for optimum diffusion	Thick walls not needed due to low BP Wide lumen decreases resistance to BF Valves present to prevent back flow due to low pressure

Arteries are the blood vessels that take oxygenated blood away from the heart to the rest of the body and have to deal with a high-pressure blood flow (BF) while the veins are blood vessels that bring deoxygenated blood back to the heart from the whole body under a low pressure system. Capillaries are the tiny vessels that mediated the change of different pressure systems and where diffusion of oxygen, nutrients and waste products can occur shown in Fig. 1.

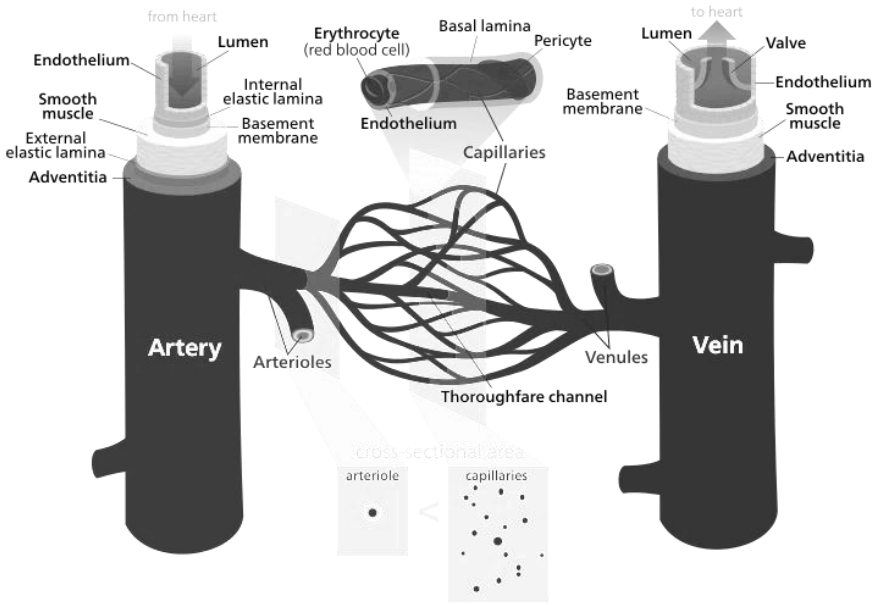

Figure 1: Artery, vein and capillary structure
Difference in structure between arteries and veins allow for different pressures and functions of this vascular system. Arteries develop into smaller arterioles before merging into the capillary bed while veins develop into venules which also run into the capillary bed. The capillary bed, which is only one cell thick, is where exchange of nutrients and removal of waste occurs [11].

6.3 Vasculogenesis

Development of the vascular system starts not long after gastrulation accompanied by somite formation. It is comprised of different vessel types and occurs via two distinct mechanisms, vasculogenesis, *de novo* vessel formation, and angiogenesis, vessel formation from pre-existing vessels. In 1988, Risau first used the term vasculogenesis to describe *de novo* blood vessel formation in embryoid bodies [12]. It has been long hypothesized, based on the close relationship between the development of the cardiovascular and the hematopoietic system that endothelial and hematopoietic cells are derived from a common precursor, known as the hemangioblast [13,14]. As seen in Fig. 2a, these multipotent stem cells give rise to both pluripotent hematopoietic stem cells that produce all blood cell lineages, as well as the pluripotent stem cell of the endothelial lineage, the angioblast [13,15]. The embryonic mesoderm, extra embryonic yolk sac, allantois and placenta have been discovered as sources of hematopoietic and endothelial progenitor cells and are also sites of vasculogenesis [16].

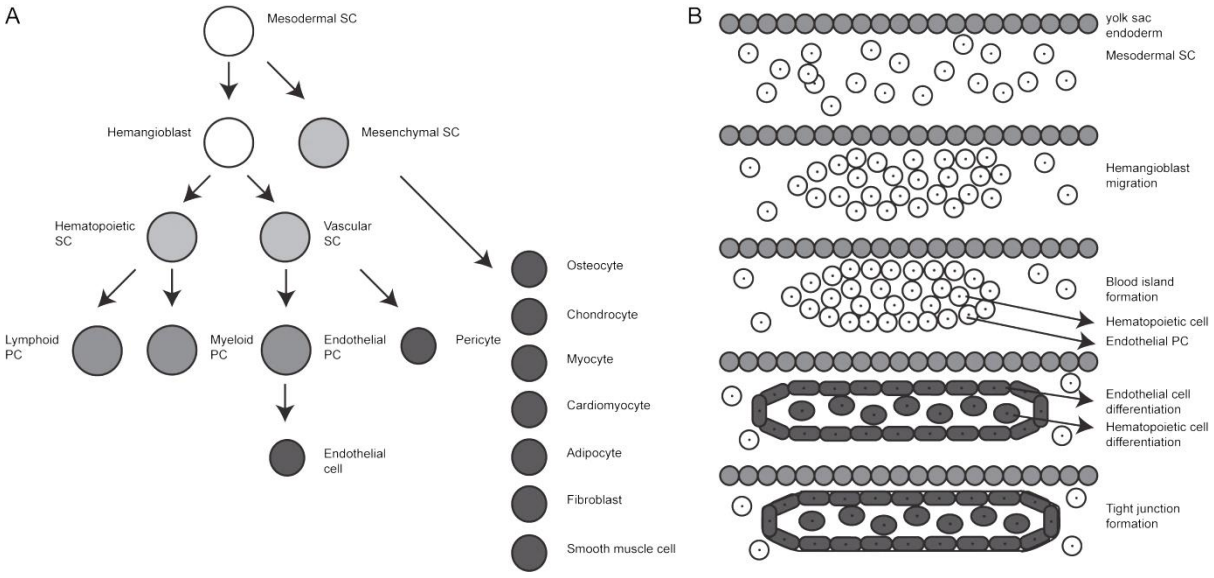

Figure 2: Origin of hematopoietic and vascular stem cells and extra embryonic vascular formation
(A) Mesodermal stem cells (SCs) are able to give rise to mesenchymal SCs, which go on to be a number of possible cell types, or hemangioblasts. Hemangioblasts can give rise to hematopoietic cells or vascular cells. (B) During vascular formation hemangioblasts migrate and cluster to form blood islands. These cells within the blood island differentiate into to hematopoietic cells or vascular cells to form blood cells or the vascular tube respectively. Modified from [15,17]

During mouse development at E7.5, within the yolk sac, there is already evidence of separate lineages, the hematopoietic and endothelial lineage which results in the development of blood islands [13]. These blood islands consist of an outer layer of endothelial cells (ECs) and an inner cluster of primitive hematopoietic cells which then extend and fuse together, allowing a primordial vascular network to develop in the extraembryonic region, seen in Fig. 2b [17,18]. It is important to state that in this case the structure of the yolk sac blood islands in the human embryo is similar to that of the mouse embryo [19]. The main function of vasculogenesis in the yolk sac is to generate the primitive vascular plexus [17].

During embryonic development, seeing as blood vessel formation is initiated in the extraembryonic regions, it was proposed that the extra embryonic vessels contributed to the formation of the blood vessels in the embryo itself, as these appear later in development via in-growth from the extraembryonic region [20]. However this was subsequently shown to not be the case. Instead, it was shown that vessels found within the developing embryo itself are formed independently via vasculogenesis [21,22]. In the case of the embryo itself, the primitive vascular network is also formed from angioblasts, although unlike the extra-embryonic angioblasts, they can develop and differentiate unaccompanied by hematopoietic progenitor cells [23]. Major embryonic vessels are formed by large aggregates of angioblasts, that then form vesicles and cords of attached vascular ECs and then undergo morphogenesis to

create epithelial tubes as seen in Fig. 3 [14,24]. In the embryo, vasculogenesis is essential for the formation of capillaries in the head mesenchyme and endocardium and by E8.5 both the intra- and extra-vascular system have anastomosed where the plexus continues and connects to the developing heart before the initial heartbeat is initiated [25,26]. Even though vasculogenesis is mainly associated with early embryonic development, it is also essential in the vascularisation of other organs such as the lungs, liver and spleen and so it is possible that angioblasts could arise *de novo* during later stages of development and arise from other mesodermal tissues such as the paraxial/ somitic mesoderm, mesodermal mesenchyme, and possibly even hematopoietic progenitors [14,27,28].

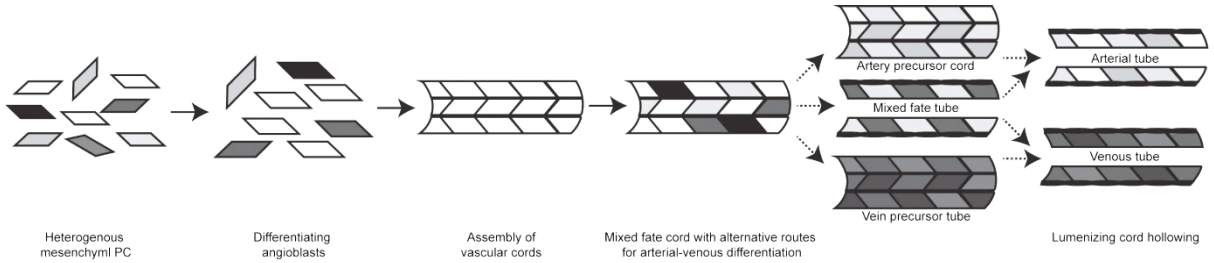

Figure 3: Vasculogenesis
The procedure of *de novo* vessel formation where a group of progenitor cells, angioblasts also known as vascular SCs, aggregate and differentiate into an immature epithelial tube which then undergo differential gene expression to give rise to distinct vascular identities. Modified from [24]

In comparison to angiogenesis, there is still little known about the signalling pathways involved during vasculogenesis and specification of vessel identity. In Table 3 is a list of critical factors known to be necessary for vasculogenesis as well as artery and vein specification, outlining the complex network of signalling pathways necessary to orchestrate such an essential process. For a long time it was hypothesized that hemodynamic forces, like BF and BP, were key players in driving vessel fate. However is has now been shown that arteries and veins contain distinct molecular markers that distinguish their identity from an early stage, even before circulation has been initiated. Table 3 demonstrates a number of known pathways involved in establishing, as well as maintaining the different vessel identities; however much is still unknown in regards to other pathways potentially involved in this process or how the synergistic or antagonistic effect of these pathways functions.

Table 3: Signalling pathways important for vasculogenesis and vascular identity

Signalling Pathway	Vascular Effect
Molecules controlling endothelial cell development and tube formation	
FGF2	Mesodermal induction and induction of angioblasts from the mesoderm [29]
IHH	Formation of blood island in yolk sac and endothelial tube in embryo [30,31]
NRP	Yolk sac vasculogenesis and formation of the primary vascular plexus [32,33]
VEGFα/VEGFR2	Blood island assembly and for their precursor cells [34–36]
TGFβ1	Yolk sac development [37]
TGFβR1/ TGFβR2	Vasculogenesis in yolk sac and embryo [38,39]
Cadherin/Connexins	Formation of EC-EC junctions [40,41]
Molecules involved in vascular identity	
Notch	Focuses vessel fate toward arterial identity [42]
EFNB2	Involved in arterial specialization [43]
EFNB4	Involved in venous specialization [43]
NRP1	Expressed in arterial endothelium [44]
NRP2	Expressed in venous endothelium [44]

The main initial players that have been identified in artery and vein identity are ephrin B2 (*Efnb2*) and ephrin B4 (*Efnb4*) respectively. Expression of both can be detected early on in development. *Efnb2* is expressed in the developing endothelium of arteries while EFNB4, its receptor, is specifically expressed in the developing endothelium in veins [43]. Knockout studies in mice showed mice lacking *Efnb2* (*Efnb2*$^{-/-}$) died embryonically due to defects in vasculogenesis, with problems in vascular patterning in both the yolk sac as well as the embryo itself. Further, EFNB2 and EFNB4 play a major role in the development of arteriovenous anastomoses by inhibiting vascular endothelial growth factor A (*Vegfa*) and angiopoietin 1 (*Angpt1*, also known as *Ang1*) induced EC proliferation and migration [43,45]. The Neuropilin signalling pathway was also shown to be a key regulator of vessel identity where neuropilin1 (*Nrp1*) is specifically expressed in arterial endothelium while neuropilin2 (*Nrp2*) expression is restricted to venous endothelium [44]. Subsequent expression pattern studies showed that neuropilins are expressed in the early stages of vasculogenesis, even before *Efnb2* and *Efnb4*, suggesting that they are primary identity markers. This suggests, that the primitive vessels of the extraembryonic vascular plexus already possess the necessary information to initiate vein and artery identity [46]. Knockout of both neuropilins leads to embryonic lethality in mice, where the developing yolk sac is avascular and the primary vascular plexus fails to develop [32]. Lastly, Notch signalling components, such as NOTCH3, delta-like 4 (DLL4) and Hes related family BHLH transcription factor with YRPW motif 2 (HEY2), have been described to be involved in the remodelling of the primary vascular plexus to develop a hierarchy of mature vascular beds and to maintain arterial fate [47,48]. For example *Dll4* heterozygous mice (*Dll4*$^{+/-}$) show reduced *Efnb2* expression but an increased *Efnb4* expression, indicating a failure in arterial differentiation implying that *Dll4* and their downstream targets are vital for promoting arterial fate [49]. The initial vascular

network has been established once the ECs have connected and formed primitive interconnecting vessels. The vasculature then undergoes a sequence of events to expand and mature the network which involves sprouting, proliferation and migration of ECs and recruitment of other cell types allowing the next phase of vascular development.

6.4 Angiogenesis

Angiogenesis is defined as the formation of vessels from pre-existing vessels and is essential for the expansion and remodelling of the vascular network [24, 50]. Angiogenesis can be separated into three distinct phases; quiescence, where the vessel is at normal or resting conditions; activation, whereby cues have been given to start branching; and resolution, where at the end the vessel must stabilize and mature to return back to the initial phase of quiescence [51].

Under normal conditions, ECs form a robust, quiescent monolayer of phalanx cells that possess a long half-life and are protected by autocrine signals such as VEGF, NOTCH, ANG1 and fibroblast growth factors (FGFs) [51]. Phalanx cells are a type of EC with a specific characteristic, they have few filopodia extensions and low migration potential in response to VEGF, have tight barrier formation and vascular lumen and they also express higher levels of molecules such as vascular endothelial-cadherin (VE-cadherin, Cdh5) [52]. These phalanx cells are what allows the monolayer, along with pericytes, to form such tight cell-cell junctions as they express VE-cadherin as well as claudins [51]. Pericytes are a cell type that display a set of characteristics consistent with muscle-cell activity and have been shown to express contractile smooth-muscle actin, however it is still unclear whether these cells are indeed smooth muscle cells (SMCs), cells with smooth-muscle-cell features or if it's possible that they can turn into SMCs when required [53]. Pericytes encase the EC vessel which allows them to maintain quiescence in a mature vessel by suppressing EC proliferation as well as releasing protective signals such as VEGF and ANG1 as mentioned previously and together these form the basement membrane as shown in Fig. 4a.

Once a vessel senses angiogenic signals, such as VEGF, FGF, ANG2 or chemokines, within the vicinity, the activation phase begins as seen in Fig. 4b. Environments such as hypoxia, inflammation, the presence of tumour cells or vascular occlusions can induce such angiogenic signals to be released [51]. Firstly pericytes, detach from the vessel wall due to the presence of ANG2 and free themselves from the basement membrane by proteolytic degradation via matrix metallopeptidases (MMPs) [54,55]. Next, ECs loosen their junctions and the budding vessel begins to dilate. This in turn allows the increased VEGF

signal to increase permeability of the EC layer allowing plasma proteins to be released which go on to form a extracellular matrix (ECM) scaffold [51]. The next signalling cascade of integrins promotes ECs to migrate along the ECM surface towards to the angiogenic signals. On top of this, further protease factors increase the local concentration of angiogenic molecules contained within the ECM, remodelling the ECM and making it a more pro-angiogenic environment [51]. At this point ECs take on different characteristics and roles to allow one cell type to migrate further and move towards the angiogenic signal, while the other cell type remains behind to form a lumen structure that will become a lumen vascular structure pictured in Fig. 4c. These different ECs are known as tip and stalk cells respectively.

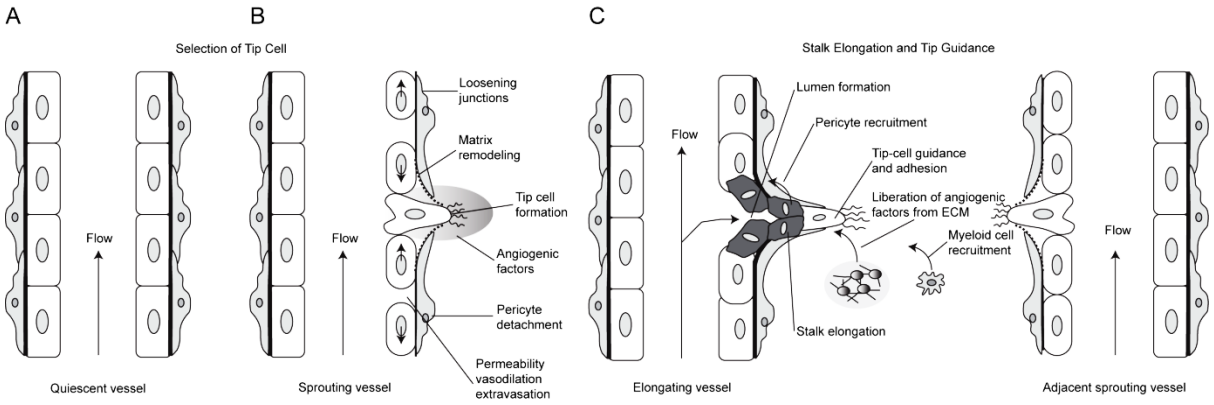

Figure 4: Tip cell selection and sprouting vessel elongation
(A) Under normal conditions ECs form a quiescent monolayer, strengthened by a basement membrane and covered with SMCs and pericytes. (B) Upon the detection of angiogenic factors, such as *Vegf*, the sprouting vessel begins to dilate allowing for EC tip cell selection via angiogenic factor gradient. To enable further invasion into the surrounding area degradation of the basement membrane, detachment of SMCs and pericytes and loosening of the other neighbouring EC junctions. Lastly an increase in permeability allows for extravasation of plasma proteins which go on to deposit a makeshift matrix layer. Proteases are also secreted to remodel the former interstitial matrix to allow cell migration. (C) Tip cells continue to move in response to further guidance signals and adhere to the newly laid down ECM. Stalk cells proliferate and elongate to form a lumen and pericytes and SMCs as well as depositing the basement membrane to stabilize the newly formed vessel. Myeloid cells are recruited and can produce pro-angiogenic factors as well as proteolytically liberate angiogenic factors from the ECM. Modified from [51]

Tip cells, stalk cells, phalanx cells and mural cells are the different cells groups that comprise a sprouting vessel, seen in Fig. 5a. Tip cells constitute a small number of ECs that take on a more motile and sprouting characteristic at the front of the sprouting vessel. These cells are able to respond to the pro-angiogenic signals, via their filopodia, where then act in accordance to positive or negative signals allowing directionality whilst preventing unorganized and random vessel growth[56]. Stalk cells on the other hand produce fewer filopodia but are instead highly proliferative, work to establish adherent, tight junctions for vascular stability and form the necessary lumen [57]. For a long time it was understood that tip

cells respond to angiogenic stimuli, such as VEGF, which is presented as a gradient and is important in controlling tip cell guidance, via the receptor VEGFR2 located on ECs [58]. Tip cells contain high levels of DLL4, unlike stalk cells, and are activated by VEGF signalling which in turn activates Notch signalling in neighbouring ECs. This signal pushes them towards a stalk cell characteristic [58]. NOTCH is then able to inhibit tip cell behaviour in these neighbouring stalk cells by decreasing levels of VEGFR2 and VEGFR3, which is needed for VEGF binding, and by increasing VEGFR1 [58,59]. VEGFR1, which is upregulated in stalk cells, binds left over VEGF to prevent tip cell formation [59]. In stalk cells, another Notch ligand, jagged1 (JAG1), is highly expressed due to its pro-angiogenic influences and is required for stalk cell maintenance [60]. JAG1 also targets DLL4 instead, thereby blocking Notch signalling allowing the tip cell to remain as such which is described in Fig. 5b [24].

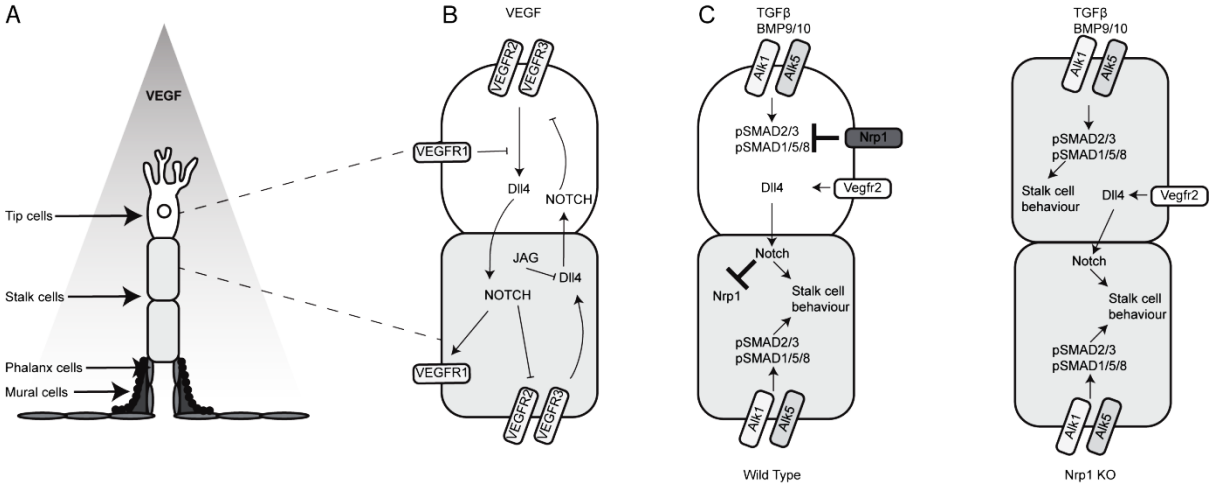

Figure 5: Sprouting cell composition and signalling mechanism
(A) In a sprouting vessel the tip cell migrates along the ECM and is guided by numerous different signals while the stalk cells proliferate to allow the sprouting vessel to move and form a lumen. Phalanx cells and mural cells are required for vascular quiescence and stability. (B) Tip cells (white) are activated via VEGF signalling which goes on to regulate Notch signalling in neighbouring stalk cells (grey) via DLL4. Notch suppresses VEGFR to allow for stalk cell behaviour. (C) Modified by [24,61,62]

In summary, tip and stalk cell specification is known to be regulated by Dll4/Notch signalling, where cells deficient for or activated by Notch signalling are either tip cells or excluded from the tip cell position respectively, and that ECs compete for the tip cell position via differential VEGFR levels under the control of Dll4/Notch signalling [59,63–65]. Recently BMP / SMAD family member 1/5 (SMAD1/5*)* signalling was also shown to affect tip/stalk cell specification, where inhibition of activin A receptor type II-like 1 (ACVRL1, as known as ALK1*)* or EC specific deletion of SMAD1 and SMAD5 results in hyper sprouting [62]. Transforming growth factor beta (TGFβ) is also known to block sprouting angiogenesis but this is highly context dependent and relies on which type I receptor is involved, ALK1 or

ALK5 [66–69]. Until recently the identity of the signal needed to switch off BMP/ALK1 signalling in tip/stalk specification was largely unknown and the link between Notch and SMAD signalling pathways had yet to be discovered. Aspalter *et al.* described a role for ALK1 and ALK5 in controlling vascular sprouting which they suggested to be downstream of Notch. As mentioned previously, NRP1 was shown to be differentially expressed and was found in arterial endothelium, tip cells included [70–72]. NRP1 is a transmembrane receptor and co-receptor to several structurally and functionally unrelated groups of ligands and signalling complexes like VEGF family members, class 3 semaphorins and TGFβ [73–76]. *Nrp1* deficient cells cannot obtain the tip cell position even when Notch is inhibited indicating that *Nrp1* operates downstream of *Notch* [62]. In another paper it had been shown that *Nrp1* is quantitatively regulated by *Notch* activity [77], therefore these results further identify *Nrp1* as the critical downstream effector of *Notch* that is needed for tip/stalk cell specification. Loss of tip cell ability and sprouting was due to the over activation of SMAD2/3 which remained consistent with the model that in stalk cells Notch is able to inhibit *Nrp1* and allow downstream activation of SMAD2/3 giving rise to stalk cell behaviour, while in tip cells NRP1 inhibits SMAD2/3 signalling allowing for tip cell response to VEGF as shown in Fig 5b and 5c [62]. How NRP1 directly inhibits SMAD2/3 or the differential roles TGFβ/ALK5 and BMP/ALK1 play still needs to be determined and better understood.

If a vessel is unable to be perfused correctly or angiogenesis has led to the overproduction of unnecessary blood vessels, then vessel pruning occurs. Vessel pruning is the trimming of a vascular network whereby regression of unwanted vessels occurs within a growing vasculature [78]. Initial triggers for regression of selected branches and the outcome of the regressing ECs are still not fully understood. EC apoptosis could be the first mechanism that results in vessel regression due to the removal of survival factors, such as VEGF, or due to activation of apoptotic signalling pathways [79,80]. One case in which this happens is in the case of pupillary membrane vessel regression and hyaloid vessel regression [81,82]. However, this has also been shown to not always be the case where even though apoptosis is involved it is not the primary, but rather the secondary effect, like during a reduction in blood-flow mediated survival signals in areas of vascular pruning [78]. Alternatively, detachment of ECs from a network as a result of migration away from an area of regression and later disassociation from the basement membrane can also lead to EC apoptosis [83,84]. Franco *et al.* used the postnatal mouse retina model to analyse vascular pruning at a high resolution and proposed a model for regression shown in Fig. 6. Firstly the branch for pruning is selected, either due to BF problems or lack of survival signals, where it constricts until occlusion has occurred and BF ceases (Fig. 6a-c). The ECs either, detach and undergo apoptosis or they migrate and reintegrate somewhere else on a neighbouring

vessel, choosing their course of action depending on the vessel involved and the context of the vascular pruning (Fig. 6d). Finally, resolution occurs when the selected vessel has fully regressed and leaves behind a collagen IV and empty basement membrane sleeve (Fig. 6e) [85]. Taken together this data would suggest that full removal and regression of a vascular network is primarily due to EC apoptosis whereas pruning of a certain vascular bed in certain conditions may be due to a combination of EC migration, redistributing and apoptosis.

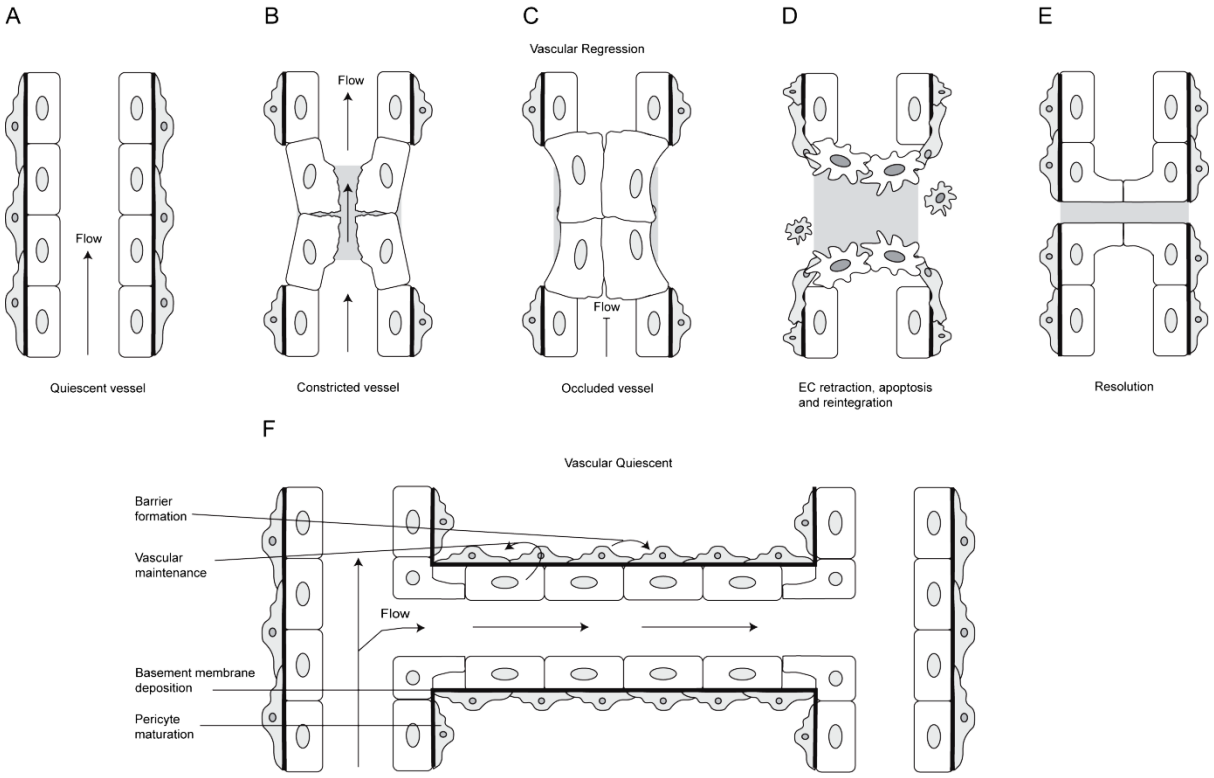

Figure 6: Vascular pruning, regression and quiescence
(A) BF can be used to select a section of a vessel for vascular regression. (B) Firstly the vessel restricts (C) until it closes and BF is blocked. (D) ECs in a regressing vessel retract and either undergo apoptosis or can reintegrate elsewhere in the vessel. Removal of these cells leaves behind an empty collagen positive basement membrane sleeve (grey area). (E) The final step in the resolution of this new vessel ends in the regression of the vessel. (F) After fusion of sprouting vessels, the lumen is formed and perfusion of the neovessel can occur. Vascular quiescence is achieved by promoting a quiescent phalanx phenotype, re-establishing EC junctions, depositing ECM, allowing maturation of SMCs and pericytes and secreting vascular maintenance signals. Modified by [51,78]

Lumen formation, depending on the type of vascular bed or the type of vessel formation, occurs via clustering of intracellular vacuoles that interconnect with vacuoles from neighbouring ECs and then go on to form a lumen known as cell hollowing or where ECs adjust their shape and junctions to allow a lumen to form known as cord hollowing [24]. Once BF is initiated into the new lumen, the vessel is able to shape and remodel its connections and respond to hemodynamic forces. Hemodynamic forces play a huge part in remodelling arteries and are essential for vessel maintenance, vessel identity and collateral vessel

expansion. It is known that non-perfused vessels are susceptible to vascular pruning and regression and that this process can be influenced by alterations in BF. Supporting this hypothesis is the need for the first heart beat to initiate BF to allow remodelling of the vascular plexus [26]. Vascular remodelling is the structural changes of vessels that involves cell growth, cell death, cell migration, and ECM synthesis or degradation and BF itself can initiate downstream effects via different signalling pathways [85]. Shear stress is the force emitted onto the endothelial layer of a vessel due to BF. High shear, like laminar flow, promotes EC survival, quiescence, alignment and secretion of vasodilation substances whilst low shear, like turbulent flow, promotes EC proliferation, apoptosis, shape change and secretion of vasoconstrictive substances [86]. Shear stress can induce AKT signalling which in turn leads to kruppel-like factor 2 (*Klf2*) activation and further upregulation of nitric oxide synthase (NOS), promoting EC survival and NO-mediated vessel dilation [83,87]. Reduction of shear has the opposite effect where this induces vasoconstriction [88]. BF itself is also able to direct EC migration during regression and its incorporation into the remaining vasculature. In quiescent vasculature ECs are known to align against the flow and this is determined by the axial polarity of the ECs golgi and nucleus [85].Though the full mechanisms of vascular pruning are not understood, in recent years, pathways such as signal transducer and activator of transcription 1 (STAT1)/ c-Jun N-terminal kinase (JNK3) and non-canonical WNT ligands have been implicated in controlling these events [89,90]. Downregulation of VEGF promotes EC apoptosis therefore inducing vascular regression, whilst DLL4/NOTCH signalling has been shown to activate pruning by altering the expression of vasoactive genes, inducing vessel occlusion, BF cessation and EC apoptosis [88]. *Ang2* is known to promote EC death and regression in the absence of VEGF and that shear stress is able to also control transcription of *Klf2*, which establishes a quiescent phenotype [54].

A major and very important step in vessel stability and maturation is the recruitment of pericytes and SMCs that will surround the newly formed vessel. Pericytes form direct contact with ECs but only in capillaries and immature vessels while SMCs and pericytes cover arteries and veins but are separated from ECs by a matrix. TGFβ signalling is needed during vessel maturation as it stimulates SMC induction, differentiation, migration and proliferation and also promotes ECM production [91]. Mural cell recruitment is controlled by a number of factors, one being platelet-derived growth factor (PDGF) and its receptor platelet-derived growth factor receptor beta (PDGFRβ) where PDGFβ is secreted from ECs that signals to PDGFRβ expressed by mural cells, effecting their migration and proliferation [24]. Loss of either the ligand or the receptor results in pericyte deficiency, vascular dysfunction and blood vessel rupturing and specifically loss of PDGFβ leads to insufficient pericyte coverage [92]. Other factors such as ANG1 are also important for recruitment of pericytes.

ANG1 is produced by mural cells and activates the endothelial-specific receptor tyrosine kinase (TEK, also known as TIE2) receptor in endothelial cells which stabilizes vessels by promotion of pericyte adhesion and firming the connection by tightening endothelial junctions [54,93]. These cells also require EFNB2 for association around ECs as well as Notch signalling for maturation and differentiation of arterial vSMCs [94,95].

Many steps are important for returning a vessel into a quiescent and stable environment as seen in Fig. 6f. Perfusion of vessels delivers oxygen and nutrients needed which in turn reduces VEGF expression and inactivates endothelial oxygen sensors, allowing the vasculature to switch from an active to quiescent state. For a vessel to fully function it is essential that the vessel must stabilise and mature which is achieved by deposits of ECM, recruitment of SMCs and pericytes, reduction in EC proliferation and increased cell junctions. Contact of tip cells with other tip cells from other sprouting vessels will interact with their filopodia and will fuse to bridge the new sprouting vessels together. Atastomosis of these vessels is established and VE-cadherin junctions allow the solidifying of these new connection. Downregulation of the tip cell behaviour will occur as a result but also the reduction in pro-angiogenic signals will contribute to the ablation of a pro-angiogenic environment allowing vascular fusion [24,51]. In addition, tissue inhibitor of metalloproteinase (TIMP) and plasminogen activator inhibitor 1 (PAI1) are circulated to allow deposition of the basement membrane where tight cell junctions can reform [96,97].

6.5 Hemodynamic forces and vascular structure in vascular homeostasis

Many different factors, such as genetic, mechanical and environmental (such as hypoxia) factors, are able to effect and alter vascular structure making this system a very complicated and dynamic system. Hemodynamics describes the fluid dynamics of blood and BF and explains these effects using physical laws that govern BF within the vessel. Our circulatory system is regulated by hemodynamic responses and mechanisms that are constantly monitored and adjusted to our body's environment. The heart is the main pump in the circulatory system where it delivers blood to the whole body through timed contractions and relaxations. There are many different factors that determine and effect hemodynamic forces that are outlined in Table 4 and shown in Fig. 7. The terms mentioned below are able to regulate gene transcription, leading to direct alterations in vascular structure which can ultimately lead to disease conditions or compensate for transient and unfavourable conditions.

Table 4: Hemodynamic terms

Term	Definition
Afterload	The pressure in the left ventricular wall during ejection
Blood flow	Volume of blood that passes through a vessel with respect to time
Cardiac output	Total blood volume pumped out of the heart in one minute
Circumferential stress	The force exerted circumferentially in both directions of a vessel
Heart rate	The number of times the heart beats per minute
Preload	The stretching pressure on CMs before contraction
Pressure	Pressure exerted from pumped blood on walls of blood vessel
Resistance	Opposition to BF within a vascular network
Shear Stress	A stress state where the stress is parallel to the vessels surface
Velocity	The distance blood travels in a vessel with respect to time

Shear stress and BP are two of the main exogenous mechanical forces that alter ECs and SMCs respectively. The endothelial layer is organized into a monolayer which acts as a barrier between the blood and the vessel but also acts as a sensor to hemodynamic forces and factors within the blood. These factors include regulators of vascular tone, recruitment of immune and mural cells and formation of new vessels. ECs are able to sense changes in their environment due to their mechanosensitive ability which allows for recognition of mechanical stimuli and coupling of these stimuli into a signalling event. Stimuli can be recognized by specific sensors on the surface of ECs and changed into a cellular signal via specialized proteins called mechanotransducers. Initial evidence indicated a role for cytoskeletal elements in transmitting signals due to shear forces throughout the intracellular network via ion channels, G-protein coupled receptors (GPCRs), the cytoskeleton, cell–cell adhesion molecules, and focal adhesions molecules [98,99]. Recent evidence now indicates that the cytoskeleton probably does not have a direct role in transmitting these signals but rather works in conjunction with other signalling mechanisms. New studies suggest that these direct signals could begin due to the appearance of multiple sensor sites on the surface of ECs, as a result of structural changes in the presence of flow causing conformational alterations in proteins or protein complexes that trigger downstream pathways. Another explanation could be due to shear stress where it is directly sensed by sensor complexes that activate specific signalling pathways that trigger downstream targets. Evidence for direct detection due to shear stress was propose when results showed that platelet/endothelial cell adhesion molecule (PECAM) acted as a direct monitor and signal transducer in response to shear stress [100,101]. PECAM can elicit a number of different responses when exposed to shear stress, such as alterations in cell shape via actin assembly, restructuring of cell adhesion complexes and adjustments in cell polarity. Further, PECAM was shown to interact with other molecules necessary for cell-cell adhesion such as CDH5 and VEGFR2. This signalling interaction evokes activation of downstream pathways, such as integrins, mitogen-activated protein kinases (MAPK) and extracellular-regulated

kinases 1/2 (ERK1/2), indicating that adhesion molecules, rather than the sensor, transmitted the transduction signal [100–102]. Application of shear stress on ECs can cause several different responses in varying timescales. For example, in a matter of seconds, activation of potassium channels, SRC family kinases and VEGFR2 occurs along with the release of NO, while within a matter of minutes GTPases, integrins, *Mapk* and Rho family members are activated [103]. Flow patterns were also shown to affect specific differential EC profiles. For example in a high shear stress environment, normal in arteries, gene expression induces an anti-proliferative, -inflammatory and thrombotic environment whereas in a low shear stress situation, hallmark of veins, gene expression increases cellular proliferation and apoptosis in a pro-inflammatory and –thrombotic setting [99,104].

Cell alignment has also been suggested as being important in transmitting the pressure from shear stress in the EC, where cells that are perpendicular to the force, defined by the cells shape and organization of its cytoskeleton, strongly increase the activation of the NF-κB pathway while cells that are parallel to the force do not strongly activate the NF-κB pathway but rather activate the eNOS-NO pathway [105,106].

SMCs act as the mechanical support for the vessel, allowing the vessel to contract or dilate according to the pressure being exerted. Many results have shown that mechanical stretch of SMCs due to BP and stress is able to regulate proliferation, apoptosis, and migration these cells as well as synthesis, degradation, and reorganization of the ECM [107].

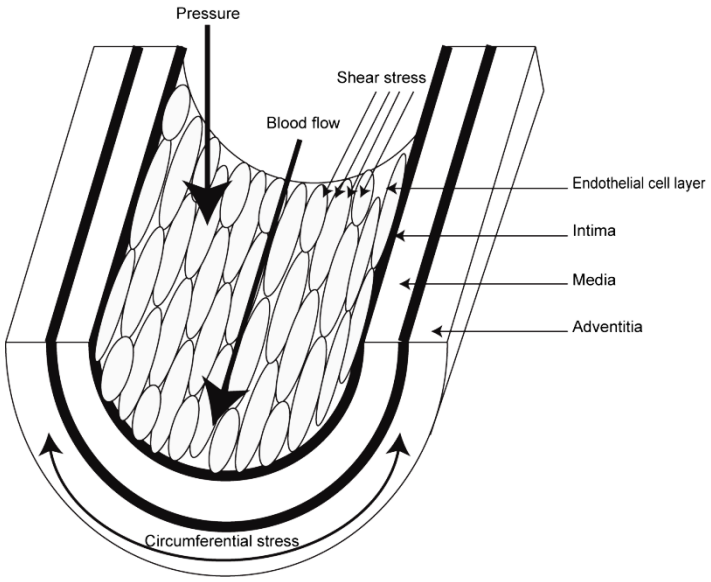

Figure 7: Role of hemodynamic forces on vascular structure
Different hemodynamic forces that are exerted upon the vascular network in response to various stimuli and factors that can alter vascular structure. Modified from [108]

6.6 BMP9 and BMP10 signalling pathway

BMP9 and BMP10 are members of the TGFβ superfamily of growth factors which include other factors such as the activin/inhibin family, GDFs, TGFs and other BMPs [109]. Members of this family regulate many different processes during early stages of development, such as induction of the three germ layers, left/right asymmetry and maintenance of pluripotency along with induction of embryonic stem cell (ESC) differentiation, and later stages of development, like haematopoiesis and organ development [109]. These growth factors have an essential role in organ development due to the role they play at a cellular level in proliferation, differentiation, apoptosis, migration and adhesion [109].

BMP9 and BMP10 are close family members that share 65 % sequence identity at a protein level although they are distantly related to other family members as seen below in Fig. 7. Both BMP9 and BMP10, as is also the case with other protein family members, are synthesised as large precursors which contains a large pro-domain needed for proper folding and a C-terminal region consisting of the active ligand [110]. Furin, an enzyme, or other proprotein convertases act to release the mature, dimeric ligand [111,112]. In the case of BMP9 it has been shown to circulate as an active ligand and this could be the case too for BMP10 although normally it circulates in its inactive form [113–115]. BMP9 is produced mainly in the liver but has also been shown to be expressed at low levels in the lungs and brain. BMP10 is expressed in the developing embryonic myocardium and is then secreted after development from the right atria of the heart through to adulthood [112,116–118]. Both BMPs have been detected in both mouse and human plasma and circulate at approximately 0.5–15 ng/mL which is necessary to bind and stimulate their receptors in the endothelium [112–114,119,120].

Interest in BMP9 and BMP10 gained attention when it was shown that both of these proteins bind with high affinity to the TGFβ type I receptor, ALK1 [113,121]. In vertebrates there are seven type I receptors, five type II receptors and two co-receptors and these receptors pair up in a number of different combinations which allows them to propagate the signals for all the TGF superfamily members shown in Fig. 8 [109]. When ligands bind to their specific type I receptor at the cell surface membrane, the receptor dimerizes and recruits their required dimeric type II receptor. Type II receptors are considered to be constitutively active and when brought into close proximity of the type I receptor, it phosporylates the type I receptor. The phosphorylation of this complex enables the recruitment of the receptor-regulated SMADs (R-SMADs) which are phosphorylated by the type I receptor. The phosphorylated R-SMAD forms a complex with the co-mediated SMAD (co-SMAD), SMAD4, which subsequently translocates to the nucleus where it accumulates and positively or negatively regulates target gene transcription [122]. BMP9 and BMP10 bind to their type I

receptor, ALK1. However when recruiting the type II receptor there is a difference in binding affinity between BMP9 and BMP10 with three possible receptors, Bone morphogenetic protein receptor II (BMPR2), Activin type receptor II A (ActR2A), and ActR2B [123]. BMP9 or BMP10 binding results in the recruitment and phosphorylation of Smad1/5/8 [112,113]. ENG, one of the co-receptors, has been shown to facilitate the binding of these ligands to ALKs which is displayed in Fig. 8 [113,121]. To date, BMP9 and BMP10 are the only ligands in this superfamily that have been shown to be able to bind directly to ENG [124]. Within this signalling pathway there is a negative feedback loop whereby the initiation of this signalling pathway induces the inhibitory SMADs (I-SMADs), SMAD6 and SMAD7. Initial studies of these I-SMADs showed they target type I receptors and are able to interact with them ultimately inhibiting further signalling and additionally have been shown to recruit SMAD-mediated ubiquitin regulatory factor (SMURF) with E3 ubiquitin ligase activity that degrade of the activate receptor complex [125].

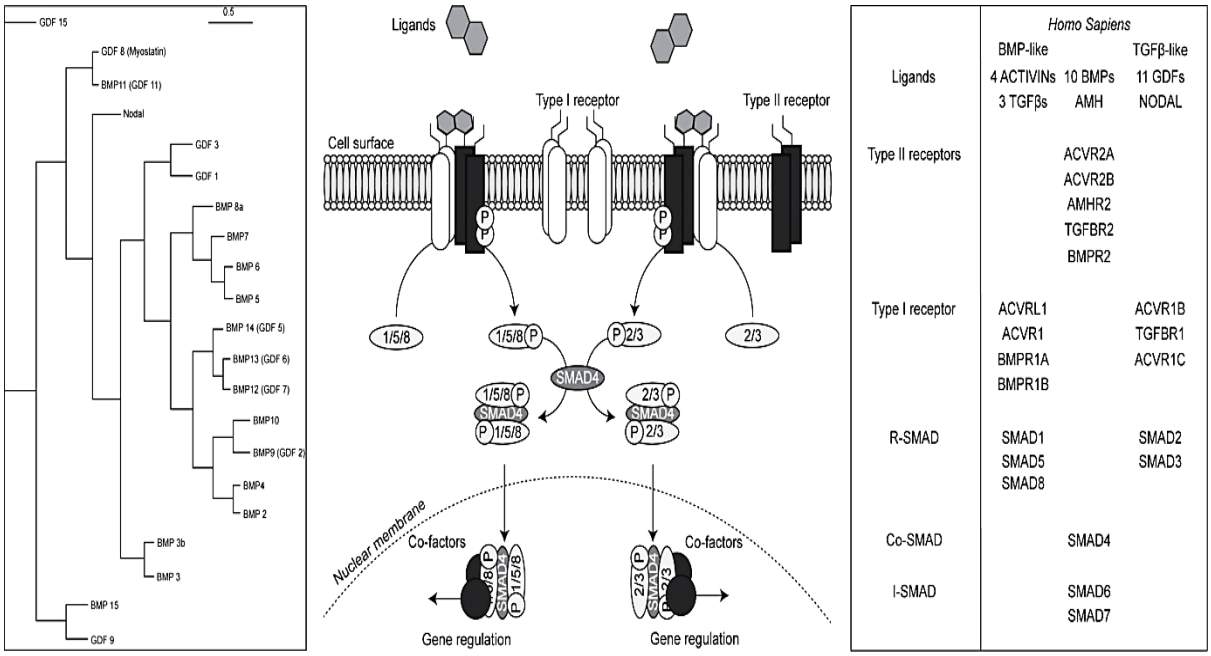

Figure 8: TGF tree, receptors and signalling pathway
(a) Phylogenetic tree of the TGF protein superfamily which shows the high degree of sequence similarity between BMP9 and BMP10 and that also these two proteins are not as highly related to the other family members. (b) Binding of ligands to their specific type II receptors and recruitment of the type I receptors allows for high combinatorial complexity allowing for regulation of numerous different downstream targets. Ligands from this signalling pathway are normally categorized into two groups, ones that activate SMAD 2/3 via ALK4, ALK5 or ALK7 or ones that activate SMAD1/5/8 via ALK1, ALK2, ALK3 or ALK6. Once these SMADs have been phosphorylated they form a complex with SMAD4 which then translocates into the nucleus. Once in the nucleus gene transcription can be directly regulated in conjunction with transcription factors, chromatin remodelling complexes and histone modifying enzymes. (c) Chart of ligands, receptors and SMADs involved in the TGF signalling pathway. Modified by [126,127]

6.7 BMP9 and BMP10 in disease and their role in vascular homeostasis

In humans hereditary haemorrhagic telangiectasia (HHT), also known as Osler-Weber-Rendu syndrome, is an autosomal dominate group of disorders that are characterized by the development of arteriovenous malformations (AVMs) in the skin, mucous membranes, and/or in internal organs such as the brain, lungs, and liver [128]. Under normal conditions, an artery feeds into a smaller sized network of arterioles which feeds into a capillary bed that are drained into venuoles that are connected to a vein as seen in Fig 9. However, in AVMs, the capillary bed is completely unorganised which leads to the situation where arteries shunt blood directly into a vein without the intervening capillary bed [129]. Therefore draining veins fail to remodel to have an arterialized characteristic and they keep their venous structure and identity which leads to rupturing and bleeding. If these AVMs are located in large organs like the brain, rupturing of these vessels can lead to seizures, a stroke or even severe and life-threatening haemorrhaging. The etiology of these AVMs is still largely unknown; however, genes that have a loss of function mutation in them have been uncovered. Most cases of HHT are congenital and develop over time due to mutations within a number of genes, however there is still approximately 15 % of patients who don't have a mutation in these known genes [130] Mutations in receptors and binding partners, for example ENG, ALK1, SMAD4 and BMPR2, have been shown to develop into different forms of HHT [128,129,131]. Although HHT is mainly congenital and was believed it was the only way AVMs could develop it is now understood that certain conditions or environments, like inflammation, trauma, stimuli promoting angiogenesis or even alterations in hemodynamic, can favour and initiate AVM formation spontaneously [132]. For example the Notch and Ephrin family members that are important in artery and vein identity, are misregulated in AVMs and it has also been shown the AVMs overproduce angiogenic factors like VEGF, ANG-2 and MMP9 but downregulate inhibitors of EC growth or vascular stabilization factors such as ANG1 [95,129]. Understanding if changes in a certain settings can initiate AVM formation and how AVMs develop is vital.

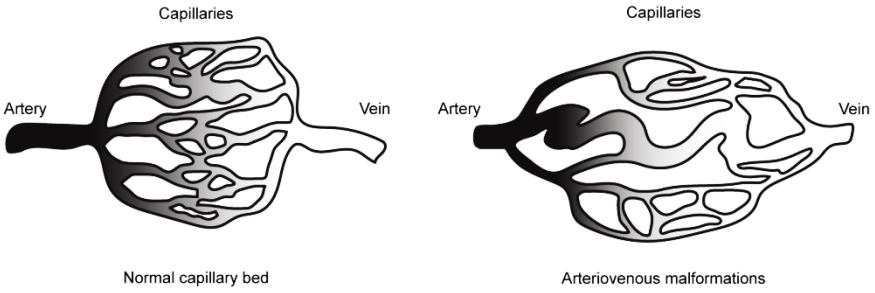

Figure 9: Arteriovenous malformations
In normal conditions areas of high pressure (dark) and low pressure (light) run into the capillary bed. Capillaries form a network of thin; one cell thick, vessels where gases and nutrients are exchanged and metabolic waste is removed. An arteriovenous malformation is when there is an abnormal connection between arteries and veins is formed, bypassing the capillary bed. In these cases vessels become dilated, fragile, and tortuous, and eventually end up rupturing. Modified from [133]

Loss of *Alk1* (*Alk1*$^{-/-}$) leads to embryonic lethality by E11.5 and histological analysis showed that before E9.5, *Alk1*$^{-/-}$ mice were indistinguishable from their WT littermates [134,135]. At E9.5 the yolk sac from these *Alk1* mutant mice possess a lack of mature vessels resulting in an interconnected knot of similar sized endothelial tubes [134,135]. The mutant embryos displayed smaller heads, were retarded in their growth and by E10.5, embryonic development was arrested [135]. At E10.5 the *Alk1*$^{-/-}$ yolk sac was avascular with few vessels showing severe signs of vascular dilation [134,135]. Two papers addressing the loss of *Alk1* during embryonic development also noted at early stages the cardiac tube was contracting in these KO embryos but that blood circulation was aberrant while at E9.5 the endocardium and myocardium were dilated and by E10.5 the pericardium was enlarged [134,135]. Urness *et al.* showed that between E7.5 – E8, angioblasts coalesced normally to form the primitive tube network with no differences between *Alk1*$^{-/-}$ embryos and WTs [134]. This was supported by Oh *et al.* that used an EC specific lacZ reporter line in the *Alk1*$^{-/-}$ background and showed the normal formation of the primary capillary plexus and that vasculogenesis was not affected [135]. Taken together, both groups hypothesis that vascular defects seen in these *Alk1*$^{-/-}$ embryos came directly after *de novo* formation of the central vascular network and that vasculogenesis was not affected, where vascular defects after E9.5 included multiple AV shunts, dilation of major vessels and excessive vessel and capillary fusion [134,135]. Expression of vSMC markers, αSMA and SM22α, were also shown to be markedly reduced in areas known to have high expression, such as the dorsal aorta (DA), heart and somites, and one SMC reporter line showed SMCs were mislocalised and not present in the perivascular region [134,135]. Urness *et al.* attributed the drastic loss of SMC to the downregulation of arterial specific marker, EFNB2. They concluded that loss of arterial identity lead to a reduced recruitment of SMCs which allowed for vascular dilation leading to fusion of vessels causing multiple AV shunts [134]. Oh *et al.* showed a dramatic increase in

plasminogen activator (PA), urokinase-type PA (uPA) and PAI1 in *Alk1* mutant mice, which are genes known to be expressed in perivascular matrix proteolysis [136]. uPA is also known to be a marker for actively migrating ECs and VEGF has been shown to increase its expression [137–139]. This increase in VEGF and uPA in *Alk1*$^{-/-}$ embryos was hypothesized to increase vascular permeability, due to perivascular proteolysis, which could allow for excessive EC migration and proliferation and this in turn results in loss of SMCs, which also cannot inhibit EC proliferation, resulting ultimately in vascular dilation and vessel fusion [135].

Seeing as early deletion of *Alk1* led to embryonic lethality, a later stage Cre was used to KO ALK1 (*Alk1* $^{L1\ Cre}$) [140]. Deletion of *Alk1* after E13.5 resulted in no mutant fetuses after E18.5 but between E15.5 – E17.5 *Alk1* $^{L1\ Cre}$ embryos were already distinguishable from their WT littermates [140]. Yolk sac analysis showed that loss of *Alk1* resulted in an increase in diameter and decrease in wall thickness of the vitelline artery, similar characteristics to the vitelline vein, suggesting the artery had lost its arterial specification as previously debated [140]. The mutant yolk sacs also showed dilated, torturous vascular networks with the presence of AVMs [140]. When analyzing the vascular network within the lung between E16.5 - E17.5, *Alk1* $^{L1\ Cre}$ lungs also displayed an irregular mesh of dilated, fused vessels and when stained with αSMA showed a reduction in the SMC layer [140].

To further investigate the role of ALK1 in the neonatal mouse, *Alk1*$^{-/-}$ mice were crossed with an EC specific Cre (*Alk1* ^{EC}) [141]. Deletion of *Alk1* in ECs led to postnatal lethality at P5 as a result of severe hemorrhaging in various organs and as seen previously in all the other *Alk1* embryonic models, these *Alk1* ^{EC} pups displayed severe dilation and tortuous vessels with the presence of numerous AV shunts as well as an uneven and depleted SMC layer which resulted in permeable and leaky vessels [141]. To achieve a better understanding of the role of *Alk1* in the adult mouse, after establishment of the vascular system, Park *et al.* generated an inducible, global deletion of ALK1 (*Alk1* ^{iCre}) via tamoxifen injection. *Alk1* ^{iCre} were injected once with tamoxifen at the age of 2 months which resulted in lethality 9 – 21 days after the injection. These mice again showed similar phenotypes to all the previous *Alk1* KO models; hemorrhaging, dilation of the pulmonary vessels, increased vascular permeability and the development of AVMs [141]. Inducing wounds in these *Alk1* ^{iCre} mice allowed for the real time monitoring of *de novo* AVMs after vessel formation. Control animals had normal arterial branches after wounding while *Alk1* ^{iCre} mice developed AVMs in the wounded area showing that this is a local response [141]. These results concluded that environmental factors, like wound healing, can induce AVM formation in adults *de novo* [141]. To address the question of how these AVMs are formed, Park et al visually monitored the process of vascular remodeling during wound healing in these *Alk1* ^{iCre} mice. During vascular remodeling, control mice formed large numbers of growing microvessels that grew towards

the center of the wound [141]. In contrast the mutants developed fewer vessels and continued remodeling at the periphery of the wound [141]. Hb (O_2) saturation levels in the controls stayed constant in the venous vessels while in the mutants Hb (O_2) levels were highly elevated in the veins, evidence of A-V shunts and lastly minor changes were made in the major arterial and venous branches of the controls during healing, while in the mutants there was an obvious and progressive dilation of vessels [141]. Taken together these papers all indicated the importance ALK1 has as an EC receptor in maintaining vascular identity and stability during embryonic and adult angiogenesis.

The involvement of BMP and TGF signalling in the maintenance of vascular homeostasis was reiterated in the discovery of the role of ENG, a co-receptor in the TGF signalling pathway, in the development of HHT in humans [142]. Similar to the *Alk1*$^{-/-}$ embryos, loss of *Eng* leads embryonic lethality by E11.5 due to defective angiogenesis and both KO's shared similar phenotypes [143]. At E8.5 ENG KO (*Eng* $^{-/-}$) embryos were indistinguishable to WT littermates where both possessed a primary vascular network but by E10.5 *Eng* $^{-/-}$ embryos were smaller in size, lacked vascular organisation and possessed cardiac defects; extra fluid was in the pericardial space, failed closure of the lumen, dilated endocardium and defects in valve formation and heart septation [143,144]. EC impairment was first detected in *Eng* $^{-/-}$ embryos between E9.5 – E10.5, where major vessels such as the DA, CA and BA, were highly disorganised and the same was clear in the yolk sac of these embryos which possessed an immature vascular plexus and undefined, disorganised vessels [143]. Although problems with EC organisation were detected around E9.5, defects with SMC coverage and differentiation were detected as early as E8.5 up till E10.5 [143]. *Eng* $^{-/-}$ yolk sacs possess endothelial tubes lacking SMC coverage by E8.5 which does not progress by E9.5 and αSMA staining confirmed fewer SMCs between the endoderm and endothelium [143]. SM22α staining at E9.5 also confirmed an inhibition in SMC development in both the yolk sacs and embryos lacking *Eng* [143]. Studies of adult mice with a heterozygous KO for *Eng* showed development of ear telangiectasia's with recurring nose or mouth bleeds, recapitulating sign in patients with HHT [144]. To understand the role of *Eng* in a cell specific context, an *Eng* EC inducible line was generated (*Eng* ^{iKO}). The retinas of P4 *Eng* ^{iKO} mice showed a denser capillary plexus and a reduction in vascular outgrowth, suggesting a delay in remodelling and a reduction in migration, which persisted until P9 [145]. AVMs were also detected at a high frequency in *Eng* ^{iKO} retinas and numerous AVMs had ruptured and were bleeding, possibly due to the increase in venous calibre and AVM enlargement [145]. There was an increased number of ECs lining the diameter of AVMs and the arteries in these AVMs had a high number of proliferating cells, where normally arteries contain non proliferating cells. Additionally αSMA expression was detected in veins in these AVMs, where αSMA is

normally only expressed in arteries. These results concluded that loss of vascular identity could play a major role in AVM development and progression [145]. Taken together these groups propose that loss of *Eng* leads to vascular instability which can lead to cardiac defects or develop diseases such as HHT and that ECs are needed to induce SMC differentiation, while SMCs are important in regulating EC organisation [143–145].

As mentioned above, BMPR2 and SMAD4 have also been implicated recently with HHT syndromes in humans [131,146,147]. Loss of *Bmpr2* leads to embryonic lethality by E9.5 and is known to be essential for gastrulation and early development due to its regulation of many different signalling ligands [148]. To overcome embryonic lethality, a knock down (KD) of *Bmpr2* was generated and showed that KD of *Bmpr2* lead to an insufficient coverage and sometimes a complete loss of SMCs in pulmonary arteries and the large intestine. The pericyte marker, PDGFRβ was also reduced in lung extracts of these KD mice. KD of *Bmpr2* in ECs also lead to an impaired angiogenic response and analysis of alterations in gene expression showed a downregulation of major components needed for vascular patterning and maturation [149]. Loss of *Smad4* also results in embryonic lethality at E7.5 in mice, where these mice showed a reduction in size, due to an impairment in cellular proliferation and with a poor definition between the embryonic and the extraembryonic regions of the embryo [150]. This group discovered a problem with mutant ESCs lacking *Smad4* during *in vitro* differentiation of the visceral endoderm and mesoderm explaining the gastrulation defects in these mutant embryos [150]. To date not much is known as to why some SMAD4 mutations can cause HHT as well as JP but in other cases it doesn't. However a possible correlation has been made where SMAD4 mutations in JP-HHT patients all have mutations clustered in one domain of the protein and this could explain a molecular mechanism for the different phenotypes [151].

To date, research has been carried out on the receptors and signalling components in the TGF signalling pathway while the ligands, BMP9 and BMP10, haven't received as much attention. BMP9 was first described as being involved in ectopic bone formation and later was shown to have a role in osteoblast differentiation as well as inducing and maintaining the neuronal cholinergic phenotype in the central nervous system [152–154]. Once it had been discovered that BMP9, along with BMP10, were the functional ligands of the ALK1 receptor, research shifted and focused on the role these two BMPs play in modulating angiogenesis [113]. Using human dermal microvascular ECs (HMVEC-d) it was shown that BMP9 binds and activates ALK1, where ENG overexpression was shown to increase this response. Stimulation with BMP9 leads to phosphorylation of SMAD1/5/8 via either BMPR2 or ACTR2A, where loss of either receptor results in a compensatory overlap from the other. Although these receptors can compensate for each other there were different cellular

responses [113,155]. Here they showed that BMP9 was able to inhibit both migration and growth of HMVEC-d's via ALK1 and this was also as the case with BMP10 [113]. BMP9 which is produced in the liver, is an active circulating factor and is found to be present in human serum that acts on ALK1 and a vascular quiescent factor *in vivo* as well as BMP10 which is produced in the right atria [112,119]. In another animal model, the zebrafish, it was shown that *bmp10* is able to limit EC number via *alk1* [115,117,120,156].

Loss of BMP9 in mice is not lethal as shown by Ricard et al as well as described in this thesis with hardly any obvious effects on angiogenesis. In contrast, loss of BMP10 leads to embryonic lethality in mice around E10.5 where cardiac defects are already observed at E9 [118,120]. Not only is BMP10 involved in maintaining vascular quiescence and homeostasis during development but it also has a unique function in cardiac development [114]. During cardiac development, BMP10 expression is detected around E8.5 and is transiently expressed in the ventricular trabecular myocardium and is involved in the process of trabeculation between E9.0 - E13.5. After this process BMP10 is no longer detected in the ventricles at E16.5 - E18.5 and is only detectable in the right atria [117,118]. In contrast, upregulation of BMP10 expression, as seen in FKBP12 deficient mice, leads to hypertrabeculation and non-compaction showing a needed for a balance in expression [118,157]. The cardiac-specific role of BMP10 is likely not restricted to its specific location but also because of its ability to regulate other important cardiac factors such as NKX2.5 and MEF2C in controlling normal cardiac function [118]. It has been hypothesized that BMP9 and BMP10 have overlapping functions during embryonic and postnatal angiogenesis. To understand the role of BMP9 and BMP10 in neonates one group used BMP9 KO (*BMP9$^{-/-}$)* mice and injected them with BMP10 monoclonal antibody. Here they showed that that loss of BMP9 together with reduced BMP10 levels in a neonate leads to more drastic vascular abnormalities in the retina where expansion of the vascular plexus was significantly delayed, vascular density was noticeably increased, vessel diameter was enlarged and affected blood vessels have reduced coverage of mural cells [114,120]. To address the question of overlapping functions during development, another group checked whether *Bmp9* can substitute *Bmp10* and fulfil its developmental role in cardiac development and angiogenesis [112,114]. Chen et al created a mouse line where the coding region of *Bmp10* was replaced by the coding region of *Bmp9, Bmp10$^{9/9}$*. At E16.5, *Bmp10$^{9/9}$* embryos did not display any major developmental angiogenic defects which was observed in *Bmp10$^{-/-}$* embryos by E9.5 [114]. *Bmp10$^{9/9}$* embryos displayed distinct DA and cardinal veins and lacked AVMs that were detected in *Bmp10$^{-/-}$* embryos. These results indicated that BMP9 and BMP10 are functionally able to overlap to allow normal early vascular development via ALK1. However by E14.5 *Bmp10$^{9/9}$* hearts were hypoplastic with thin ventricular walls and showed pericardial

edema and by E17.5, the hearts had grown in size, altered in shape and a majority of them also had ventricular septal defects which were all similar to previous results in *Bmp10*$^{-/-}$ embryos [114]. Around E16.5 *Bmp10*$^{9/9}$ embryos were also affected by haemorrhages and edema, which increased in severity as the embryos developed. Seeing as early vascular development in *Bmp10*$^{9/9}$ embryos was mostly normal they hypothesized that the late vascular phenotype may be a secondary effect due to defects in heart development. Taken together these results clearly show that BMP9 is able to compensate for loss of BMP10 during vascular development but BMP10 has a very specific role in cardiac development that cannot be replaced and impairment in cardiac development leads to later vascular abnormalities.

6.8 Thesis aim and overview

To date, little is known about the role of BMP9 and BMP10 in the adult cardiovascular system and how they maintain vascular quiescence. The aim of this thesis was to use different mouse models and *in vitro* analysis to study the role of both BMP9 and BMP10 individually as well as their possible overlapping roles and how they affect vascular homeostasis. To achieve this, a constitutive BMP9 single knockout line (SKO) was generated along with a conditional BMP10 single knockout line (cKO) which was under the control of ANF Cre, to bypass the embryonic lethality. These two SKO lines were then crossed to generate a BMP9/BMP10 double knockout line (DKO). Using these two SKO lines and DKO line I have investigated overall cardiac function and structure by using techniques such as magnetic resonance imaging (MRI) and micro computed tomography (µCT) to determine if cardiac function was compromised. Vascular structure and changes in vascular homeostasis was measured by using numerous different hemodynamic factors as read outs, such as BF, blood velocity (BV), heart rate (HR) and BP. Along with structural and functional readouts I was able to use these different lines to decipher and understand the changes and alterations in gene and protein expression that shed light onto the mechanisms that can lead to CVDs, as well as vascular diseases such as HHT, and an overall view on how vascular homeostasis is maintained.

7 Materials and Methods

7.1 Animal Experimentation

7.1.1 Isolation of mouse embryos from the uterus

Breeding female mice were checked for a vaginal plug formation, indicating mating has usually occurred. When this plug is formed, it is counted as E0.5. Embryos at E14.5 and E16.5 were required and these developmental stages were calculated by counting from the positive plug formation to these final time points.

Pregnant female mice were killed via cervical dislocation as anaesthetics can have unwanted effects on the embryos. The abdominal cavity was opened and the uteri were removed and placed in to cold PBS. A small part of the embryo, usually the tail, was used for genotyping.

7.1.2 Magnetic Resonance Imaging

MRI was used for cardiac functional analysis and was carried out by our in house service group. A Bruker Pharmascan 7.0 T machine, fitted with a 300 mT/m gradient system and a custom-built circularly polarized birdcage resonator, was used for analyzing our samples. An Early Access Package for self-gated cardiac imaging was used (Intragate, Bruker, Ettlingen, Germany) and all data were analysed via the Qmass digital imaging software (Medis, Leiden, the Netherlands).

Before analysis mice had to be anaesthetized using 5 % Isofluorane /O_2 to ensure a reduction in movement during measurements. The mice were then fixed in a dorsal orientation in a specialized mount to further ensure a more permanent position during measurement. The mice were then placed into a magnetic field where they were, kept at a constant temperature of 37 °C, via the systems thermostatic regulatory system and continually anaesthetised with a mask that produced 2 % Isoflurane/O_2.

We wanted to understand the cardiac function of our DKO mice in comparison to their littermate controls and both the SKO mice over an extended period of time. Therefore we began measurements at 1 month of age and then measured the same mice again at 3, 6, 9 and 12 months from all groups. By using MRI we were able to determine cardiac wall

thickness, ejection fraction (EF), stroke volume (SV), left ventricular mass (LVM) as well as end diastolic (ED) and end systolic (ES) volume over a long period of time.

7.1.3 Magnetic Resonance Angiography

Two angiography techniques based on physical properties of flowing blood are most commonly used: The Time Of Flight method is based on the principles of in-flow of the fresh, unsaturated blood into the imaging plane and on the other side the Phase Contrast Angiography uses alternating flow encoding gradients to produce an angiogram. Both techniques provide an insight into morphology, but PCA additionally allows a mapping of the average blood velocities (PC-MRA).

3 and 6 month old mice were measured under anesthesia (1.2 – 1.8 % Isoflurane in 0.5 L/min O_2 and 0.5 L/min air) in the 7.0 T superconducting magnet (Bruker Biospin, Pharmascan, 70/16, 16 cm; Ettlingen, Germany) equipped with an actively shielded imaging gradient field of 300 mT/m, and, after an upgrade, of 760 mT/m respectively. The frequency for the ^{1}H isotope is 300.33MHz. The body temperature was maintained at 37 °C by a thermostatically regulated water flow system during the entire imaging protocol.

For a rough positioning in the magnetic field a spinecho sequence, for exact positioning RARE-(Rapid acquisition with relaxation enhancement) sequences in coronal, sagittal and axial orientation was used. The interesting blood vessels are subsequently presented in an axial orientation with the 2D TOF-MRA: TE (echo time) = 2.9 ms, TR (repetition time) = 25 ms, FOV (field of view) =3.7x3.7 cm, MTX (matrix size) = 256x256, slice thickness = 0.8 mm, slice overlap = 0.5mm and 150 slices. Subsequently a three-dimensional reconstruction (MIP) was calculated with the imaging software Paravision 5.1 (Bruker, Ettlingen, BRD).

For the following flow quantification via velocity mapping it is important to set the slice orientation strictly perpendicular to the target vessel, using an in-house-developed program [158]. For the PC-MRA we use the following parameter: TE= 4.0ms; TR= 35 ms; Venc= 60 cm/sec, FOV = 4.0x2.5x2.0 cm, MTX =256x256x40 and slice thickness = 20 mm. The quantitative flow values are obtained by integrating across manually drawn regions of interest (ROI) that enclose the vessels (Paravision 5.1, ROI Tool, Bruker, Ettlingen, Germany). For the increase of accuracy magnitude images are used to define vessel walls and for a reduction of the influence of possible segmentation errors a velocity threshold is defined: Only pixels with a velocity >0 in the direction of flow are used.

7.1.4 Micro computed tomography

µCT was performed at the Vascular Research Centre, Frankfurt am Main by Dr. Christoph Schürmann [159]. Mice were killed and perfused with vasodilation buffer (4 mg/L Papaverine, 1 g/L Adenosine in PBS, Sigma-Aldrich, Taufkirchen, Germany) for 5 min, followed by fixation for 15 min with 4 % PFA. After PFA fixation, the mouse was perfused with the radiopaque contrast agent MicroFil (Flow Tech, Carver, MA, USA) with a pressure of 100-120 mmHg until the silicon polymer had set. Mice were stored overnight in 4 % PFA at 4 °C and scanned using a Skyscan 1176, Bruker micro-CT (Kontich, Belgium). Data reconstruction was done using the NRecon/InstaRecon CBR Server – Premium software (Skyscan, Kontich, Belgium/ InstaRecon, Champaign, Illinois, USA) and image analysis, segmentation of µCT data and quantification of vessel lumen area was performed with the Imalytics Preclinical Software (Gremse-IT, Aachen, Germany).

7.1.5 Retina Assay and Immunofluroescence Histochemistry

The protocol for mouse retina extraction was described by Stahl *et al.* 2010 [160]. To begin to process the eyes, they were firstly fixed in 4 % PFA for 1 h on ice. The eyes were then transferred to cold PBS where they were dissected and processed. Retinas were then blocked for 1 h in C-Buffer (1 % BSA, 3 % FBS, 0.5 % Triton, 0.5 % Tween-20, 0.01 % Sodium-Deoxy-Cholate in PBS) before antibody staining. Primary antibody was diluted in 50 % C-Buffer/PBS and incubated overnight (O/N) at 4°C. Retinas were then washed in PBSA (PBS with 1 % BSA) + 0.1 % Tween-20, 3 times for 10-15 min each time. Secondary antibody is diluted in 50 % C-Buffer/PBS and incubated for 1 h at room temperature (RT) rotating in the dark. Retinas were again washed in PBSA + 0.1 % Tween-20, 3 times for 10-15 min each time.

For lectin staining retinas were washed in pBLEC (1 % Tween-20, 0.1 mM $CaCl_2$, 0.1 mM $MgCl_2$, 0.1 mM $MnCl_2$ in PBSA at pH 6.8) for 30 min. Isolectin B-4 antibody was diluted at 1:100 in pBLEC and incubated at RT for 2 h. Retinas were washed one in pBLEC for 30 min, then once in PBSA-Tween-20 for 30 min and lastly in PBSA for 30 min.

To check for cellular proliferation, 5-ethynyl-2´-deoxyuridine (EdU) was injected at 50 µg/g body weight i.p into P5 pups and the pups were left for 3 h, to allow for EdU incorporation. The P5 pups were killed via decapitation, as cervical dislocation is not possible. When staining for EdU incorporation, retinas were washed twice with 3 % BSA in PBS. Each retina was then incubated at RT for 20 min in 500 µL 0.5 % Triton-X100/PBS to permeabilize the samples. Retinas were then washed again twice in 3 % BSA/PBS. The EdU reaction cocktail was prepared according to the company's protocol and 100 µL of this

reaction cocktail was added to each retina and left at RT for 30 min rotating. The samples had to be protected from the light. The retinas were finally washed once with 3 % BSA/PBS and further staining's were then performed.

For nuclear staining, DAPI was used at a 1:1000 dilution in PBSA and incubated for 15 min while rotating at RT. Retinas were finally washed twice with PBSA for 10 min each. Retinas were mounted onto cover slides using MOWIOL and stored at 4°C.

7.1.6 Blood Pressure Measurements

BP of the control and DKO mice was determined using implantable telemetric transmitters (DSI, TA11PA-C10). Firstly the mice must weigh a minimum of 27 g before the catheter of the transmitter is inserted into the left carotid artery. Data was set to record every 30 min for 180 s and this lasted for 7 days per treatment. The first recordings are performed 7 days after implantation of transmitter to allow the mice time to recover after the surgery and reach basal levels.

Two different chemical compounds we used to invest potential alterations in BP were Captopril and L-NAME at a concentration of 600 µg/mL and 500 µg/mL, respectively. These compounds will be administered by dissolving them in the drinking water where the mice drank them *ad libitum,* as a non-invasive method. The water was changed on a daily basis to ensure the chemicals were still present and effective. One week's period was given between each treatment to make sure the mice had recovered and returned to their normal basal levels before the next set of measurements.

Data was sampled with Dataquest A.R.T. 4.0 with a sample rate of 500 Hz and with a filter cut-off of 100 Hz. Data reduction is performed by Dataquest A.R.T. 4.0 by calculating the reduced mean for the sampled signals. From these devices diastolic, systolic, pulse pressure (PP), activity, BP and HR were measured. The mean of these values were then calculated separately for day- and night-time.

7.2 Molecular Biology

7.2.1 Genomic tail and tissue DNA Isolation

Tail cuts or small pieces of embryonic tissue were digested in 500 µl TENS Buffer (100 mM EDTA pH 8.0, 100 mM NaCl, 50 mM Tris-hydrochloric acid (HCl) pH 8.0 and 1 %

SDS), together with 200 µg/mL Proteinase K at 56°C O/N. The next day, the samples were spun at 12,000 x g for 10 min and 500 µl Isopropanol was then added to precipitate the DNA. Samples were left to stand for 10 min before being centrifuged again at 12,000 x g for 15 min. The DNA pellet was then washed with 700 µl 70 % Ethanol (EtOH) and centrifuged further. The pellet was then let dry for 5-10 min before adding 100 µl of ddH_2O. To elute and re-suspend the DNA, the samples were left to shake O/N at 56°C. This extracted DNA was then used for genotyping.

7.2.2 Polymerase Chain Reaction and Genotyping Protocols

Polymerase chain reaction (PCR) was performed to determine mice genotypes as well as determining optimal primer conditions. For each setup PCR buffer (20 mM Tris/HCl pH 8.4, 50 mM KCl), 2 mM $MgCl_2$, 10 mM dNTP´s (0.2 mM per nucleotide), 10 mM forward primer, 10 mM reverse primer and 0.2 units Taq DNA-polymerase were added to 1 µl genomic DNA. The total volume of each reaction was 25 µL and the difference in volume was made using ddH_2O. The primers (Table 5) and protocols (Table 6) used for each genotype are mentioned below.

Table 5: Mouse genotyping primers

Genotype	Forward Primer	Reverse Primer
Apelin Mutant	ATG TCT GGG TGT AGG TCC ATA AAG G	GAC AGT TTC TCT AAC TCA AAG GGC C
Apelin Wild Type	ATG TCT GGG TGT AGG TCC ATA AAG G	GCT TCC TTC TTC TAG TCC TGT TCC A
BMP10	AAC AGG CCC GCA TCA TTT AT	TGG CCC AGG GGC CTA TTC TTT G
BMP9 Mutant	CTG TGG TCC ACC AGG ATA CG	ACA CCG GGA TTC TCC CAA TC
BMP9 Wild Type	GTC ACT GTT CCC CCA CTA GC	GAA AGG GGA AGT CCT CCG TG
General Cre	CCA GGC TAA GTG CCT TCT CTA CA	AAT GCT TCT GTC CGT TTG CCG GT

Table 6: Specific genotyping protocols

Apelin	BMP10	BMP9 Mutant	BMP9 Wild Type	General Cre
94°C – 5 min	95°C – 5 min	95°C – 5 min	95°C – 5 min	95°C – 4 min
94°C – 10 s	95°C – 30 s	95°C – 30 s	95°C – 30 s	95°C – 1 min
58°C – 10 s	58°C – 30 s	50°C – 30 s	65°C – 30 s	67°C – 1 min
72° - 40 s	72°C – 1 min	72°C – 45 s	72°C – 40 s	72°C – 1 min
Go to 2 repeat 40x	Go to 2 repeat 40x	Go to 2 repeat 35x	Go to 2 repeat 35x	Go to 2 repeat 30x
72°C – 5 min	72°C – 5 min	72°C – 5 min	72°C – 5 min	72°C – 10 min
4°C - ∞	4°C - ∞	4°C - ∞	4°C - ∞	4°C - ∞

7.2.3 RNA isolation

Trizol (Invitrogen) was used to extract RNA from both tissue and cells in accordance with manufacture's protocol. To obtain homogenous tissue samples, the samples were ground with sterile steel balls and then processed using a tissue homogeniser.

Tissue samples were normally suspended in 1 mL Trizol, whereas cells collected from smaller plates were placed in 500 µL Trizol (in this case the other components volume though out the protocol were also halved). 200 µl of chloroform was added to allow for separation of RNA from unwanted components such as, proteins. The samples were centrifuged at 4°C for 5 min at 12,000 x g. Once each aqueous phase had been separated clearly the top layer containing the RNA was removed and placed in 500 µL of cold Isopropanol. The samples were mixed and left on ice for 5-15 min to allow for the RNA to precipitate. Samples were centrifuged at 12,000 x g for 15 min, the pellet was collected, supernatant removed and the pellet was washed twice with 1 mL 75 % EtOH. After the samples had been washed they were dried carefully, so as not to dry out the pellet, and the pellets were then resuspended firstly in 25 µL of DEPC water (0.1 % v/v DEPC in ddH_2O). DEPC is used because it inactivates RNAses and autoclaving before it's used is necessary to deactivate the DEPC. To determine the concentration of each sample, a Nanodrop photospectrometer was used.

7.2.4 Reverse Transcription and (semi)Quantitative Reverse Transcription PCR

For Quantitative Reverse Transcription PCR (qRT-PCR), reverse transcription of RNA into cDNA is first needed. RT-PCR was performed using the Superscript II kit according to the manufacture's protocol.

To begin 1 µg, in a total of 10 µL DEPC H_2O, of isolated RNA was incubated with 1 µL $Oligo(dT)_{T15}$ and 1 µL 10 mM dNTP at 65°C for 5 min. Samples were then put on ice and in each sample a mixture was added. This mixture contained 4 µL 5x First strand buffer, 2 µL 1 M DTT, 1 µL RNAsin and 1 µL SuperScript™ II reverse transcriptase. The samples were then heated at 42°C for 60 min and then at 70°C for 15 min. Samples were then put on ice and then diluted at 1:4 using ddH_2O.

To be able to measure the differences in differential gene expression, SYBR®Green I (Thermo Fisher) was used, and RT-PCRs were performed using a iCycler Multicolor Real Time PCR machines. The setup up used was according to manufacturing suggestions with the majority of PCRs run at an annealing temperature of 60°C. All setups used 25 µL

reaction mix which contained 5.5 µL ddH_2O, 12.5 µL 2x SYBR®Green, 1 µL 2.5 mM primers, both forward and reverse, and 5 µL of cDNA that had been further diluted at 1:10.

To calculate the relative expression of each sample, the cT values quantified by the PCR machine were used. Samples then had to be individually normalised by using the expression of the housekeeping genes, such as acidic ribosomal protein (Arp) for the mice samples or Glyceraldehyde-3-Phosphate Dehydrogenase (GAPDH) for the human samples.

Table 7: qRT-PCR protocol

Temperature (°C)	Duration (s)	Cycles
95	30	
95	07	
60	20	max. 40
72	03	
50	10	100 (+0.5 °C per step)

Table 8: qRT-PCR primers

Gene Name	Species	Forward	Reverse
ALK1	Mouse	GAG GAT TAC AGG CCA CCT TTC	GGA TTG TGA CTG AGC TTC TGC
ANP	Mouse	GGA TTT CAA GAA CCT GCT AG	TGC TTT TCA AGA GGG CAG AT
αSMA	All	GTG CTA TGT CGC TCT GGA CTT TGA	ATG AAA GAT GGC TGG AAG AGG GTC
APLN	Mouse	GAG GAA ATT TCG CAG ACA GC	GGG ACC ATC AGC AGC TAG AA
APLN	Human	AAG GGA CCC ATG CCT TTC	CAC TGG TGG CTA CAG CAG GT
APLNR	Mouse	TGG CCA CAG CAG TCT TAT GG	AGG TCA CTA CAA GCA CCA CG
APLNR	Human	CCT GCA TCA GCT ACG TCA ACA	GGG ATG GAT TTC TCG TGC ATC T
ARP	Mouse	AAG CGC GTC CTG GCA TTG TCT	CCG CAG GGG CAG CAG TGG T
BMP10	Mouse	GCT AAC ATC ATC CGG AGC TTC	CTC TGT TGA TAC TAA GAC CAG C
BMP9	Mouse	CTC CCA GGA CAA AAC CAG AG	TGT GCT TCT GAA AGG GGA AG
BNP	Mouse	GCA ATT CAA GAT GCA GAA GC	AAG AGA CCC AGG CAG AGT CA
CCNA2	Mouse	GCC TTC ACT CAT TGC TGG AG	TGA CTG TTG GGC ATG TTG TG
CD34	Mouse	GGT AGC TCT CTG CCT GAT GAG	TGG TAG GAA CTG ATG GGG ATA TT
CD34	Human	GCA AGC CAC CAG AGC TAT TC	TGC ATG TGC AGA CTC CTT TC
GAPDH	All	ACC ACA GTC CAT GCC ATC AC	CAT GCC AGT GAG CTT CCC GT
HEY1	Human	TGC GGA CGA GAA TGG AAA CTT GAG	CGG CTT TTT CTA GCT TAG CAG ATC CCT
PECAM	Mouse	AGT GAC AGC GGG GAG TAC AG	TAC TGG GCT TCG AGA GCA TT

7.2.5 Gene Array Protocol

The gene array was performed according to the manufacture's manual from Affymetrix.

7.3 Biochemistry

7.3.1 Protein isolation from tissue

Samples, which had been snap frozen and kept at -80°C, were crushed using a chilled mortar and pestle and were ground into a fine powder. The fine sample powder was then added to a new tube and 300 µL protein extraction buffer (0.1 M Tris/HCl pH 8.0, 0.01 M EDTA, 10 % SDS and protease and phosphatase inhibitors 4 µg/mL aprotinin, 500 µg/mL benzamidine, 4 µg/mL leupeptin, 1 mM Na_3VO_4, 20 mM NaF and 2 mM PMSF) was added.

The samples were then sonicated for 20 s for 5 cycles and afterwards were centrifuged. At this stage samples should not be viscous. If that was the case, more sample buffer was added and samples were again sonicated.

To determine the concentration of the samples, to allow for equal loading on a Western Blot, a small amount of sample was removed and a Bio-Rad assay was performed.

Before loading onto a gel, 0.04 M DTT was added to the samples. The samples were then heated at 98°C for 5 min and then centrifuged before loading. Samples could be stored at -20°C or -80°C for long term storage.

7.3.2 Protein isolation from cell culture

Adherent cells were washed once in PBS and protein extraction buffer was added. The samples were scrapped into a new tube, sonicated and centrifuged for 10 min at 20,000 x g. The supernatant was placed into a new tube, 0.04 M DTT was added and the samples were incubated at 98°C for 5 min and centrifuged again before use.

7.3.3 Protein concentration measurement

To measure the protein concentration of each sample, the DC™ protein kit (BioRad) was used. A standard curve was prepared by using known, different concentrations of

bovine serum albumin (BSA). The samples were prepared according to the company's protocol. The samples were then measured by using the Flurostar and the concentration could be measured via an absorption measurement at 750 nm.

7.3.4 Sodium Dodecyl Sulfate-Polyacrylamide Gel Electrophoresis

Gels for sodium dodecyl sulfate-polyacrylamide gel electrophoresis (SDS-PAGE) were self-made according to Table 9 below. To begin an empty 1 mm gel chamber was filled three quarters fill with the resolving gel mixture and left for about 30-40 min until they had set. Once dry the chamber was then filled with the stacking gel and a comb was inserted at the top of the chamber. When the stacking gel had set the complete gel could then be used for gel electrophoresis. The chamber was then fixed into a western blot chamber, SDS running buffer was poured in (2.5 mM MES, 2.5 mM Tris, 0.05 % SDS, 50 mM EDTA) and the prepared protein samples were loaded. At the beginning electrophoresis was at 60 volts (V) until the samples had passed though the stacking gel and then the volts were increased to 140 V until the samples were separated accordingly.

Table 9: Resolving and stacking gel for SDS-PAGE

Resolving Gel (10 mL)					**Stacking Gel (10 mL)**	
Components	8 %	10 %	12 %	15 %	Components	5 %
Water	4.60	4.00	3.30	2.30	Water	6.80
30 % acryl-bisacrylamide	2.70	3.30	4.00	5.00	30% acryl-bisacrylamide	1.70
1.5 M Tris-HCl (pH 8.8)	2.50	2.50	2.50	2.50	1.5M Tris-HCl (pH 8.6)	1.25
10 % SDS	0.1	0.1	0.1	0.1	10% SDS	0.1
10 % APS	0.1	0.1	0.1	0.1	10% APS	0.1
TEMED	0.006	0.004	0.004	0.004	TEMED	0.01

7.3.5 Western Blot Image Processing and Analysis

Wet transfer was used to transfer the proteins from the gel onto a nitrocellulose membrane. The transfer chamber was lined with sponges that had been soaked in transfer buffer (12.5 mM Bicine, 12.5 mM Bis-Tris, 0.8 mM EDTA, 20 % Methanol). Next Whatman filter paper was placed followed by the gel and then the membrane. Lastly another Whatman filter paper and then soaked sponges were added. This chamber was loaded and filled with transfer buffer and run at 30 V for 2 h. To check for equal loading and a proper transfer, the blots were later stained with *Ponceau* S *red* staining solution.

To stain the membrane for the specific antibody, the membrane was firstly blocked with 5% skim milk powder in TBST at 4°C O/N. This was followed by the primary incubation step at RT for approximately 5 h with the first required antibody (Table 10). Next the

membrane had to be incubated with a horse-radish-peroxidase (HRP-) coupled secondary antibody (Table 10). If it was necessary to use a membrane twice for the detection of two different proteins, then the membranes were stripped with Restore™ PLUS Western Blot Stripping Buffer (Thermo Scientific, 46430) for 10 min and then washed 3 times with TBST (20 mM Tris, 140 mM NaCl, 0.1 % Tween-20) and blocked again O/N using 5 % skim milk powder in TBST at 4°C before the next antibody was used.

To detect the protein signal, chemiluminescence was used with the SuperSignal™ Femto kit (Pierce) and imaged using a VersaDoc™ 3000 Imaging system. To quantify the protein signal, the software “Quantity One” was used.

Table 10 Antibodies and working dilutions used for western blotting

Name	Dilution	IgG	Source
Actin	1:1000	rabbit	Sigma, A2668
ANP	1:1000	rabbit	Novus Biologicals, NBP2-14873
pSMAD1/5/8	1:1000	rabbit	Cell Signalling Technology, 9511
pSMAD2	1:1000	rabbit	Cell Signalling Technology, 3101
α-rabbit (HRP)	1:300	goat	Pierce, 31460

7.4 Histochemistry

7.4.1 Cryosectioning and Paraffin Sectioning

For immunohistological analysis cryosectioning was performed. To prepare for cryosectioning tissues were fixed by O/N incubation in 4 % PFA/PBS. They were then transferred into 15 % sucrose/PBS O/N and then 30 % sucrose/PBS O/N respectively. Samples were then placed into moulds and embedded in Tissue-Tek® O.C.T. Polyfreeze™, and frozen using dry ice. Samples were kept long term at -80°C. Sections were made using a cryostat-microtome (Leica) and sectioning was performed at between -20 and -25°C. The cryostat was set to cut at a thickness of 8 µm. The sections were placed on microscope slides and stored at -20°C.

Paraffin sections were used for histochemical staining. To prepare organs for paraffin sectioning, the mice were first perfused with PBS and then secondly with 4 % PFA. The organs were excised from the mouse and kept O/N at 4°C in 4 % PFA. Next they were washed twice in 1x PBS and then added to 70 % EtOH O/N at 4°C. Following this they were put into 80 % EtOH followed by 90 % EtOH and twice 100 % EtOH for 2 h at each point at RT. Next the samples were put into isopropanol O/N at RT and then were placed in a 1:1 mixture of isopropanol/Paraffin O/N at 65°C. The samples were left in 100 % Paraffin at

65°C all day and then were placed in a vacuum oven at 65°C for 2 h. After this the samples could then be embedded. Sections were performed on a Leica RM2125RT microtome at RT. and samples were placed in a water bath at 42°C before putting them on a slide. Slides were dried O/N on a hot plate at 42°C and sections were then kept at RT.

7.4.2 Hematoxylin and Eosin Staining

Firstly the paraffin sections had to be deparaffinized by placing the samples twice in Xylol for 5 min each time. The samples were then passed through 100 % EtOH, 90 % EtOH, 80 % EtOH and 70 % EtOH for 2 min each time. The sections were then placed in ddH_20 for 2 min followed by Meyer's Hematoxylin for 10 min. Next the sections were twice dipped and quickly passed through ddH_20 before being put into normal, running water for 10 min. Samples were then dipped 10 times in HCl and again placed into normal water for 10 min. Samples were added to Eosin for 10 min and the sections passed through 70 %, 80 % and 90 % EtOH. Samples were left for 10 min in 100 % EtOH and xylol twice for 5 min each time. The slides were mounted using Entellan.

7.4.3 Masson's Trichrome Staining

Paraffin sections were deparaffinised by placing the samples twice in Xylol for 5 min each time and then by passing them through 100 % EtOH, 90 % EtOH, 80 % EtOH and 70 % EtOH for 2 min each time. The slides were placed in ddH_2O for 2 min before they were placed into preheated Bouin's Solution at 56°C. They were left in the Bouin's solution at 56°C for 15 min. The slides were washed in running tap water for 20-25 min until the yellow colour was removed as much as possible.

The slides were rinsed in ddH_2O briefly before they were put into Mayer's Hematoxylin for 5min. Again the sections were rinsed in running tap water for 5 min and then dipped briefly in ddH_2O. The sections were then stained in Biebrich Scarlet-Acid Fuchsin solution for 5 min and rinsed again briefly in ddH_2O. A solution with Phosphotungstic/Phosphomolybdic acid/ ddH_2O at a ratio of 1:1:2, respectively, was prepared and the slides were placed in the solution for 5 min. Next the slides were further stained by adding them to Anilin Blue solution for 5 min. The slides were added to 1 % Acetic Acid for 2 min and then washed in ddH_2O before they were dehydrated. Dehydration of the slides was performed by dipping the sections in 96 % EtOH and then placing them in twice in 100 % EtOH for 2 min each time. Slides were then placed in Xylol twice for 10 min each time and then mounted with Entellan.

7.4.4 Toluidine Blue Staining

Firstly 0.1 g of toluidine blue powder was dissolved in 100 mL of water and filtered. Sections were then stained for 2-3 minutes with toluidine blue dye and washed 3 times in water before mounting with Mowiol.

7.4.5 Immunoflurosecence Antibody Staining

Sections were fixed using 4 % PFA for 15 min and to permeabilize 0.2 % Trition X-100 in PBS was added for 5min. Sections were washed three times in PBS before they were incubated for 1 h with Blocking Solution (5 % FCS, 1 % BSA, 1x Gold Buffer [20 mM Tris, 0.155 M NaCl, 2 mM EGTA, 2 mM $MgCl_2$ at pH 7.5]) at RT. After blocking, the primary antibody (Table 11) was diluted in 1 % BSA and 1x Gold Buffer and incubated O.N. at 4°C. Following that the sections were washed 3 times in PBS and incubated with the correct corresponding secondary antibody in 1 % BSA/1x Gold Buffer at RT. for 1 h. Slides were again washed 3 times in PBS and mounted using a glass cover and Mowiol. Sections were left to dry O.N. and then stored at 4°C.

Table 11 Antibodies and working dilutions used for immunofluorescence

Name	Dilution	IgG	Source
αSMA	1:1000	Mouse	Sigma, C6198
ERG1/2/3	1:1000	Rabbit	Santa Cruz, sc-353
Ki-67	1:1000	Rabbit	Abcam, ab15580
MF20	1:50	Mouse	Hybridoma Bank, MF 20
PECAM	1:500	Rabbit	Abcam, ab28364

7.4.6 Electron Microscopy

Mice were perfused and the tissues were fixated in fixation buffer (1.5 % Glutaraldehyde and 1.5 % Paraformaldehyde in 0.15 M HEPES Buffer at pH 7.3) for 24 h at 4°C. The tissue was that contrasted using 1 % osmium tetroxide followed by washing in distilled water and embedded in hypoxic resin. Next the samples were contrasted using uranyl acetate and dehydrated by placing the samples in an increasing percentage of alcohol. Finally the samples were embedded in agar100 and ultra-thin slices were made with an ultra cyrotome and analysis was performed using a transmission electron microscope (TEM, Zeiss EM 902).

7.5 Cell Culture

7.5.1 Adult Mouse Cardiomyocyte Isolation

The adult CM Isolation protocol was based and modified from a previous publication [161]. To begin the mice were killed and the hearts were directly removed from them. In the aorta a cannula was placed and fixed to allow for perfusion and finally was arrested and then perused with approximately 20 mL Calcium-Free Buffer (113 mM NaCl, 4.7 mM KCl, 0.6 mM KH_2PO_4, 0.6 mM Na_2HPO_4, 1.2 mM $MgSO_4x7H_20$, 12 mM $NaHCO_3$, 10 mM $KHCO_3$, 10 mM Hepes, 30 mM Tarin, 10 mM 2,3-Butanedionemonoxime, 5.5 mM Glucose). To dissociate the CMs, 20 mL Enzyme Buffer (0.25 mg/mL Liberase DH, 0.14 mg/mL Trypsin, 12.5 µM $CaCl_2$) was used. The heart turned pale and swelled slightly to indicate that perfusion was carried out properly and was complete. The aorta was then removed from the heart and then the ventricles were separated from the rest of the heart and chopped into small pieces. These small ventricle pieces were then added to 5 mL Stop Buffer 1 (Enzyme Buffer, 10 % FCS, 12.5 µM $CaCl_2$). The pieces were continuously resupsended by pipetting up and down with a wide-mouth pipette. The cell suspension was then moved into a 50 mL falcon tube and the cells were allowed to settle down to the bottom of the tube. The supernatant was removed and placed into a new tube which was then centrifuged for 1 min at 300 x g. Both pellets, one from the cells that has settled and two from the cells that had been spun down, were then resuspended in 5 mL of Stop Buffer 2 (Enzyme Buffer, 5 % FCS, 12.5 µM $CaCl_2$), combined and then filtered using a 100 µm cell strainer.

An important note to remember was to keep the Ca^{2+} levels at a final concentration of 1 mM. Again the samples were centrifuged for 1 min at 300 x g and the supernatant was finally removed, leaving the CMs in the pellet. The CMs were resuspended in the appropriate cell culture medium (M199 medium from Gibco, 5 mM Creatinine, 2 mM L-carnitine in HCl, 5 mM Taurin, 25 mM Hepes, 1% Penicillin/streptomycin, 5 % FCS, 1 % Its supplement from Sigma) and then plated on laminin-coated slides. They were left to attach for 4 h and then were fixed and stained with MF20 and DAPI (Table 11). Adult CMs were then analysed, firstly by taking images on a Zeiss Z.1 Axio Imager 2 microscope and then the area of 200 CMs was calculated using ImageJ.

7.5.2 Adult Mouse Smooth Muscle Cell Extraction, Culturing and Stimulation

A 6 well plate should be coated in 1% Gelatin for at least 30min before plating the cells. For mice to be able to plate 1 well in a 6 well plate, between 6-8 mice were needed at approximately 8-10 weeks of age. Mice were killed via CO_2 as cervical dislocation could

destroy the aorta. Once the mice were dead the aorta was removed and put into a dish with ice cold HBSS. The adventitia was removed by using two serrated bent forceps and by gently pulling it away from the aorta. Each aorta was then immersed and gently moved through 70 % EtOH for 2-3sec. The aortas were then washed three times in HBSS before mincing them into small pieces. The aortas were then digestion according to the following instructions three times. Firstly they were digested in 10ml Digestion Buffer (1 mg/ml Collagenase, 0.5 mg/ml Soybean trypsin inhibitor, 0.3 mg/ml BSA) for 40-60 min in a shaking water bath at 37°C. Every 15-20min the pieces were pipetted a number of times to ensure no clumps formed and to allow for more efficient digestion. After each digestion step, the pieces were let settle to the bottom of the flask and the supernatant was centrifuged at 120xg for 5min. Then 10ml new Digestion Buffer was added to the cell pieces and the second digestion step was carried out while the cell pellet was then resuspended in SMC medium (Glutamax (Invitrogen, 10569010), 1 % P/S, 10 % FCS, 10 % mouse serum, 0.5 % Amphotericin) and plated into one gelatin coated well. This process was carried out three times and on the third time the supernatant was passed through a 100 µm filter before plating and all cell mixtures were combined in 1 well. The cells were then left untouched for one week before the first medium change was performed.

To starve these mouse SMCs the media had to be switched down over a couple of days. Firstly in the morning of the first day the medium was changed to Glutamax with 2% FCS and 2 % mouse serum and then in the evening the media was again changed to Glutamax plus 2 % FCS. The next day the medium was exchanged for Glutamax without any serum and then finally the next day the cells were stimulated in Glutamax without any serum.

Cells were stimulated with BMP9 (R&D 5566-BP-010) or BMP10 (R&D 6038-BP) or both together, at 1 ng/mL and 25 ng/mL respectively.

7.5.3 Adult Rat Smooth Muscle Cell Extraction, Culturing and Stimulation

Rat smooth muscles cells (rSMCs) were isolated according to the protocol described by Owens et al [162]. A 60 mm plate was coated in 1 % Gelatin for at least 30min before plating the cells. 4-5 Sprague-Dawley rats approximately 150-175 g in weight were used. Rats were killed via CO_2 and the aortas were put into a dish of M199 media (ThermoFischer, 12340-030) containing 1 % P/S. The loose fat and connective tissue was gently removed from the aorta and was then placed in a new dish with M199 and 1 % P/S. The aortas were placed in the enzyme solution (25 ml per 5 aortas, 1 mg/ml Collagenase II, 1 mg/ml Soybean trypsin inhibitor, 0.25 mg/ml Elastase and 1 % P/S made up to 25 ml Hank's HBSS at a pH

of 7.2) and preincubated for 20 min at 37 °C. Aortas were then placed into M199 and 1 % P/S and the enzyme solution was rinsed away and then the adventitia was removed from the media. A longitudinal incision was made along the aortas where pieces with adventitia still attached were removed and the intimal surface of the aorta was gently scraped. The aortas were rinsed to wash off the intimal cells and then placed in the above enzyme solution and cut up into small pieces and then incubated at 37 °C for 1 h. Free cells were collected and rinsed in M199 and 1 % P/S to remove the excess enzyme solution and then passed through a filter for plating. Media containing 10 % FBS is needed to inactivate the enzyme solution and the cells are then centrifuged, counted and plated according to the needed cell density. Media should be changed after about a week and cells shouldn't be passaged until cells are subconfluent to allow for proper cell growth and expansion. Cells were grown in SMC growth medium plus supplements (Provitro, 200 0601 – prf) containing 1 % P/S and 0.1 % Amphotericin-B (rSMC media). For splitting and before stimulation the smooth cells were kept in a media mixture at a 1:1 ratio of rSMC growth media and Media199 with 1 % P/S, 10 mM HEPES, 0.1 % Amphotericin-B and 10 % FBS.

To starve rat SMCs the medium is changed to Medium 199 and 10 % FBS on the first day, the next day the medium is changed to Medium 199 without FBS and the following day the cells were stimulated in Medium 199 only. They were stimulated with BMP9 (R&D 5566-BP-010) or BMP10 (R&D 6038-BP) or BMP9 and BMP10 together, at a concentration of 1 ng/mL and 25 ng/mL respectively or with Apelin-13 (Bachem, H-4568) at 1mM and FGF2 at 20ng/mL used as a positive control. When rSMCs were directly stimulated with BMP9 and BMP10 they were stimulated after starvation O/N in M199 or M199 with 1 % FCS.

7.5.4 Smooth Muscle Cell Proliferation and Migration Assay

To determine the effects of BMP9, BMP10 and Apelin (APLN) on rSMC proliferation, cells were plated at a density of 5,000 cells in a 96 well plate. To test for cellular proliferation an MTT assay (Vybrant® MTT Cell Proliferation Assay Kit, ThermoFisher V13154) was used and performed according to the company's manual. The medium from the cells was removed and replaced it with 100 µL of fresh starvation medium. A stock solution of 12 mM MTT had been made and 10 µL was added to each well. As a negative control 10 µL of the MTT stock solution was added to 100 µL of the starvation medium alone. The cells were incubated at 37°C for 4 h. Next 100 µL of the SDS-HCl solution was added to each well and mix thoroughly. The cells were further incubated at 37 °C for 4 h before each sample was mixed the absorbance read at 570 nm.

To understand the migratory effects these different compounds have on rSMCs, the cells were first plated in a 24 well plate and let grow till fully confluent. The cells then underwent the starvation process mentioned before. When in starvation media a small scratch was made down the center of each well, the cells were then washed once or twice before starvation media containing the difference compounds being tested was added. Photos were made of the scratched area which was then taken again after 24 h of stimulation. Brightfield images were taken as were immunofluorescent pictures of Dapi stained.

7.5.5 Human Umbilical Vein Endothelial Cell Culturing and Stimulation

Human Umbilical Vein Endothelial Cell (HUVECs) were obtained from Lonza (CC-2519) were cultured in Endothelial Basal Medium (CC-3121) combined with 10% FCS and EGM™ SingleQuots™ (CC-4133), which contained growth factors, cytokines, and supplements.

Cells were plated in T75 cell culture flasks for maintenance at 37 °C and 5 % CO_2. When needed for stimulation the cells were split maximum 1:6 onto 15 cm cell culture plates. To starve the HUVECs, the media was switched to Endothelial Basal Medium without FCS and the EGM™ SingleQuots™ but just contained 0.1 % BSA for 6 h.

After HUVECS were starved for 6 h, they were stimulated with BMP9 (R&D 5566-BP-010) or BMP10 (R&D 6038-BP) or BMP9 and BMP10 together, at a concentration of 1 ng/mL and 20 ng/mL respectively. TGF-β was used at a concentration of 5 ng/mL.

Cells were stimulated for 6 h before the media was changed or cells were collected for further experiments.

7.6 Analysis Programs

7.6.1 Statistical Analysis

All graphs and data are shown as mean ± standard error (mean ± SEM). To calculate the difference between each of the groups and to determine their *P* values, the two-tailed student's t-test was performed using the statistical analysis program from GraphPad Prism version 6.07 (GraphPad Software, La Jolla California USA, www.graphpad.com). From the program the *P* values were defined as *p<0.05, **p<0.01, p***<0.001, ****p<0.0001, non-significant (ns) p>0.05.

7.6.2 Gene Ontology Term Analysis

To determine changes in global gene sets of the different arrays performed, a **G**ene **O**ntology en**RI**chment ana**L**ysis and visua**L**iz**A**tion tool (GOrilla) was used [163]. This program gave an overview into biological processes that were both up- and down-regulated when comparing DKO to WT samples or stimulated and none stimulated samples.

7.6.3 Gene Set Enrichment Analysis

Another program used to analysis gene sets from the array data was Gene Set Enrichment Analysis (GSEA) [164,165]. This program was used to give insight into global changes happening within the different gene set samples.

7.6.4 Venn Diagram Generation

To determine overlapping genes within the various gene array sets, Venn diagrams were generated using an online tool [166].

7.7 Generation of Mouse Lines

7.7.1 BMP9 SKO Line

Bmp9 (also known as GDF2) targeted ESCs were bought from EUCOMM (MGI: 1321394, project: VG10018) and upon homologous recombination the entire coding region of *Bmp9* was replaced with a lacZ cassette, resulting in targeted deletion of *Bmp9* shown in Fig. 10. These targeted ESCs were then injected into blastocysts of fertilized female mice and backcrossed for 5 generations to generate the *Bmp9*$^{-/-}$ SKO (BMP9 SKO) line.

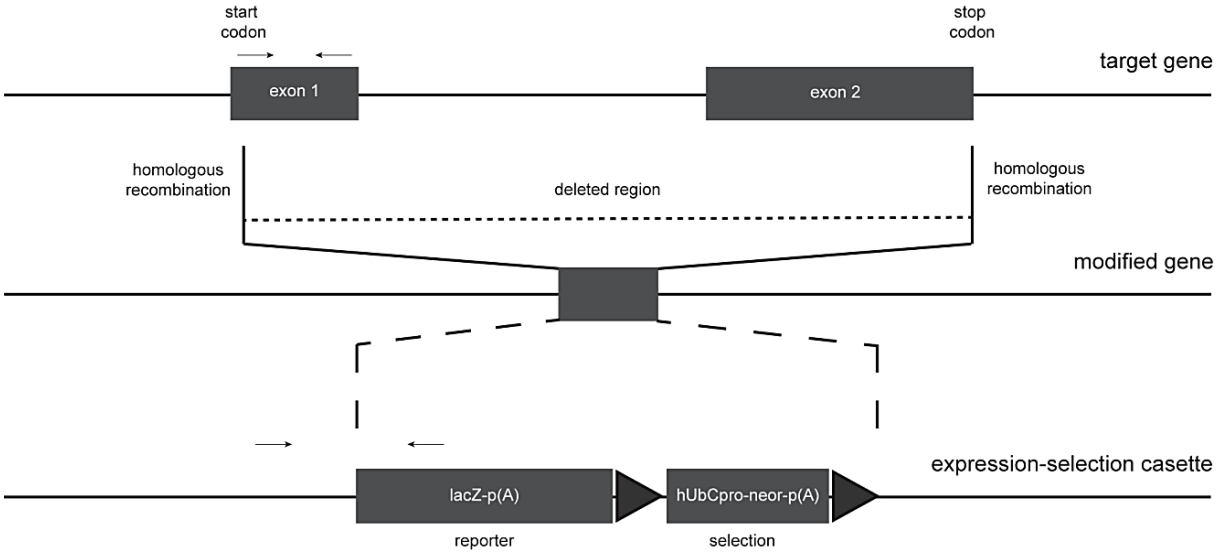

Figure 10: BMP9 SKO mouse line schematic
BMP9 was generated by inserting a cassette, containing a lacZ reporter and neo^{r} selection, into the coding region of BMP9 via homologous recombination, therefore generating a constitutive knockout mouse. Arrows indicate general location of the genotyping primers used.

7.7.2 BMP10 cKO Line

The *Bmp10* heart specific conditional knockout mice (BMP10 cKO) were generated and described by Bücker [167]. A BAC containing 61.5Kb (87339721-87401265) genomic DNA of chromosome 6 was obtained from BACPAC Resources Center (BPRC) (bMQ438f03). A 12.4 kb fragment (BamHI-HindIII) was subcloned into pKODTA vector by homologous recombination in SW102 cells. 5' and 3' recombination arms were inserted into pL451 vector containing a FRT flanked Neomycin selection cassette with a single LoxP site. The XhoI/SacII digested fragment was introduced into the first intron by recombination. For insertion of a second LoxP site, 5' and 3' recombination arms were inserted into pL452 vector containing a Neomycin selection cassette flanked by two LoxP sites. A KpnI/SacII

fragment was introduced into intron 5 by homologous recombination. For gene targeting, 20 µg of NotI-linearized BMP10 cko-targeting vector DNA was electroporated into 129/Bl6 F1 hybrid ES cells. Targeted clones were selected for neomycin resistance and were confirmed by Southern blotting (EcoRI digest: WT, 18.8 Kb; mutant, 8.9 Kb) and PCR with primers surrounding the single loxP site in the long homolog arm. The same PCR reaction was used to genotype resulting recombinant mice after injection of selected ESCs into blastocysts of fertilized female mice and backcrossed for 5 generations. To remove the neomycin cassette these mice, carrying the targeted *Bmp10* allele, were crossed with a Flp deleter mouse line. Once the neomycin cassette was removed there mice were then backcrossed for five generations to remove the Flp deleter. For heart specific conditional Cre-mediated recombination, *Bmp10*$^{fl/fl}$ mice were bred with *Nppa* Cre (also known as ANF Cre*)* transgenic mice as shown in Fig.11 [168].

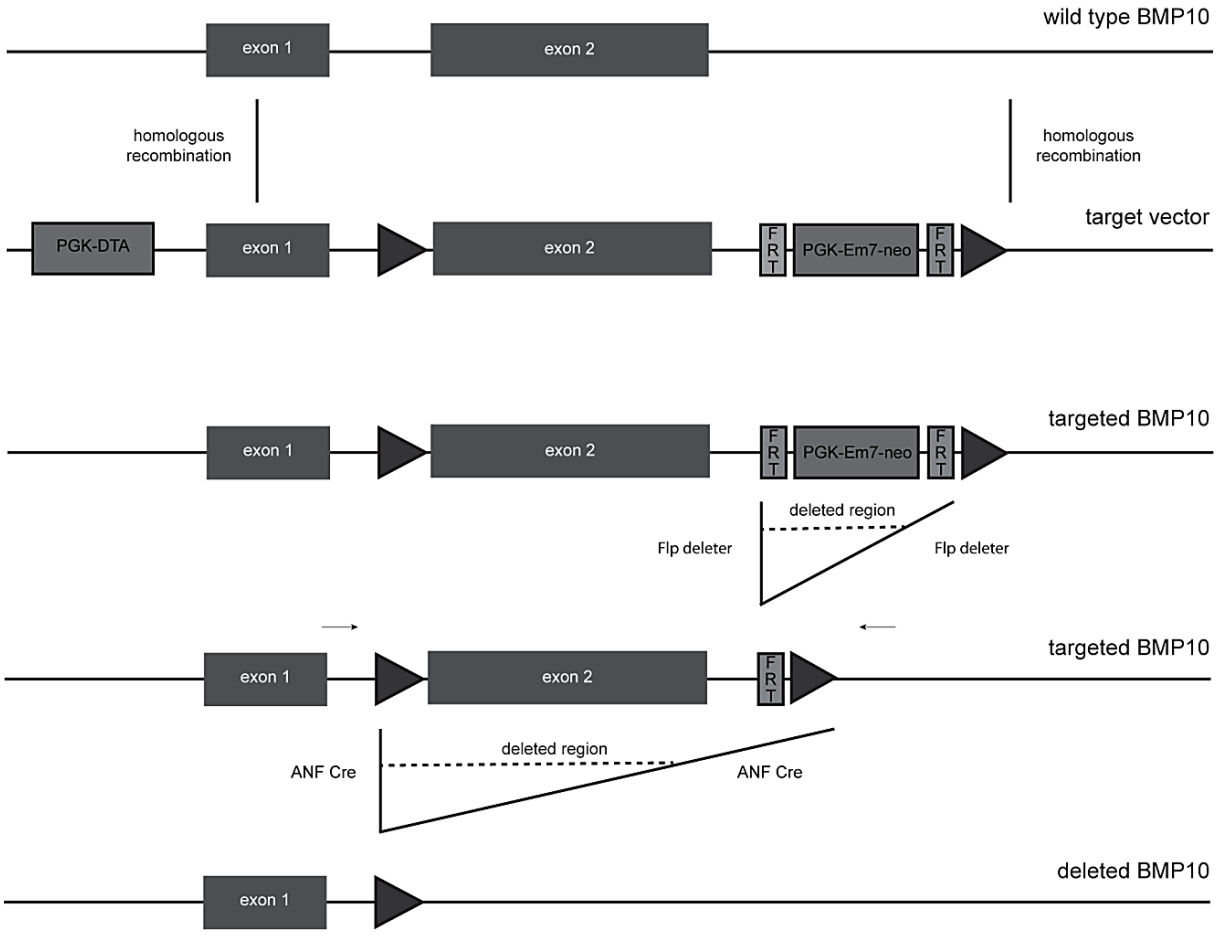

Figure 11: BMP10 cKO mouse line schematic
LoxP sites (triangles) were inserted into the area of interest via homologous recombination. These sites were excised and exon 2 of the gene was removed when in the presence of ANF Cre to give a heart specific conditional knockout line. Arrows indicate general location of the genotyping primers used.

7.7.3 BMP9 and BMP10 DKO Line

BMP9 and BMP10 DKO mice were generated by crossing *ANF-Cre^{pos}Bmp10$^{fl/fl}$* with *Bmp9$^{-/-}$* mice on a C57/BL6 background to give *ANF-Cre^{pos}Bmp10$^{fl/fl}$Bmp9$^{-/-}$* (DKO) mice. These mice were then backcrossed for 5 generations.

7.7.4 BMP9, BMP10, Apelin TKO Line

Apelin KO (*Apln$^{-/-}$*) mice described by Kuba et al [169]. To remove *Apln* a targeting vector that replaced exons 2 and 3, the complete coding area of *Apln*, was constructed using the self-excision ACN-Neo cassette as seen in Fig. 12 below. The ACN-Neo cassette contained a testis-specific ACE promoter–driven Cre recombinase and a PGK promoter–driven neomycin resistance gene which was flanked by loxP sites and in the mouse testis, the whole ACN-Neo cassette is excised through Cre-lox–mediated recombination.

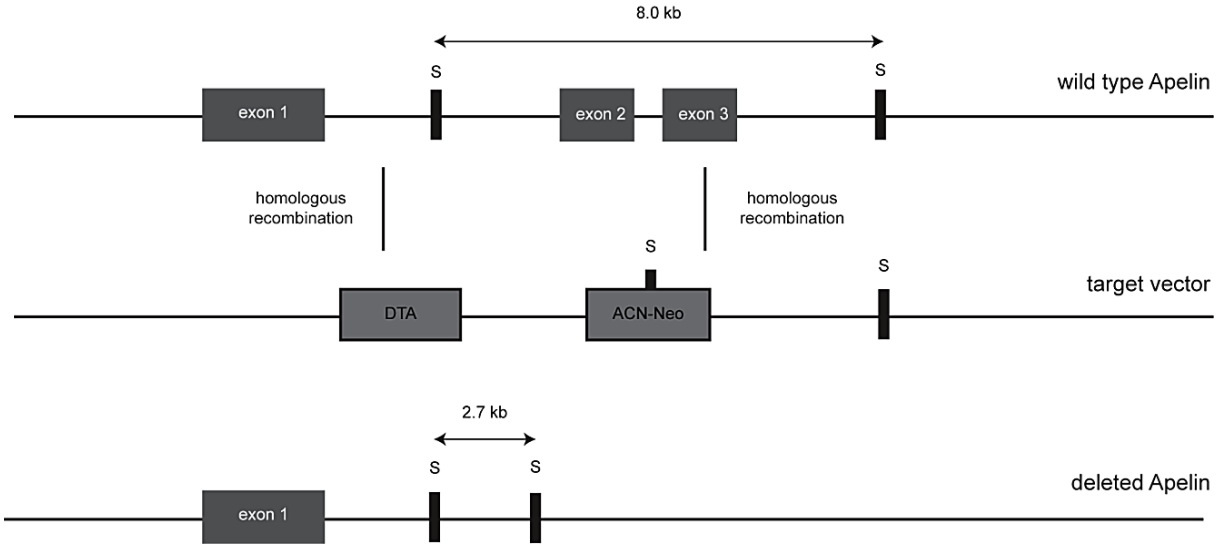

Figure 12: Apelin KO mouse line schematic
Apln coding area, exons 2 and 3 were substituted with the ACN-Neo self-excision cassette via homologous. In the testis self-excision of the ACN-Neo cassette occurred, resulting in the removal of the ACN-cassette. Diphtheria toxin A (DTA) was used as a negative-selection cassette and the *Sac*I (S) digestion sites are also shown.

Bmp9, *Bmp10*, *Apln* triple knockout (TKO) mice were generated by crossing *ANF-Cre^{pos}Bmp10$^{fl/fl}$Bmp9$^{-/-}$* mice with *Apln$^{-/y}$* males or *Apln$^{+/-}$* (Apelin heterozygous) females, resulting in *ANF-Cre^{pos}Bmp10$^{fl/fl}$Bmp9$^{-/-}$Apln$^{-/y}$* males or *ANF-Cre^{pos}Bmp10$^{fl/fl}$Bmp9$^{-/-}$Apln$^{-/-}$* females.

8 Results

8.1 Loss of BMP9 and BMP10 does not result in embryonic lethality or developmental issues

To ensure that *Bmp9* and *Bmp10* expression were depleted in their respective mouse models, qRT-PCR was used detect their expression patterns. Two different organs were analysed to ensure a systemic knockout of *Bmp9* and *Bmp10*. The liver, where *Bmp9* is secreted from, and the heart, which is *Bmp10*'s secretary organ, was analysed at 1 and 2 months of age. Results showed that at both time points *Bmp9* was clearly ablated in the liver of both BMP9 SKO mice and DKO compared to WT littermates (Fig. 13 A) and absent from the heart as expected (Fig. 13 C). *Bmp10* expression was absent in the heart of BMP10 cKO and DKO mice (Fig. 13 B) as well as the liver (Fig. 13 C). This confirms successful targeted depletion of both *Bmp9* and *Bmp10*. At 1 month of age, both SKOs and DKO mice did not display obvious postnatal growth problems, shown by their normal body weights (Fig. 13 D) and all groups survived with no noticeable problems for more than 1 year (Fig. 13 E).

Since loss of *Bmp10*, *Alk1* or *Eng*, results in embryonic lethality, it was important to determine if either SKOs or the DKO mice resulted in embryonic or postnatal lethality. Litters were counted to ensure that the number of each genotype was represented according to normal Mendelian ratios. Each breeding scheme set up is described below and showed that mice from all genotypes were born at the expected Mendelian ratios (Fig. 13 F).

Loss of *Alk1* or *Eng* leads to embryonic lethality due to severe vascular abnormalities during development. Therefore, E14.5 control and DKO embryos were collected and immunostained for PECAM and αSMA to determine the coverage of ECs and SMCs respectively. At E14.5 there was no obvious difference between PECAM and αSMA suggesting that the DKO mice do not suffer any vascular defects during embryonic development (Fig. 13 G).

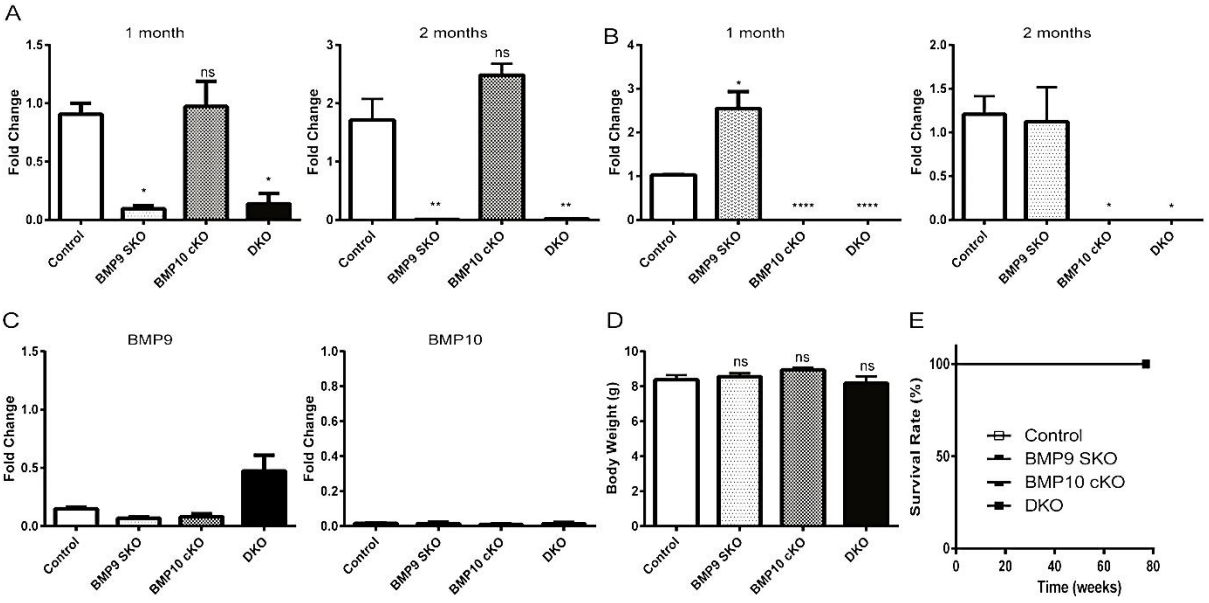

F

Parental Cross	Offspring	Expected	Observed
BMP9$^{+/-}$ x BMP9$^{+/-}$			
	BMP9$^{+/+}$	10	8
	BMP9$^{+/-}$	20	20
	BMP9$^{-/-}$	10	12
ANF-Cre^{pos}BMP10$^{fl/fl}$ x ANF-Cre^{neg}BMP10$^{fl/fl}$			
	ANF-Cre^{neg}BMP10$^{fl/fl}$	20	19
	ANF-Cre^{pos}BMP10$^{fl/fl}$	20	21
ANF-Cre^{pos}BMP10$^{fl/fl}$BMP9$^{+/-}$ x ANF-Cre^{neg}BMP10$^{fl/fl}$BMP9$^{+/-}$			
	ANF-Cre^{neg}BMP10$^{fl/fl}$BMP9$^{+/+}$	6	4
	ANF-Cre^{pos}BMP10$^{fl/fl}$BMP9$^{+/+}$	6	14
	ANF-Cre^{neg}BMP10$^{fl/fl}$BMP9$^{+/-}$	12	4
	ANF-Cre^{pos}BMP10$^{fl/fl}$BMP9$^{+/-}$	12	19
	ANF-Cre^{neg}BMP10$^{fl/fl}$BMP9$^{-/-}$	6	3
	ANF-Cre^{pos}BMP10$^{fl/fl}$BMP9$^{-/-}$	6	4
ANF-Cre^{pos}BMP10$^{fl/fl}$BMP9$^{-/-}$ x ANF-Cre^{neg}BMP10$^{fl/fl}$BMP9$^{-/-}$			
	ANF-Cre^{neg}BMP10$^{fl/fl}$BMP9$^{-/-}$	26	23
	ANF-Cre^{pos}BMP10$^{fl/fl}$BMP9$^{-/-}$	26	29

G

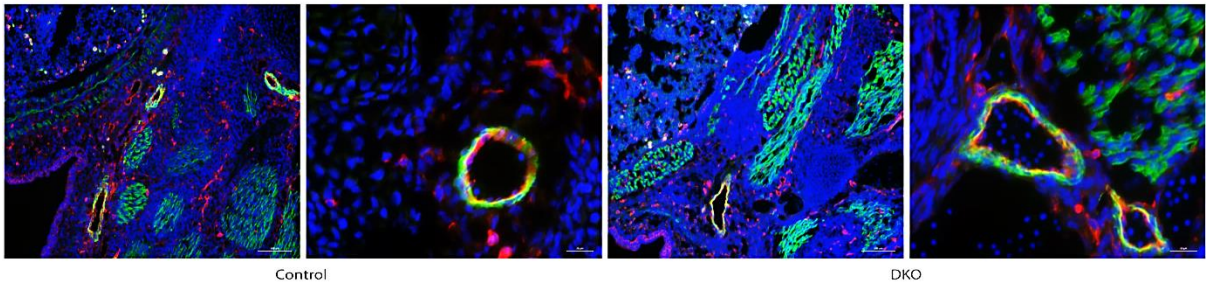

Figure 13: Loss of BMP9 and BMP10 does not lead to embryonic or postnatal lethality or vascular abnormalities during development

(A) RT-PCR shows *Bmp9* expression in the liver at 1 month (L) and 2 months (R). (B) RT-PCR shows *Bmp10* expression in the heart at 1 month (L) and 2 months (R). (C) Control RT-PCR shows specific tissue expression, where *Bmp9* and *Bmp10* are not expressed in the heart (L) and liver (R) respectively at 1 month. (D) Body weights of P21 pups reveal no difference between SKO and DKO mice compared to controls during postnatal development and (E) Survival curve showing the loss of BMP9 and 10 does not affect viability. (F) Calculations of the expected embryo Mendelian ratios also occur as expected. (G) Immunofluorescent staining's showed no vascular abnormalities at E14.5, PECAM (red), αSMA (green) and DAPI (Blue). *p<0.05, **p<0.01, ****p<0.0001, non-significant (ns) p>0.05

8.2 DKO mice develop cardiac hypertrophy and impaired cardiac function

Using MRI it is possible to determine cardiac function and structure using a number of different parameters. Each group was measured at different time points to determine if mutant mice displayed signs of age-dependent cardiac failure.

Ejection fraction (EF) is the percentage of blood pumped out of the heart with every heartbeat. Normally a low EF is used as an indicator of HF, resulting from insufficient blood volume being pumped out of the heart. Functionally, the heart has to increase its contractility which can ultimately leads to HF. MRI analysis showed that the DKO mice had a significantly lower EF at 6 months of age. This was not evident at 1 month while both SKO mouse groups did not display any significant changes in EF (Fig. 14 A). This data showed that the loss of BMP9 and BMP10 leads to reduced EF indicating impaired cardiac function.

SV is the amount of blood pumped out of the heart during each contraction and is calculated by measuring the difference between the ventricular end-diastolic volume (EDV) and the end-systolic volume (ESV). The EDV is the volume of blood in the ventricle at the end of chamber filling (diastole) and ESV is the volume of blood in the ventricle at the end of a contraction (systole). By 1 month, the DKO mice showed an increase in SV in comparison to the other groups which more than doubled in volume by 6 months of age (Fig. 14 B). This increase in SV showed an increase in blood volume in the heart and again demonstrated a change in cardiac function.

It is also possible to measure the left ventricular mass (LVM) using MRI as well as the thickness of the LV wall during both diastole and systole phases. Again, by 1 month of age, it was already clear that the LVM of the DKO mice was significantly greater than the control mice as well as both SKO mice, although they displayed a slight increase in size in comparison to the controls (Fig. 14 C). A significant two-fold increase in LVM was evident in the DKO compared to controls by 6 months whereas there was only a slight increase seen in the SKO mice (Fig. 14 C). This demonstrates that loss of BMP9 and 10 leads to cardiac hypertrophy.

This was further verified when the ventricular wall thickness was calculated in the diastole phase where an increase in thickness was already evident by 1 month in the DKO and was more pronounced at 6 months in comparison to the other groups (Fig.14 D). Dilated cardiomyopathy is a condition whereby the heart becomes enlarged and cannot pump blood efficiently which normally leads to a thinning of the ventricular wall [170]. Even though the DKO hearts were enlarged, this data clearly shows there was no sign of ventricular wall dilation,

as the wall thickness was increased in the DKO animals. Taken together, these results showed an increase in overall heart size of the DKO mice, already beginning at 1 month of age, with an increase in blood volume but an overall reduction in pumping and ejection efficiency. This overall increase in heart size, without cardiac dilation and the increase in blood volume could be an explanation as to why these DKO mice are able to survive and function normally although they have a reduction in EF.

Hearts from each group were collected at 1 and 6 months of age to visualize the difference in heart size and overall structure. Hematoxylin and Eosin Staining (H&E) staining confirmed there was an overall increase in the whole heart size at 1 month of age in the DKO mice compared to the other groups (Fig. 14 E). At 6 months the difference in heart size of the DKO mice was still significantly larger than in the other groups, consistent with the MRI analysis (Fig. 14 F). Measurement of the heart weight to the tibia length further showed the hypertrophic phenotype of the DKO mice beginning at 1 month of age which was still seen at 6 months (Fig. 14 G).

Cases of cardiac hypertrophy, even if just in specific areas, for example in the right atria due to valve stenosis or atrial septal defect, are normally correlated with cardiac dysfunction [171]. This can be a result of an increase in ECM components which restricts CM contractility. Seeing as the DKO mice display cardiac dysfunction and hypertrophy it was essential to determine the extent of cardiac fibrosis, as this could have been a reason for cardiac impairment. At 1 month and 6 months, hearts from DKO mice did not display cardiac fibrosis (Fig. 14 E). This revealed that the lower EF in the DKO mice is not due to excess fibrosis but rather due to an overall increase in size (Fig. 14 F). It was recently published that *in vitro* BMP9 acts as a profibrotic factor and so lack of BMP9 in these mutant mice could also explain why there is no increased fibrosis [172]. During HF, dilation can occur along with morphological changes such as increase in CM apoptosis and fibrosis [173]. However this situation does not occur in the DKO mice meaning they may undergo compensatory hypertrophy where fibrosis is not necessary as the CM increases in size in response to an increase in work load [173].

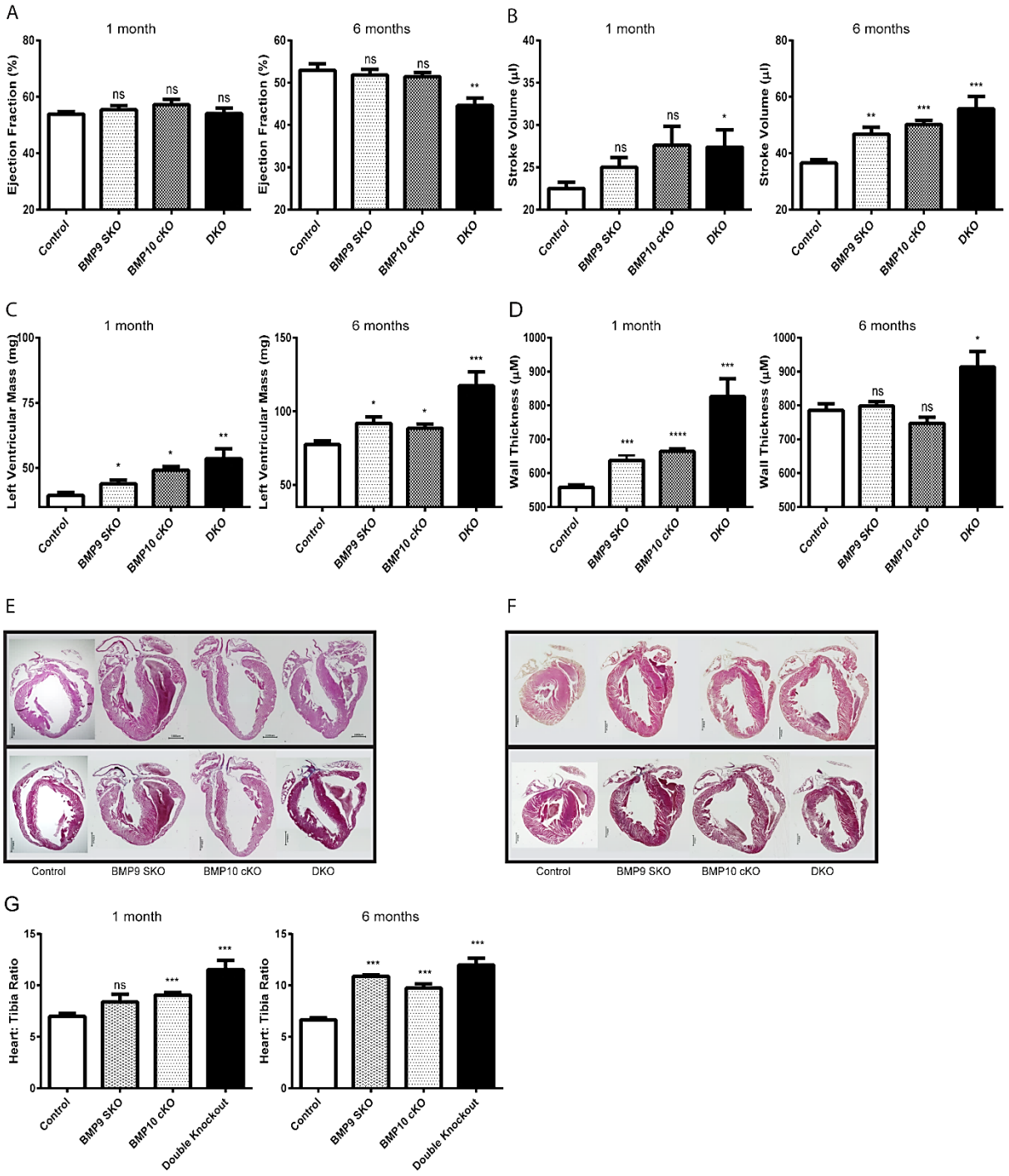

Figure 14: DKO mice display cardiac impairment with an overall increase in heart size but do not exhibit significant fibrosis

(A) The EF of each mouse group at 1 (L) and 6 (R) months shows a decrease in the DKO over time. (B) The SV of each mouse group at 1 (L) and 6 (R) months shows an increase over time. (C) The LVM of each mouse group at 1 (L) and 6 (R) months shows a major increase in size especially in the DKO. (D) The wall thickness was measured during the diastole phase at 1 (L) and 6 (R) months showing a thickening in the wall of the DKO. (E) H&E staining (top) and Trichrome (bottom) of all mouse groups at 1 month shows the overall increase in heart size of the DKO mice without the presence of fibrosis. (F) H&E (top) and Trichrome (bottom) staining of all mouse groups at 6 months show that over time there is no presence of fibrosis even though the heart increases in size. (G) The heart: tibia ratio all mouse groups at 1 (L) and 6 (R) months shows the hypertrophic nature of these DKO hearts. *p<0.05, **p<0.01, p***<0.001, ****p<0.0001, non-significant (ns) p>0.05

To determine if cardiac hypertrophy was due to an increase in size or overall number of CMs, adult CMs were isolated and the area of CMs was calculated. CMs isolated from DKO mice had a higher % of larger CMs; approximately 60 % were between 2000-3000 μm^2 (Fig. 15 A), in comparison to the control and the SKO mice, where approximately 60 % were between 1500-2000 μm^2 (Fig. 15 A). These results were further analyzed via immunofluorescence staining (Fig. 15 B) and the average size of CMs from each genotype was calculated showing that DKO CMs were significantly larger (Fig. 15 C). P5 hearts from each group, that were injected with EdU, were sectioned, stained and quantified for cellular proliferation, as EdU is a quantitate chemical that follows newly synthesized DNA via detection of the incorporation of a deoxyribonucleoside analog. EdU and DAPI positive cells were counted and compared to determine overall proliferation of cells within the heart. Analysis of these sections showed there was no significant change in proliferation in the DKO mice compared to controls (Fig. 15 D).

During HF and adverse cardiac remodelling, CMs react to stress signals by activating pathways that induce pathological hypertrophy. These changes that occur during HF and remodelling are similar to the processes seen during fetal cardiac development where CMs must grow in size. Normally the heart responds by reactivating the fetal gene program where the heart switches expression of structural proteins from the adult form back to the fetal isoforms [174]. Analysis of fetal gene expression were analysed by qRT-PCR and revealed an increase in both *Anp* (*Nppa*) and *Bnp* (*Nppb*) levels in DKO mice at 2 months as well as in the SKO mice, confirming reactivation of the fetal gene program under cardiac hypertrophy and stress (Fig. 15 E).

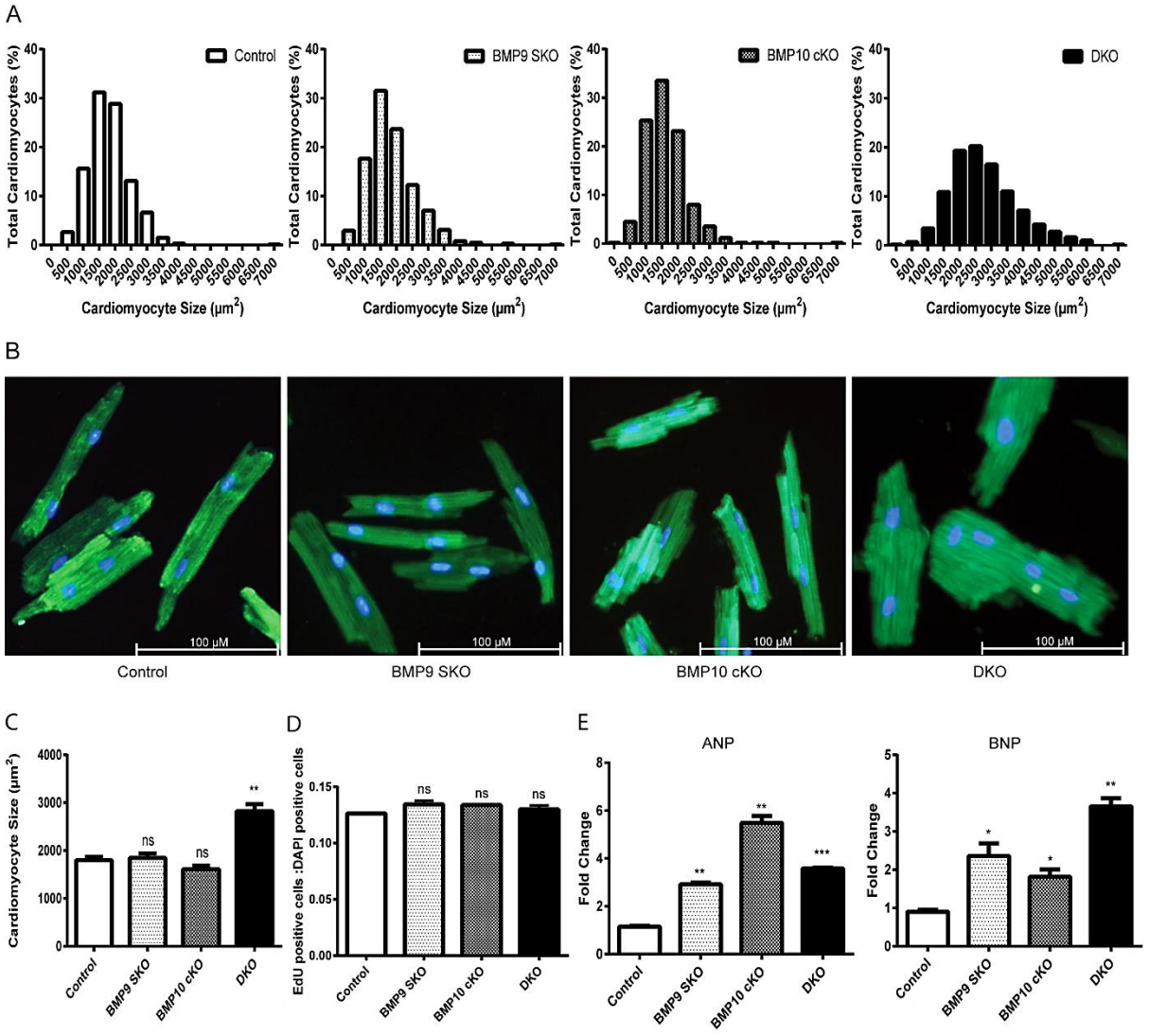

Figure 15: DKO adult CMs are larger but do not display increased proliferation
(A) Calculation of the total area of adult CMs shows a shift in the DKO CMs towards a higher percentage of larger CMs. (B) Immunofluorescent staining with MF20 (green) and DAPI (blue) demonstrate CM an increase in size of the DKO CMs compared to controls. (C) The average area of adult CMs shows the significant increase in CM size of the DKOs. (D) Analysis of proliferating adult CMs using EdU shows there is no increase in proliferating CMs in any of the groups. (E). RT-PCR for *Anp* (L) and *Bnp* (R) levels at 2 months indicates an increased hypertrophic response in the DKO hearts. *p<0.05, **p<0.01, p***<0.001, non-significant (ns) p>0.05

8.3 DKO mice show changes in vascular structure leading to changes in vascular homeostasis

As BMP9 and BMP10 are known to be involved in vascular homeostasis, µCT analysis was used to determine the vessel structure and dynamics. From the images taken it was again clear that the DKO mice were characterized by an overall increase in heart size compared to control mice (Fig. 16 A). Aside from the increase in heart size, it was shown that the DKO mice have an increase in vessel diameter of the coronary arteries (Fig. 16 B). This was determined by measuring the diameter of the main coronary artery from the aortic

valve until the first bifurcation process. This increase in vessel dilation was concomitant with an increase in the vessel volume in the DKO mice compared to controls (Fig. 16 C). Interestingly, it was also shown that there was an increase in branch numbers in the DKO mice compared to the control mice (Fig. 16 D). This increase in branch number could be due to the lack of BMP9 and BMP10, which are vascular quiescent factors, leading to a continuation of vascular expansion or due to the fact that there is an increase in vessel diameter meaning there is better perfusion for visualization.

Due to changes in vascular structure of the DKO mice it was important to determine changes in vascular hemodynamics, as changes in vascular structure will ultimately affect hemodynamic forces and vice versa, with changes in both having adverse effects on the heart. Telemetric devices were implanted into adult mice for 1 month where the basal BP was measured, as was BP in response to stimulation with vasoconstrictive or vasodilative compounds. At basal levels, DKO mice displayed significantly reduced BP compared to the controls (Fig. 16 I) however there were no changes in HR in either of the mice groups (Fig. 16 J) demonstrating bradycardia was not the cause of the hypotension seen in the DKO mice.

Captopril is an angiotensin-converting enzyme (ACE) inhibitor and is used to induce vasodilation via the angiotensin II pathway. After administration of Captopril the DKO were able to respond and further dilate resulting in a further reduction in their BP (Fig 16 H) similar to controls (Fig. 16 G). When compared with the control mice it was still clear that the DKO mice had a significantly lower BP even after Captopril administration meaning they still kept the dilated phenotype (Fig. 16 I) and this overall vessel dilation could explain the chronic hypotension seen in these DKO mice.

Nitric oxide synthases are a group of essential enzymes needed to catalyse NO production from L-arginine. NO is a cellular signalling molecule that is involved in vascular tone, angiogenesis and other important functions. NG-nitro-L-arginine methyl ester (L-NAME) has been widely used to inhibit constitutive NOS which results in vasoconstriction. When L-NAME was administered to control mice, a significant increase in BP was observed (Fig. 16 G). In contrast, there was a slight increase in BP seen in the DKO mice compared to their basal BP (Fig. 16 H). When compared with control mice, DKO mice had a significantly blunted response to L-NAME administration indicating that these mice have a defect in their SMCs to respond to signals that induce vasoconstriction (Fig. 16 I).

Another method used to determine changes in hemodynamic forces was angiography imaging as it was possible to visualize the vascular network of adult mice in the tail region and to measure the BF and BV at 6 months of age (Fig. 16 E-F). This showed a consistent and significant change in both the BF and BV in the DKO mice when compared to the control mice.

Taken together these results show an overall change in hemodynamic forces due to a systemic increase in vessel diameter. Since there was no change in heart rate, it showed that this was not the main cause of hypotension seen in the DKO mice but that it was more likely due to vasodilation. Chronic vasodilation causes the BP to drop, which was seen in the DKO mice, and a decrease in BP effects vascular resistance therefore allowing for an increase in BV and BF.

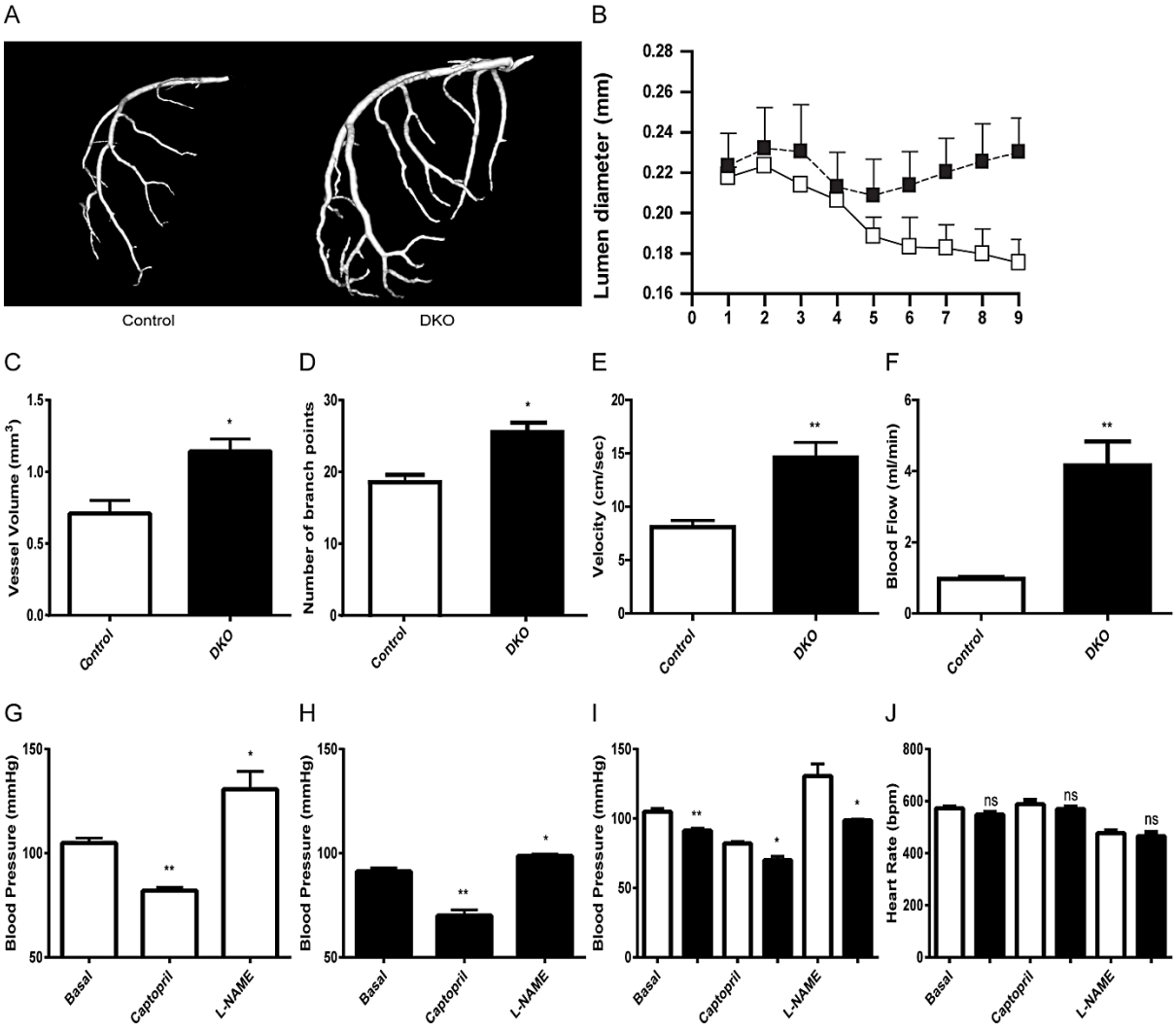

Figure 16: µCT analysis clearly shows a dilation of major coronary vessels in the heart with an increase in blood volume, velocity and flow in the DKO mice

(A) µCT images of main coronary artery from the control (L) and DKO (R) mice where there is a clear dilation of the artery in DKO mice.(B) µCT analysis from the aortic valve till the first bifurcation point show an increase in lumen diameter of the DKO (black boxes) vessel in comparison to the control (white boxes). (C) Measurement of vessel volume of coronary arteries using µCT shows an increase in DKO mice. (D) Quantification of branch point numbers from the coronary artery clearly shows an increase in the DKO hearts. (E) Measurement using angiography analysis of BV and (F) BF shows an increase in both in the DKO mice at 6 months. (G) BP measurements of control mice under different conditions. (H) BP measurements of DKO mice under different conditions. (I) Comparison of control (white) and DKO (black) mice at basal levels and after captopril and L-NAME treatment shows the DKO mice had lower BP and are unable to respond fully to L-NAME. (J) HR of control (white) and DKO (black) mice at basal levels and after captopril and L-NAME treatment show no major changes. *p<0.05, **p<0.01, non-significant (ns) p>0.05

8.4 Retina assay shows changes in vascular network of DKO mice during postnatal development

To study vascular development and cellular migration and proliferation, the *ex vivo* retina assay model was used. The main advantage for using this model is that the retina of mice are avascular after birth which then becomes highly vascularized after a number of days. By collecting retinas at P5, early sprouting angiogenesis can be studied. During this time frame, vasculature development and EC migration and proliferation can be monitored. Using P21 retinas allows for the monitoring of later stages of development when vascular remodelling and maturation occurs.

Images from P5 retinas showed a clear difference between the DKO retinas and the other groups where there was a severely impaired outgrowth of the vascular network from the optic nerve to the periphery of the retina (Fig. 17 A). This could be due to problems and perturbations in chemical cues that guide ECs while proliferating and migrating. ERG is a member of the ETS family of transcription factors and is known to be expressed in the nucleus of ECs [175]. Staining for ERG allowed for the visualization of ECs (green) in DKO retinas at P5. This revealed a clear increase in ERG positive cells (Fig. 17 A). When quantified the DKO retinas showed there was a trend in an increase in ERG/ EdU double positive cells at the vascular front compared to the other groups (Fig. 17 D). BMP9 and BMP10 are EC quiescent factors so in their absence, an increase in proliferating ECs would be consistent with their known proposed function. Not only was the outgrowth hindered but the vascular networks that had formed leaned towards a denser network in the DKO seen in the PECAM coverage in both the outer and inner areas of the retina (Fig.17 B). Quantification of numbers of protruding filopodia and branch points also showed an increase suggesting an active, immature network that was still proliferating and unable to switch to a mature and quiescent network (Fig. 17 C). Taken together these results indicate that BMP9 and BMP10 play a role in endothelial tip cell migration which ultimately leads to prolonged proliferation resulting in a denser, unorganized network that causes vascular abnormalities. Two recent publications used two different methods showing the effects of the loss of BMP9 and BMP10. Ola *et al.* injected postnatal pups from P2 to P4 with BMP9 and BMP10 blocking antibodies and collected the retinas at P5 which clearly showed the presence of AVMs, an increase in vascular area and branching in retinas blocked for BMP9 and BMP10 [176]. Meanwhile Ruiz et al demonstrated that immunoblocking of BMP9 and BMP10 via transmammary delivery also lead to an increase in vascular density and number of AVMs in P6 pup retinas [177]. Taken these recent papers and the data shown in Fig. 19, loss of BMP9 and BMP10 leads to vascular abnormalities where AVMs are formed and the retinal vascular has an increased density and branching points.

As it is known that ECs are able to recruit SMCs when in a quiescent phase, it was next investigated how the loss of BMP9 and BMP10 affected SMC coverage in the retina. Quantification of αSMA showed a declining trend in its overall expression in the DKO retinas, again highlighting the vascular defects seen in these DKO mice (Fig. 17 E). Retinas blocked with BMP9 and BMP10 antibodies, as well as endothelial specific ALK1 KO, were stained for αSMA showed a decrease in coverage of arteries and an increase in SMC coverage of veins involved in AVM formation [176]. Taken together this indicates the need for EC quiescence to allow for the recruitment of SMCs and that impaired or improper coverage of SMCs could be involved in the development of vascular abnormalities such as AVMs.

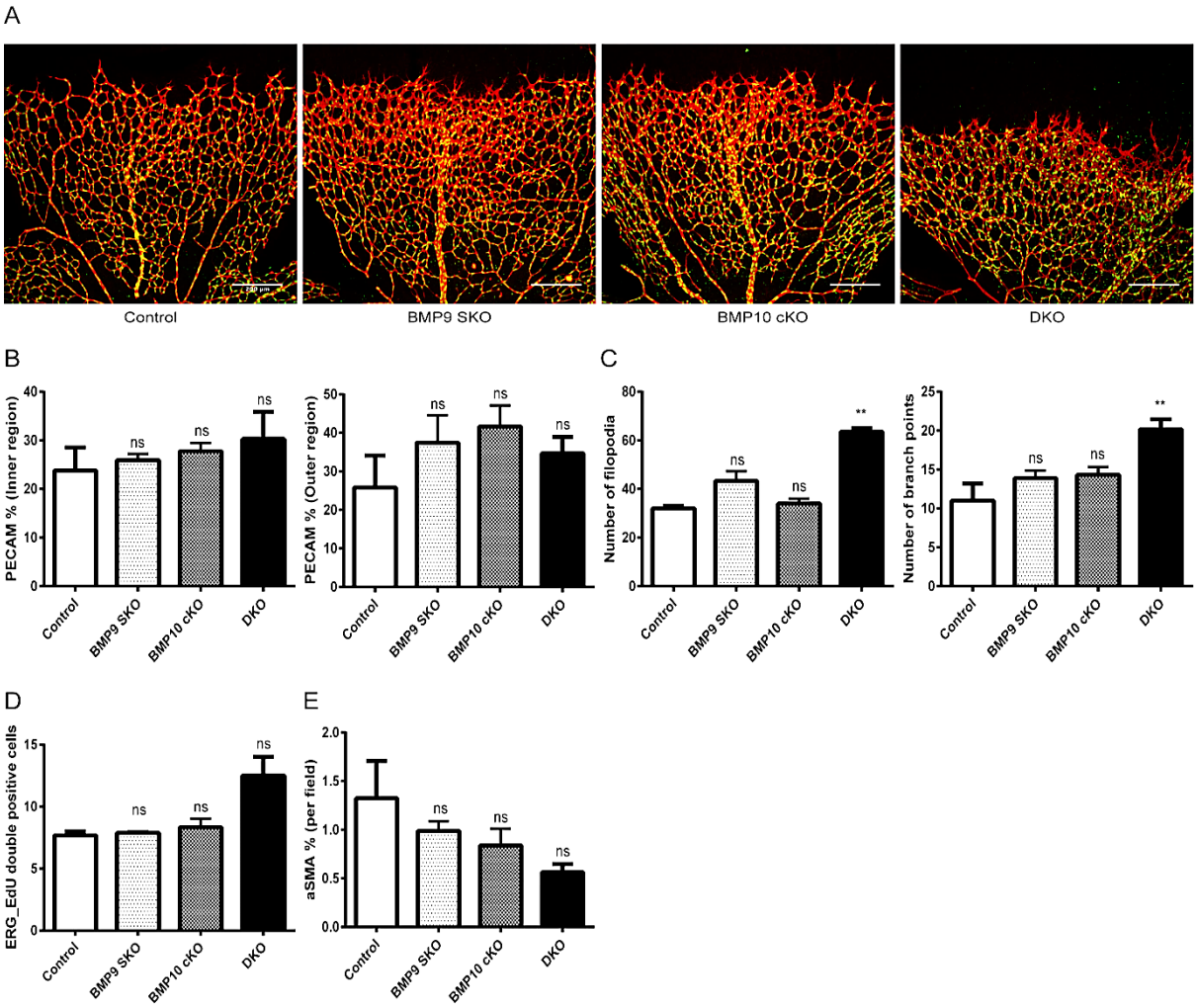

Figure 17: Loss of BMP9 and BMP10 disturbs vascular outgrowth during early vascular development and effects vascular quiescence in P5 retinas
(A) P5 retinas stained with ERG (green) and PECAM (red) show a reduced outgrowth in the DKO retinas with an increase in vascular density at the periphery. (B) Quantification of PECAM in the outer (L) and inner (R) areas of the retina shows a trend towards an increase in DKO retinas. (C) In the DKO retinas there is a significant increase in both the number of filopodia and branch points. (D) Quantification of double positive cells for ERG and EdU shows an increase in proliferating ECs in DKO retinas. (E) Analysis of αSMA shows a reduction in coverage of the DKO retinas. **p<0.01, non-significant (ns) p>0.05

Around P21 the retinal vasculature responds to factors that suppress angiogenic sprouting leading to a mature, quiescent network. Proliferation and migration of ECs is suppressed, which in turn allows the recruitment of perivascular cells to stabilize and reinforce the vascular network. Once this has occurred and perfusion has begun, pruning is needed to remove regressing vessels that are not in use. In the DKO retinas at P21 it is clear that the retinas have a much denser network with higher levels of connecting vessels from PECAM (green) staining (Fig. 18 A). To quantify this, PECAM coverage was analysed at both the inner and outer part of the retinas where an overall increase was seen in the DKO retinas (Fig. 18 D). This result clearly demonstrates that the DKO retinas have not reached a quiescent state. Quantification of the total coverage of αSMA also indicated a lack of SMC coverage which would also account for an unstable environment (Fig. 18 C). Reduced SMC coverage and active ECs leads to weakened vessels that are not able to maintain their shape and rigidity. Measurements of the artery and vein diameter showed an increase in their size due to increased EC number that are not reinforced properly due to absence of SMCs (Fig 18 B). $Alk1^{-/-}$ and $Eng^{-/-}$ mice are known to lead to tortuous vascular beds that exhibit a higher degree of permeability leading to haemorrhaging and in these models, severe and lethal AVMs are present. Although our mice are viable, the presence of tortuous vascular beds was seen in the DKO retinas as well as misalignment of the veins, where the vein is no longer parallel to the arteries but perpendicular (Fig. 18 A, white arrow). The presence of AVMs was also present in the DKO retinas but never seen in the controls or SKOs, where an artery feeds directly into a vein (Fig. 18 A, white arrows). Although loss of BMP9 and BMP10 does not lead to lethality, unlike their receptor KOs, there are still AVMs and vascular abnormalities, although at a lower frequency, meaning other factors may bind to ALK1 in their absence in an attempt to maintain vascular homeostasis.

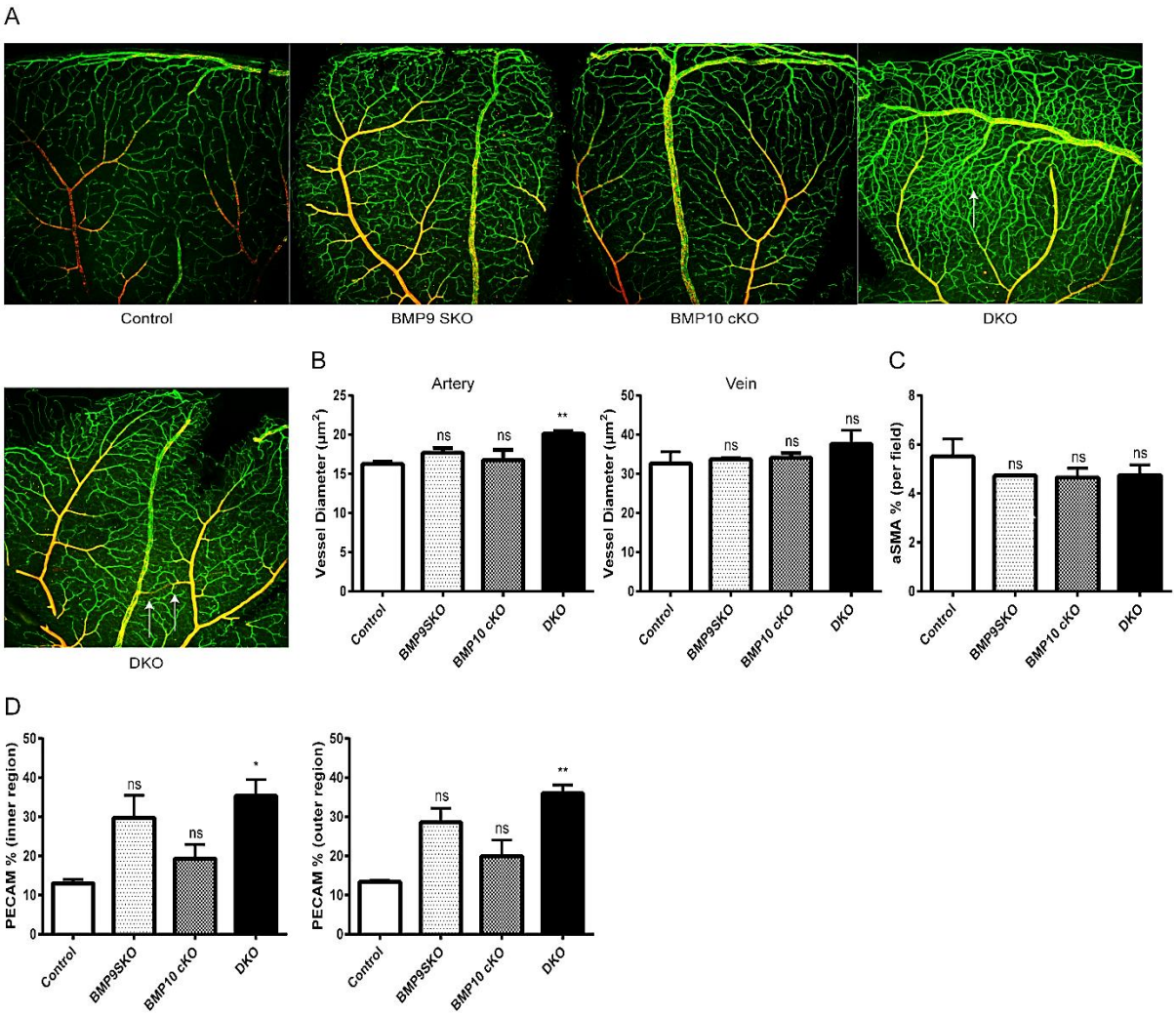

Figure 18: Absence of BMP9 and BMP10 leads to vascular abnormalities during vascular remodelling and maturation in P21 retinas
(A) P21 retinas stained with PECAM (green) and αSMA (red) show the presence of AVMs and torturous vascular beds in the DKO retinas (white arrows). (B) Analysis of artery and vein diameter showed dilation in the arteries of the DKO retinas. (C) Quantification of total αSMA coverage shows a trend towards less coverage in DKO retinas. (D) Quantification of PECAM coverage at the inner (L) and outer (R) regions of the retina shows an overall increase in DKO mice. *p<0.05, **p<0.01, non-significant (ns) p>0.05

8.5 DKO mice lose SMC number and coverage resulting in dilated vessels

Due to the obvious vascular defects seen in the DKO retinas together with the changes in hemodynamic forces it was important to determine how the loss of BMP9 and BMP10 affects the cellular structure and coverage of the vasculature. Already at 1 month of age there is a clear reduction in *Acta2* (also known as *αSMA*) expression in the heart of DKO mice compared to control mice (Fig. 19 A). This reduction was still evident in DKO hearts at 2 months of age but had clearly not worsened over time (Fig. 19 A). In hearts from

DKO and SKO at 1 month of age, an increase in *Pecam* levels was observed however no significant increase could be detected at 2 months of age in any of the groups (Fig. 19 B). These results suggested that loss of BMP9 and BMP10 play an active role in EC quiescence which in turn allows for either direct or indirect SMC recruitment that establishes a quiescent mature vessel. To compliment the qRT-PCR expression data, immunofluorescent staining for PECAM and αSMA of control and DKO hearts at 2 months was performed. This confirmed a reduction of αSMA in the DKO mice in comparison to the controls with a slight increase in PECAM (Fig 19 E).

To further investigate the vascular abnormalities resulting from the loss of BMP9 and BMP10, transmission electron microscope (TEM) was carried out on 6 month old hearts. Consistently, the images showed that DKO mice had reduced SMC numbers and that the SMCs instead of being “brick like” in appearance are very thin and appear to stretch around the vessel (Fig. 19 C). At higher magnification it was clear that the structure of the vessel in the DKO mice was disrupted and their SMCs had lost their size and structure in comparison to the controls (Fig. 19 D). Such a high loss of SMC number, as well as their overall coverage, explains why these DKO mice have such dilated vessels and that it is mainly due to the loss of vascular tone and stability. The level of dilation and the incapability of the DKO vessels to respond to vasoconstrictors explain why they have a lower BP and an impaired response. Due to a non-quiescent state, vital cross talk between the ECs and SMCs is likely inhibited preventing recruitment of SMCs and subsequent maturation.

To quantify vessel diameter and wall thickness, control and DKO aorta’s were collected at P21 and stained with Toluidine Blue. Quantification showed that loss of BMP9 and BMP10 leads to a clear increase in aortic diameter and that the DKO mice have a thinner aortic wall in comparison to the control and SKO mice (Fig. 19 F and G).

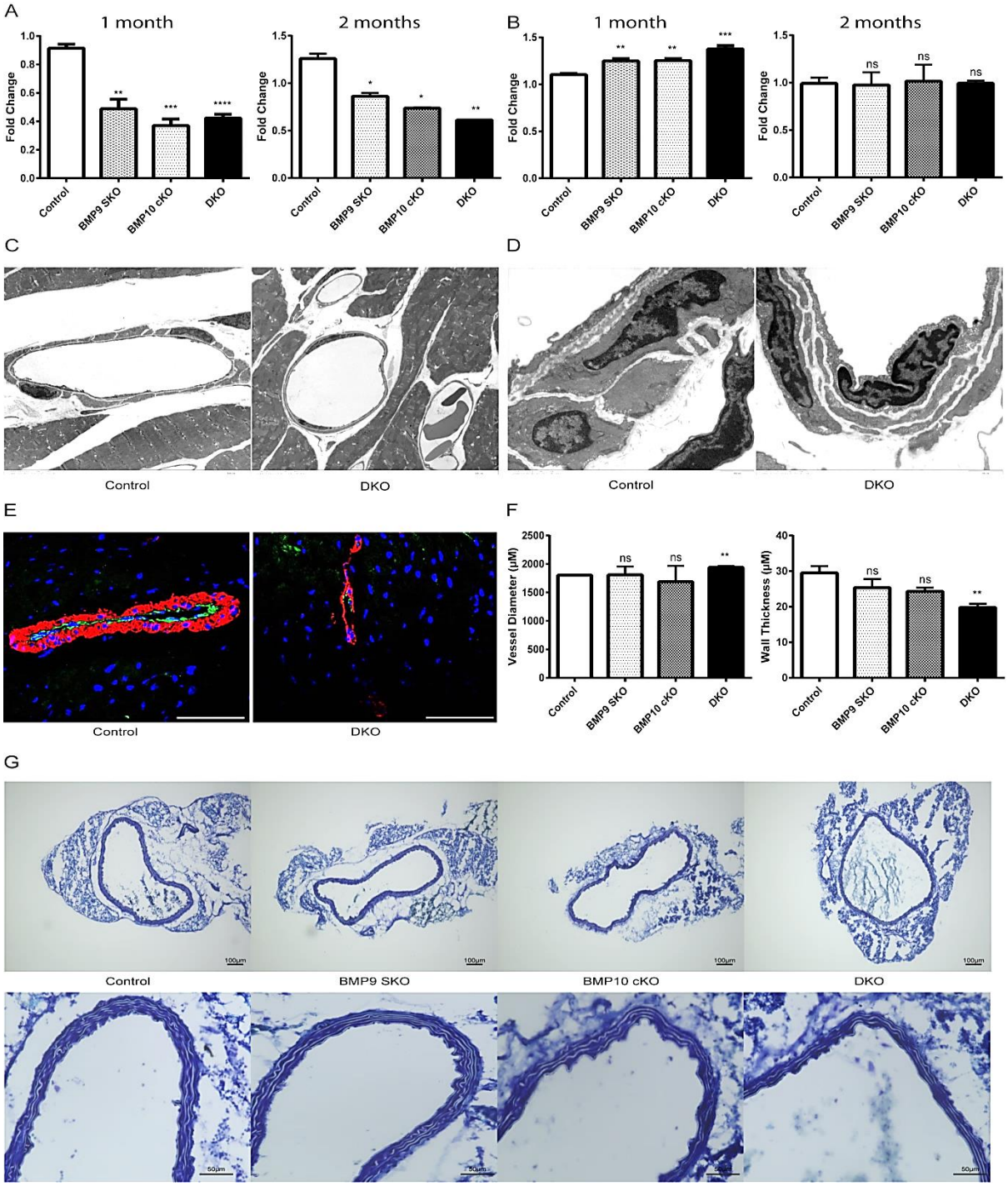

Figure 19: Loss of BMP9 and BMP10 leads to a reduction in SMC number and coverage, leading to changes in the vascular structure

(A) RT-PCR of *αSma* in 1 month (L) and 2 month (R) old hearts shows a massive decrease in expression in DKO hearts. (B) RT-PCR of *Pecam* in 1 month (L) and 2 month (R) old hearts shows a slight increase in expression in the DKO samples at 1 month. (C) Electron microscope image on 6 month old heart samples shows the reduction in SMC number and a thinner layer in DKOs. (D) Higher magnification of 6 month old heart samples shows the smaller SMCs and disruption of the vascular structure in DKOs. (E) Immunofluorescence of PECAM (green), αSMA (red) and DAPI (blue) on 2 month old heart samples shows a clear reduction in αSMA in the DKOs. (F) Quantification of vessel diameter and wall thickness of P21 aortas shows the DKOs have a thinner wall and are more dilated. (G) Toluidine Blue staining of P21 aortas shows the DKO aortas are dilated and has a thinner wall. *p<0.05, **p<0.01, p***<0.001, ****p<0.0001, non-significant (ns) p>0.05

8.6 BMP9 and BMP10 effect endothelial cell proliferation and alter genes involved in differentiation and cell cycle

BMP9 and BMP10's primary receptor, ALK1, is known to be expressed in ECs. qRT-PCR revealed that it was also expressed at high levels in SMCs but not CMs (Fig. 20 A). To date, ALK1 has been described mainly as an EC receptor. Intriguingly, this qRT-PCR data suggests BMP9 and BMP10 could potentially bind directly to SMCs .To date BMP9 and BMP10 are known to directly target ECs and induce their quiescence. To determine their functioning concentration on ECs *in vitro*, HUVECS were stimulated with different concentrations of BMP9 and 10 to confirm activation of SMAD1/5/8 occurs (Fig. 20 B). Stimulation of HUVECs with BMP9 and BMP10 showed the optimal concentrations, 1 ng/mL and 20 ng/mL respectively, were able to induce pSMAD 1/5/8 expression. Stimulation of HUVECs with TGFβ showed its optimal concentration to be 5 ng/mL and that TGFβ is able to stimulate both pSMAD 1/5/8 as well as pSMAD2. This result showed that other ligands, such as TGFβ, could activate SMAD 1/5/8 signalling in ECs *in vitro* in the absence of BMP9 and BMP10, consistent with other publications [66,135,178].

As a proof of principle experiment, EC proliferation was assessed on HUVECs stimulated with BMP9 and BMP10 (Fig. 20 C). TGFβ was also included because TGFβ has been shown to induce EC proliferation and functions with BMP9 and BMP10 to achieve a balance between EC proliferation and inhibition. Stimulation of HUVECs with BMP9 and BMP10, singularly and combined, resulted in a significant reduction in EdU incorporation, showing that these two factors do directly inhibit EC proliferation, reiterating that they are important quiescent factors (Fig. 20 C) While TGFβ had no significant effect on proliferation alone, when stimulated with BMP9 and BMP10 there was a slight increase in HUVEC proliferation compared to stimulation with BMP9 and BMP10 on their own (Fig. 20 C).

In order to determine downstream targets of BMP9 and BMP10, RNA array analysis of HUVECs stimulated with BMP9 and BMP10 was performed and from this array two genes were validated using qRT-PCR (Fig. 20 D). *HEY1*, which is upregulated in HUVECs stimulated with BMP9 and BMP10, is known to be involved in Notch signalling and is important in angiogenesis and has been previously shown to be upregulated in the presence of BMP9 and BMP10 [120,179]. CD34 is thought to be a ECs progenitor marker and has been shown to be expressed in tip cells during active angiogenesis, therefore reduction in CD34 would suggest activation of cellular quiescence (Fig. 20 D) [180]. A previous publication also showed that BMP9 and BMP10 could affect APLN expression levels, therefore analysis of *APLN* expression following BMP9 and 10 stimulation at different time points was tested [120]. The result in HUVECs revealed a dramatic and significant downregulation of *APLN* expression by 1 hour that was still evident after 4 hours that was maintained right through to overnight (Fig. 20 E).

This result suggested that BMP9 and BMP10 may directly inhibit *APLN* expression and that APLN could have an important role in vascular quiescence. Recent work by Kasai et. al showed that blocking *Apln* via siRNA lead to an increase in EC proliferation which in turn resulted in a reduction in pericyte recruitment, which is similar to what we observed in our DKO mice [181]. To further understand APLN expression and its relationship to BMP9 and BMP10 expression, its expression was then further investigated in the hearts of the DKO mice.

GOrilla analysis was performed to gain further insight into the global biological processes that were altered in HUVECs after BMP9 and BMP10 stimulation. Processes of interest that were upregulated in the presence of BMP9 and BMP10 included regulation of cell differentiation, regulation of pathway-restricted SMAD protein phosphorylation, BMP signalling pathway, regulation of cell migration and blood vessel morphogenesis (Supp. Fig A). Genes involved in regulation of cell differentiation overlapped with genes involved in SMAD protein phosphorylation and BMP signalling pathway. The genes included *BMPR2* and *ENG*, showing BMP9 and BMP10 signalling were activated, along with *TGFβ2* and *TGFβ1* and other receptors such as *BMPR1A*, *ACVR2A* and *ACVR1*. BMP9 and BMP10 have been reported to work in concert or opposition with TGFβ under differing conditions to induce or inhibit EC proliferation and migration [182]. BMP9 and BMP10 induce quiescence by activating stalk cell genes, via crosstalk with Notch signalling, such as *JAG1*, *ID1*, *ID2*, *HEY1* and *VEGF*, which was clearly seen in the gene sets involved in the regulation of cell differentiation and blood vessel morphogenesis [62,120,183]. Another upregulated factor important in endothelial cell differentiation was TMEM100, which is also a known downstream target of BMP9 and BMP10 signalling, where loss of TMEM100 is able to recapitulate the *Alk1*$^{-/-}$ phenotype [184]. Lastly, genes involved in cell migration, that were upregulated included *PDGF*, integrin's, *TGFβ*, heparin-binding egf-like growth factor (*HB-EGF*) and *VEGF*. Interestingly the majority of these candidates are essential for the migration and recruitment of SMCs [185,186].

Gene processes downregulated in HUVECs stimulated with BMP9 and BMP10 mainly included cell cycle, cell division and DNA replication (Supp. Fig. B). Many genes overlapped in these processes, including *CCNA1* and members of the KIF and CDC family's. This result clearly backs the evidence that BMP9 and BMP10 are involved in inhibiting EC proliferation.

Taken together gene analysis of HUVECs showed the involvement of BMP9 and BMP10 in differentiating ECs and induction of quiescence. This in turn would allow for stable interaction with neighbouring cells, such as SMCs and pericytes, shutting down cell cycle progression and enabling stabilization of the vascular network.

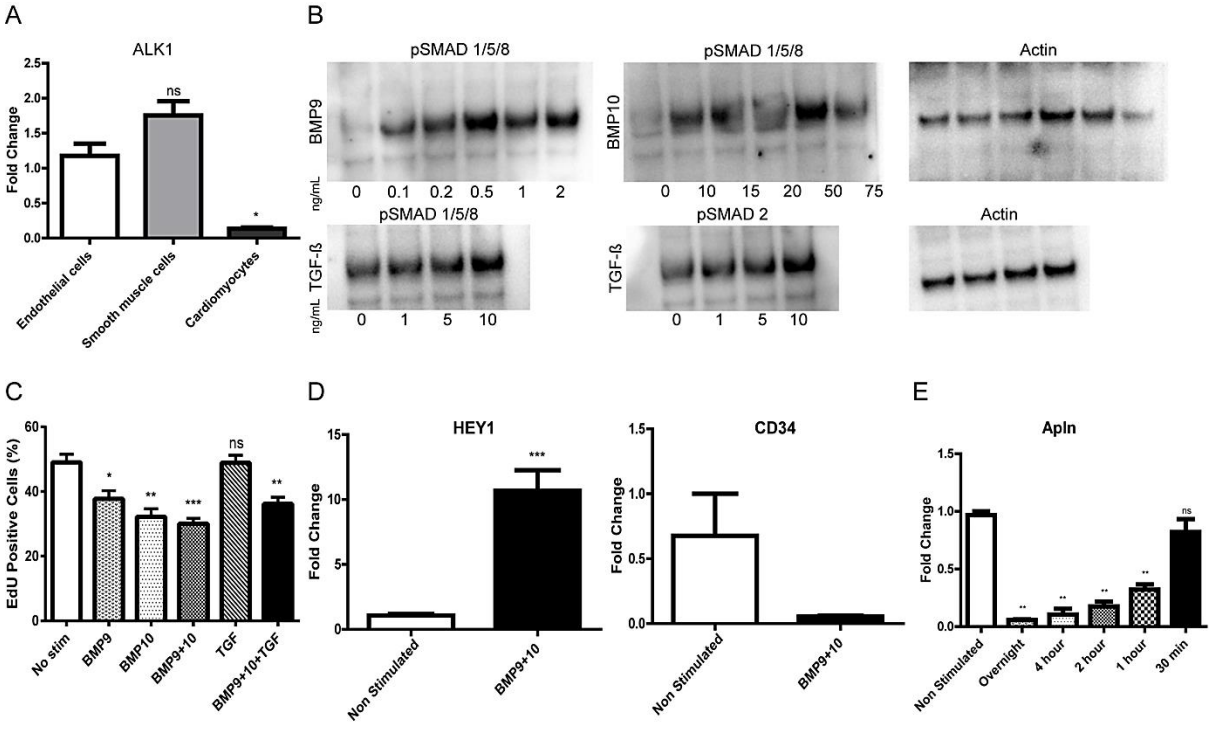

Figure 20: BMP9 and BMP10 directly reduce EC proliferation and decrease APLN expression

(A) RT-PCR analysis of *Alk1* shows it is expressed in ECs and SMCs but not in CMs. (B) Western blot analysis of HUVECs stimulated with different concentrations of BMP9, BMP10 and TGFβ after 30 minutes. Activation of pSMAD1/5/8 was used to confirm the working concentrations of BMP9 and BMP10, while pSMAD2 was used for TGFβ signalling. (C) HUVECs stimulated with BMP9 and BMP10 overnight showing they are able to inhibit proliferation, while TGFβ does not. (D) RT-PCR validation of candidate genes from the array. (E) Time course of *APLN* expression in HUVECs when BMP9 and BMP10 are present shows they are able to reduce *APLN* expression after 1 hour. *p<0.05, **p<0.01, p***<0.001, non-significant (ns) p>0.05

8.7 Loss of BMP9 and BMP10 in the heart of DKO mice leads to changes in vascular quiescent and response to stimuli

ALK1 is not expressed on CMs (Fig. 20 A) making it very unlikely that BMP9 and BMP10 exert direct effects on CMs. Hence, it was more important to look for secreted factors that could affect the vasculature as well as CMs. Gene array analysis of the total heart was performed to gain a global insight into changes within the cardiovascular system of control versus DKO mice. Gain-of-function (GOF, where HUVECs were stimulated), and Loss-of-function (LOF, where heart and aorta of DKO mice were analysed) approaches were analysed to discover direct targets of BMP9 and BMP10 that are involved in cardiovascular homeostasis. GO analysis of processes upregulated in DKO hearts showed changes in biological processes such as GPCR signalling pathway, ECM structure organization, angiogenesis, epithelial cell migration and cell division (Supp. Fig C). Genes involved in GPCR signalling pathway, included *Apln* and endothelin-1 (*Edn1*), were upregulated in the

DKO hearts which are important factors regulating cardiac hypertrophy, vascular tone and blood pressure (Fig. 21 A) [187]. This result was intriguing as upregulation of such potent factors could explain for the phenotype seen in the DKO hearts, making them interesting potential downstream targets. *APLN* levels were dramatically reduced in HUVECs stimulated with BMP9 and BMP10 (Fig. 20 E), the opposite of what was seen in the DKO hearts (Fig. 22 A), while *EDN1* remained unchanged in the absence or presence of BMP9 and BMP10 making *Apln* a potential downstream target of BMP9 and BMP10.

Many of these gene processes had overlapping players that are normally associated with active angiogenesis including *Ccn2a*, *Cdk*, *Kdr* and *Vegf* (Fig. 23 B-C). Genes such as *Nos3* were also upregulated which could explain the excessive vascular dilation seen in the DKO hearts and higher levels of hypoxia-inducible factor 1α (*Hif1α*) would suggest these DKO mice have a slightly higher hypoxic environment as a result. Changes in the expression of genes important for ECM structure organization were also detected including collagen, *Tgfβ* and elastin. Upregulation of these genes is explained by the constant active angiogenic environment in the DKO hearts but also due to the fact that the DKO hearts have remodelled, become overall hypertrophic, so that it can remain functional and the mice viable. These findings altogether strengthen the role BMP9 and 10 in angiogenesis and cardiovascular homeostasis.

Gene targets from the array that were involved in the various processes mentioned were validated by RT-PCR, for example *Ccn2a*, *Cd34* and *Apln* (Fig. 21 A). Comparison of the HUVEC array and DKO heart array showed an overlap of 15,000 genes in the form of a Venn diagram (Fig. 21 B). From these 15,000 genes, significant targets from both sets with a fold change greater than 1.20 and lower than 0.80 were analysed. From these criteria 130 genes were found and a comparison was made between genes that were highly expressed in the DKO hearts but lower expressed in stimulated HUVECs and vice versa to decipher direct downstream targets of BMP9 and BMP10. GO analysis of genes expressed at high levels in DKO hearts compared to HUVECs were analysed and shown to be mainly involved in cell cycle and division (Supp. Fig D). These results would suggest that even though a global analysis of the whole heart was performed the majority and most significant changes in gene transcription are all related to ECs proliferation and angiogenic processes.

The effects of APLN as well as BMP9 and BMP10 on CMs are not clear. To further understand the role of APLN, BMP9 and BMP10, rCMs were isolated and stimulated *in vitro* for 1 week. As a positive control to induce a hypertrophic environment, FGF2 was used as it is a known inducer of CM hypertrophy, which was confirmed as seen in Fig. 21 C-E [188]. Preliminary results show that BMP9 stimulation alone has no significant effect on

cardiomyocyte hypertrophy seen by the same basal ANP expression as the control and the few number of cardiomyocytes with protruding filopodia (Fig. 21 C-E). When BMP9 is added along with FGF2, an increase in ANP expression and protruding filopodia is detected however this is just a response from FGF2, as FGF2 stimulation alone has similar results (Fig. 21 C-E). However when BMP10 was added separately to cardiomyocytes there was a clear reduction in ANP levels and this was also evident in the reduced number of extending filopodia compared with the control (Fig. 21 C-E). Moreover these initial results would also suggest that in a hypertrophic environment, BMP10 and FGF2 together, BMP10 is able to block cardiomyocyte hypertrophy as ANP expression is lower than in FGF2 alone (Fig. 21 C-D). This result is also evident in bright field images where there is a clear reduction in filopodia extensions (Fig. 21 E). To date conflicting results for the role of APLN in cardiomyocyte hypertrophy makes it difficult to understand its direct function in the heart. However these first results also do not give a clear insight into the role of APLN because at basal levels APLN does not increase ANP expression nor does it exasperate FGF2 induced hypertrophy (Fig. 21 C-E). These findings support the ideas from different publications that BMP10 does play a specific role in the heart, which BMP9 does not, and higher expression levels of BMP10 blocks cardiomyocytes hypertrophy [114,189]. Further work on APLN detailing its effects on cardiomyocyte hypertrophy is still needed.

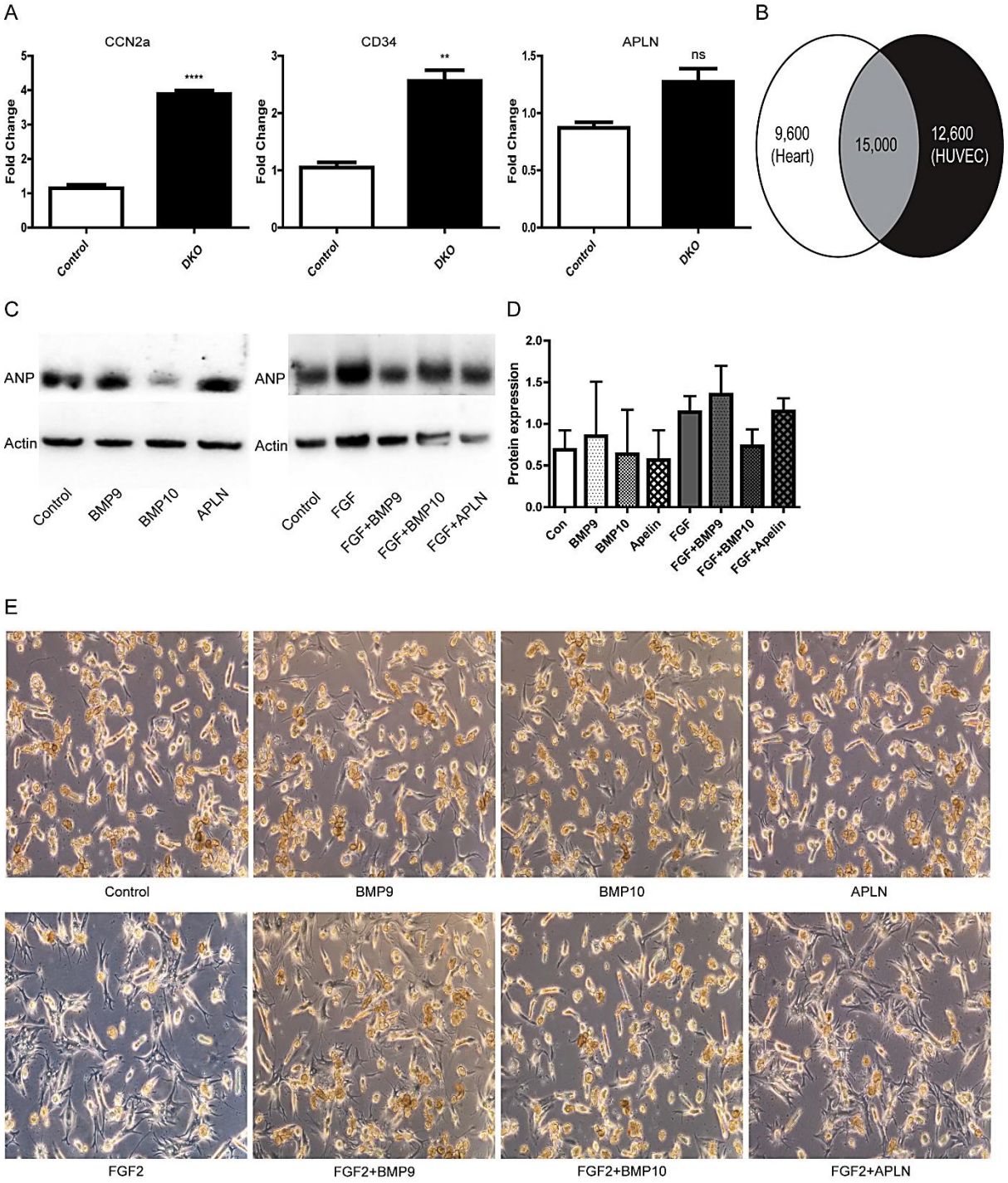

Figure 21: BMP9 and BMP10 effect vascular stability and quiesence in DKO hearts resulting in an increase in APLN levels, along with changes in the hypertrophic response

(A) RT-PCR analysis validating targets upregulated in DKO hearts. (B) Venn diagram comparing overlapping genes in the DKO heart and stimulated HUVEC array. (C) WB analysis for ANP on rCMs stimulated with different factors to check for the hypertrophic response (D) Quantification analysis of WB for ANP with different stimulation factors normalised to Actin. (E) Bright field images of rCMs after stimulation with various compounds. **p<0.01, ****p<0.0001, non-significant (ns) p>0.05

8.8 Loss of APLN in the DKO mice does not rescue the cardiovascular phenotype

Taken together, since loss of BMP9 and BMP10 led to an increase in APLN levels (Fig. 22 A) and HUVEC stimulation with both BMPs led to a drastic decrease in APLN expression (Fig. 20 E), it was postulated that loss of *Apln* (*Apln*$^{-/-}$) in the DKO mice could lead to a rescue of the cardiovascular phenotype. TKO mice were generated by breeding DKO mice with APLN SKO mice (Fig. 12). qRT for *Apln* expression was then performed on the TKO mice to ensure deletion of *Apln*, where results showed that *Apln* expression was efficiently decreased in the TKO line (Fig. 22 A). The two parameters used to determine if loss of *Apln* in the DKO background could rescue these mice was the return of the hypertrophic heart to a normal size and secondly the return of SMCs to the vasculature allowing for the reduction of vascular dilation. qRT-PCR for αSMA performed on TKO hearts showed that there was no increase in *αSma* expression and that it was still significantly lower than the control mice, although not as low as the DKO samples (Fig. 22 B). Measurement of the heart: tibia ratio also showed there was no reduction in cardiac hypertrophy in the TKO and that they still resembled the DKO phenotype (Fig. 22 C). Histochemistry staining confirmed these hearts to be large in size, with an overall hypertrophy and no signs of fibrosis (Fig. 22 D). Aorta's from TKO mice and control mice at 2 months were collected and stained for Toluidine blue to determine if vascular dilation was still present and if they still presented a thinner aortic wall. Quantification of the aorta's showed that the TKO mice have a tendency towards a more dilated vessel in comparison to the control mice (Fig. 22 E). Along with this finding the TKO's also possess a thinner aortic wall when compared to controls (Fig. 22 F).

Taken together initial results would suggest that loss of *Apln* does not rescue the DKO mice phenotype. In these circumstances loss of one gene alone may not be enough to account for all the phenotypes seen and therefore cannot rescue our DKO mice. As shown above many different factors are changed in our DKO mice which have a very complex system involved, with numerous different pathways cross talking and interacting together or in opposition to each other. One explanation could involve a second ligand that has been published that binds the APLN receptor, known as apelin receptor early endogenous ligand (*Apela* also known as *Ela*) [190]. qRT-PCR and PCR for *Ela* was unsuccessful as it was undetectable in either PCRs which used both mouse and human samples. This could be due to the fact that *Ela* is located is a non-coding region which gives rise to a small hormone peptide that undergoes further cleavage making it hard to detect [191]. Therefore it is not known whether this ligand's expression is increased to compensate for the loss of *Apln* and cannot be ruled out.

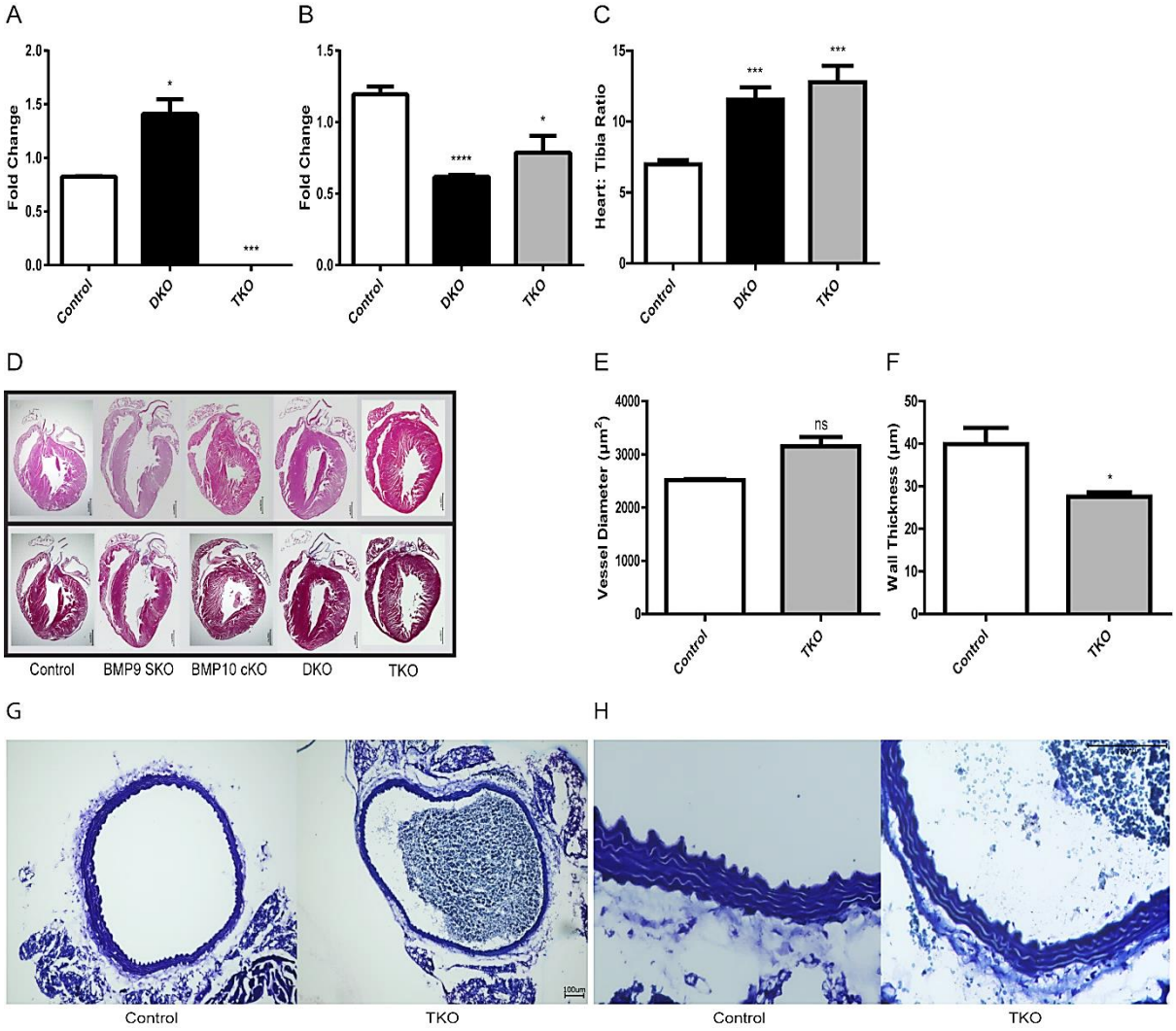

Figure 22: Loss of Apelin in the DKO background rescues the SMC phenotype but not always the cardiac hypertrophy
(A) qRT-PCR shows higher expression of *Apln* in the DKO hearts but no expression in the TKO hearts at 2 months. (B) Loss of *Apln*, *Bmp9* and *Bmp10* in TKO mice does not increase *αSma* expression at 2 months. (C) Calculation of the heart: tibia ratio of TKO hearts compared to control and DKO hearts at 2 months shows they are still hypertrophic with no reduction in size (D) H&E (upper panel) and Trichrome (lower panel) staining shows an overall increase in cardiac morphology in the TKO hearts and no sign of fibrosis at 2 months just like the DKO hearts. (E) Analysis at 2 months shows there is a slight increase in vascular diameter of the TKO aorta compared to the control. (F) Analysis at 2 months shows a decrease in the wall thickness of the TKO aorta compared to the control. (G) Toluidine blue staining of the aorta at 2 months for control and TKO samples. (H) Higher magnification of aortas from control and TKO mice show the difference in structure and thinner wall layer. *p<0.05, p***<0.001, ****p<0.0001, non-significant (ns) p>0.05

8.9 BMP9 and BMP10 induce expression of contractile markers and are involved in SMC differentiation and recruitment

To date ALK1 is considered primarily an EC receptor, although others have reported its expression on other cell types, qRT-PCR analysis shows *Alk1* expression in SMCs also (Fig. 20 A) [192].The expression of ALK1 in SMCs leads to question whether or not BMP9 and

BMP10 have direct effects on SMCs and this question was addressed *in vitro* with isolated SMCs. To therefore also determine whether the phenotype in the DKO mice was due to a problem in EC to SMC cross-talk, primary SMCs from the aorta of DKO mice were isolated and a gene array was performed to monitor global changes and co-cultures *in vitro* were also setup.

Direct stimulation of mSMCs *in vitro* with BMP9 and BMP10 followed by IF staining showed a remarkable increase in αSMA (red) expression (Fig. 23 A). This was further quantified using qRT-PCR, where the expression of *αSma* was dramatically increased when compared to non-stimulated cells (Fig. 23 B). Normally when isolated and cultured, SMCs lose their contractile phenotype and αSMA is amongst a number of markers whose expression is dramatically downregulated [193]. This data indicated that BMP9 and BMP10 could be important in directly maintaining SMC contractility *in vivo*. In our lab it was published that loss of mir143 and mir145 results in a loss of contractility in SMCs [194]. It was reported that loss of these two mirs led to a reduced contractile state in SMCs, where contractile markers were decreased and there was a reduction in media thickness of the femoral artery, as well as having low basal BP [194]. Therefore to test how potent BMP9 and BMP10 were at increasing αSMA levels, SMCs from mice heterozygote for mir143 and mir145 were isolated and stimulated. Although not as extreme as in WT SMCs, stimulation of SMCs heterozygote for mir143 and mir145 showed BMP9 and BMP10 together were able to activate *αSma* expression, as this is not normally the case (Fig. 23 C), making these BMPs good candidates for promoting SMC contractility.

To test the roles of BMP9 and BMP10 in SMC proliferation, rSMCs were isolated and a Vybrant assay was performed after 7h stimulation with BMP9, BMP10, Apelin-13 and FGF2. Stimulation of all compounds caused an increase in cellular proliferation, although stimulation with BMP9 and BMP10 gave the highest increase in proliferation along with Apelin-13 (Fig. 23 D). However stimulation with BMP9, BMP10 and Apelin-13 sees a reduction in proliferation compared to Apelin-13 or BMP9 and BMP10 alone, indicating that BMP9 and BMP10 are able to inhibit the proliferative effects of APLN *in vitro* (Fig. 23 D). This evidence was further supported as stimulation of both SMCs and HUVECS with BMP9 and BMP10 leads to a dramatic decrease in *Apln* expression (Fig. 20 E, 23 E) along with its receptor, *Aplnr* (also known as Apj) (Fig. 23 F).

As mentioned previously mentioned ECs receive signals from within the blood and then signal to SMC via secreted factors, such as PDGF, to recruit or differentiated SMCs [195,196]. To uncover potential secreted factors from ECs on SMCs that could affect SMC recruitment, co-culture experiments were performed where HUVECs were stimulated with

BMP9 and BMP10 and the stimulated media was then put onto mSMCs. This stimulated HUVEC media that was put onto mSMCs also induced a reduction in *Apln* expression (Fig. 23 G). When *αSma* expression was analysed it was shown that upon reduced APLN levels, αSMA expression was increased (Fig. 23 H). Taken together, these results show that a reduction in APLN could lead to higher expression of contractile markers, such as αSMA, in SMCs.

Recruitment of SMCs is needed for vascular maturity and stability to induce vascular quiescence. To understand the affects BMP9, BMP10 and APLN have on rSMC migration, a migration assay was performed. To date there are conflicting results as to whether or not APLN promotes or inhibits SMC migration [197,198]. Results from the migration assay would suggest that BMP9 and BMP10 along with APLN are not potent factors involved in SMC migration, unlike FGF2 (Fig. 23 I).

GSEA analysis of aortas from DKO mice showed an increase in genes expressed in regulation of respiration and metabolism (Fig. 23 J) while genes involved in cell division and maturation were downregulated (Fig. 23 K). Genes involved in aerobic respiration and cellular respiration included genes involved in the succinate dehydrogenase complex and ubiquinol-cytochrome c reductase genes. This upregulation in respiration could be due to higher mitochondria production or mitochondria number in SMCs, seeing as there is a loss of SMC coverage. Gene's downregulated in DKO aortas were involved in cell division and maturation. This result is not surprising as these mice have a severe reduction in SMC coverage and number. Gene's downregulated in cell division included *Myh9*, *Myh10* and *TGFβ*. MYH9 and MYH 10 are non-muscle myosin proteins expressed in numerous cells in the heart and are important factors in the contractile properties of SMCs while TGFβ has been shown to been important for SMC differentiation [199,200]. When looking at genes downregulated in cell maturation, genes such as *Adam12* and *Ereg* were amongst some of the significant hits. Not much is known about these factors but recent papers have revealed the importance ADAM12 plays in inducing differentiation of mesenchymal SCs into SMCs via TGFβ signalling and how ADAM12 was able to induce αSMA expression [201]. Recent findings have shown EREG to be a potent SMC mitogen, whose expression was controlled by factors such as ANG2 and EDN1, and may have an important role in SMC proliferation and remodelling [202].

In vitro BMP9 and BMP10 are able to induce expression of αSMA in mSMCs while also being able to suppress APLN signalling. Co-culture experiments were able to confirm that factors secreted from ECs are important and capable of also re-expressing αSMA and suppress APLN signalling, although it is not as dramatic. BMP9 and BMP10 allow rSMC

proliferation *in vitro* and can also inhibit proliferation induced by APLN stimulation. This data was further supported by gene array analysis of aorta's lacking BMP9 and BMP10, where genes involved in cell division and maturation are downregulated. Taken together these results would suggest that BMP9 and BMP10 play a role in SMC proliferation and maturation, where they also help to maintain the SMCs contractile phenotype. These results then lead to the question of whether BMP9 and BMP10 can directly affect SMCs *in vivo* and what role they play and to address this question an *Alk1* SMC specific KO mouse line is needed.

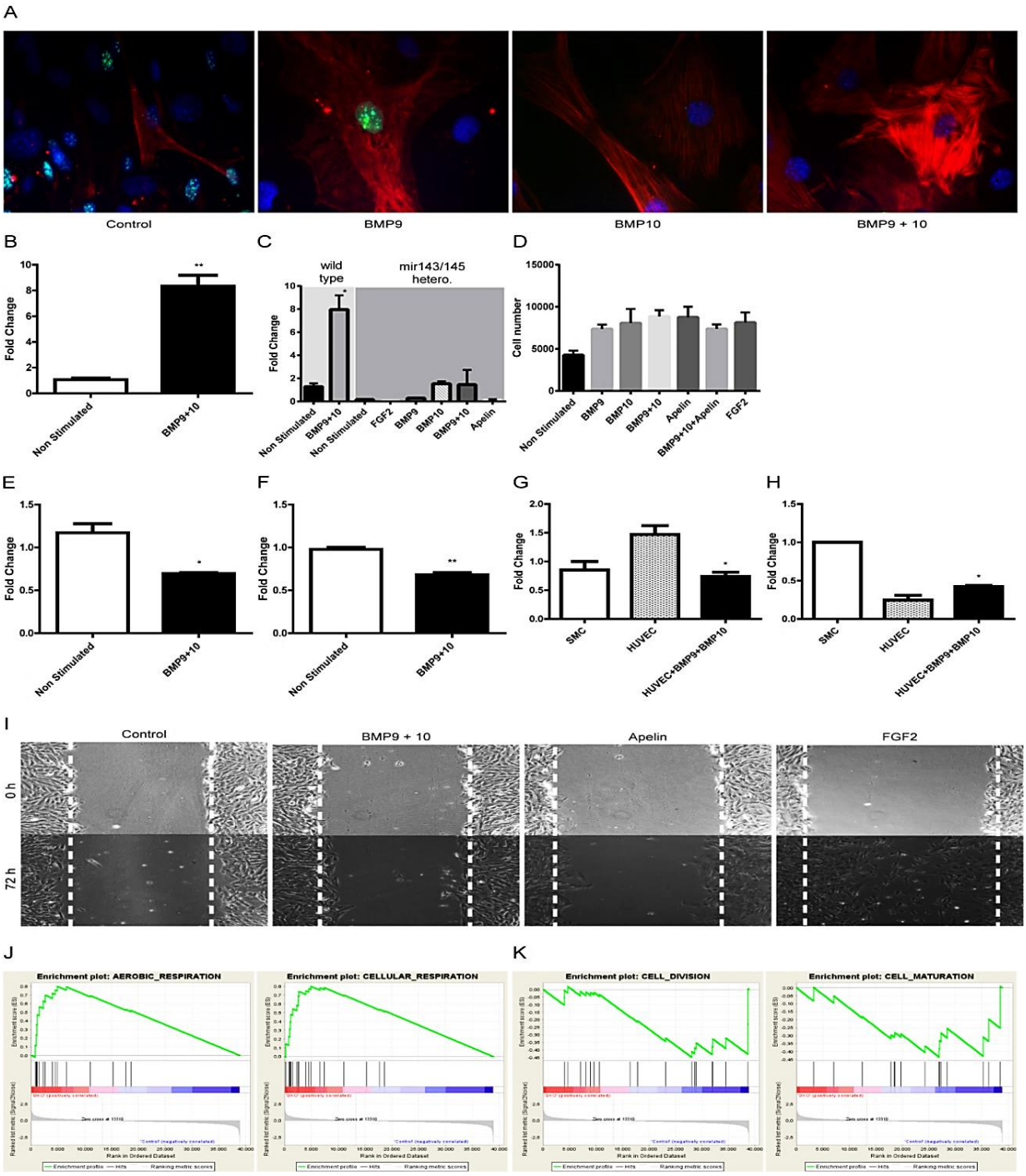

Figure 23: BMP9 and BMP10 increases levels of αSMA in SMCs and inhibits APLN expression while also affecting SMC proliferation and migration
(A) Immunofluorescence staining of mouse SMCs (mSMCs) with ki-67 (green), to monitor proliferation, and αSMA (red), to determine contractile phenotype. BMP9 and BMP10 together are able to induce re-expression of αSMA (B) qRT-PCR showed the higher level of αSMA in mSMCs stimulated with BMP9 and BMP10 (C) Heterozygous KO of mir-143 and mir-145 in mSMCs leads to the absence of αSMA, where stimulation with BMP9 and BMP10 is able to slightly increase its expression levels. (D) Rat SMCs (rSMCs) were directly stimulated and a Vybrant assay was performed to test for proliferation. (E) qRT-PCR of stimulated mSMCs showed a significant decrease in APLN expression (F) qRT-PCR of stimulated mSMCs showed a significant decrease in APLNR expression. (G) Co-culture experiments, where HUVECs were stimulated with BMP9 and BMP10 and the media was put onto mSMCs, showed that APLN expression was decreased. (H) Co-culture experiments, where HUVECs were stimulated with BMP9 and BMP10 and the media was put onto mSMCs, showed that αSMA expression was increased. (I) Migration assay performed on rSMCs showed there was hardly a response to stimulation with BMP9 and BMP10 or APLN after 72 hr compared to the control group stimulated with FGF2. (J) GSEA analysis of DKO aortas showed an increase in genes related to cellular respiration and aerobic respiration. (K) GSEA analysis showed that loss of BMP9 and BMP10 in the aorta led to a decrease in genes involved in cell division and cell maturation. *$p<0.05$, **$p<0.01$

9 Discussion

9.1 The role of BMP9 and BMP10 in cardiovascular homeostasis

BMP9 and BMP10 are part of a complex and interconnected signalling pathway, the TGF-β superfamily signalling pathway, which control and modulate numerous important biological processes. To understand the specific role of each of these players in this pathway and their implications in human diseases, many different mouse models have been utilized [203–205]. Not only do they orchestrate a fine balance within their own signalling pathway to maintain homeostasis but TGF signalling family members are also known to interact with other signalling pathways such as MAPK pathway, PI3K/AKT, WNT and Notch signalling [205,206].

To date no research has been published on the loss of both BMP9 and BMP10 in a mouse model to address their role in cardiovascular homeostasis or how they may contribute or protect against disease development and progression. BMP9 and BMP10 are secreted from the liver and the right atria respectively and loss of these two ligands was confirmed via qRT-PCR [112,120]. Loss of *Alk1* and *Eng*, the binding receptors of BMP9 and BMP10, leads to embryonic lethality when constitutively knocked out [135,140,143,144,207]. While *Alk1* ^{EC} in ECs and *Alk1* ^{iCre} KO in the adult leads to lethality after P5 and P21 respectively, *Eng* ^{iKO} KO results in vascular abnormalities but the mice are viable [141,145]. These results reveal the complex role of BMP9 and BMP10 and their binding partners in angiogenesis and vascular homeostasis. The approach taken here allowed a systematic characterisation of the role of BMP9, BMP10 and their overlapping function as the main mediators of ALK1 signalling. Loss of *Bmp9* and *Bmp10* did not result in embryonic lethality which strengthens the argument that other ligands are able to bind ALK1, such as TGFβ1 and TGFβ3, and also work to maintain vascular homeostasis [192,208]. This point was further supported by the fact that DKO embryos at E14.5 displayed no signs of abnormal PECAM or αSMA coverage unlike *Alk1*$^{-/-}$ and *Eng*$^{-/-}$ embryos that already have problems with EC and SMC coverage between E8.5 and E9.5 [134,143]. Further, loss of *Bmp9* and heart specific deletion of *Bmp10*, to overcome embryonic lethality seen in constitutive BMP10 KO mice, does not result in any major developmental problems in either the SKOs or DKO suggesting that BMP9 and BMP10 have redundant functions in the adult. This is consistent with previous work revealing that *Bmp9* can compensate for the loss of *Bmp10* in modulating developmental

angiogenesis and maintaining vascular homeostasis but not BMP10's specific role in early cardiac development [114].

The comprehensive analysis of heart morphology and cardiac function revealed some intriguing insights into the role of BMP9 and BMP10. Cardiac failure can be defined by a decrease in SV, due to systolic or diastolic dysfunction, where the heart has problems with contractility (systolic dysfunction) or problems with chamber filling due to stiffness of the heart (diastolic dysfunction) leading to a decrease in EF [209]. These changes result in an increase in ventricular end diastolic pressure. To normalize this increase in preload, the heart dilates which over time can lead to cardiomyopathy and ultimately HF [209]. Although the DKO hearts show clear signs of cardiac hypertrophy, via MRI analysis, heart: tibia comparison and histochemistry, by 1 month of age they do not show a severe reduction in EF. However by 6 months of age these DKO animals display a higher increase in LVM and a significant reduction in EF but these symptoms did not progressively get worse, suggesting the system was able to stabilize and cope with these adverse effects hence why these mice survived. What causes the observed increase in LVM in the DKO mice can be explained by the increase detected in SV along with EDV, which in known to increase preload exerted on the heart [210]. Preload is defined as the stretching of CMs before contraction and according to the Frank Starling mechanism, an rise in SV increases the volume of blood in the heart, by stretching the ventricles which expand during diastole [211]. This increase in blood volume enhances the force of contraction and therefore also increases the blood pumped out during diastole [211]. Normally a significant decrease in EF is a hallmark of cardiac failure. However in the case of the DKO mice, the reduction in EF did not significantly worsen over time suggesting that this adaptation was more physiological rather than pathological. Overall loss of BMP9 and BMP10 results in a decrease in EF and increases in LVM, SV and wall thickness. This concludes that although the EF is lower, the SV is higher and the heart functional as there are no signs of a thinner ventricle wall, though the LVM is significantly increased, meaning a sufficient amount of blood is being pumped around the system and is not detrimental to the animal.

Another hallmark of cardiac failure that leads to reduced EF is the presence of fibrosis, meaning the heart is no longer effectively pumping [212]. The lack of fibrosis in DKO hearts at 1 month or at 6 months of age revealed these hearts do not suffer from contractility problems. These images of the DKO mice also showed that they did not suffer from specific areas of cardiac hypertrophy, i.e. right atria seen in PH, but rather the whole heart was enlarged in size [213]. These images again argued for a lack of pathological hypertrophy, where an increase in interstitial fibrosis correlates with the degree and initiation of LV hypertrophy, but rather argue towards an adaptive response due to the changes in the

vascular system [214,215]. Recently it was published that BMP9 is a profibrotic factor that, via ALK1 and ALK5 signalling, promotes ECM protein production meaning that under stress conditions loss of BMP9 is unable to elicit this response [172]. However the more likely explanation is that the heart adapts to altered cardiac output and pressure in a physiological way, as seen in athletes who undergo different types of training [216].

It has been long established and accepted that after birth, adult cardiomyocytes do not undergo proliferation but rather respond to injury or stress by increasing their area, which was the case for the DKO hearts [217]. This hypertrophy could have occurred as a result of increased blood volume, which is known to stretch CMs making them hypertrophic, or due to the secretion of hypertrophic stimuli under stress conditions [211]. ANP and BNP are small peptide hormones that are important during development where they have been shown to be involved in many important biological processes such as regulation of blood pressure, monitoring salt and water balance, vasodilation to ensure proper blood supply to the embryo and cardiogenesis [218]. Re-expression of ANP and BNP are common markers used to determine cardiac hypertrophy as these two peptides are secreted upon cardiac wall strain and are also known to play a role in preventing increased cardiac hypertrophy and fibrosis [219–223]. qRT-PCR confirmed an increase in these hypertrophic markers, *Anp* and *Bnp*, in the DKO and SKO hearts. These results suggested that hypertrophic stimuli, like ANP and BNP, play a role in the enlargement of the DKO hearts due to the increase in cardiac strain and may also contribute to vasodilation. Stimulation of cardiomyocytes with BMP9 and BMP10 show that loss of BMP10, not BMP9, could also result in the increase in ANP expression resulting in cardiomyocyte hypertrophy.

ALK1 is not present on CMs, but rather ALK3, suggesting that BMP9 and BMP10 do not cause hypertrophy directly but it is possible that the hypertrophy is a secondary effect due to changes in the vascular network or initiation via a different signalling pathway [189]. Due to the fact BMP9 and BMP10 are quiescence factors, loss of both results in an increase in vascular dilation because of active ECs and a lack of SMCs. This hypothesis was addressed already in both papers studying the loss of *Alk1* and *Eng*, where the vascular defect was developed first leading secondly to cardiac developmental defects [134,135,143]. This is due to the important relationship between vessel diameter, BF, BV and BP which play an important role in vascular homeostasis and changes in any of these can have pathological effects [156,224,225] . Arteries normally deal with higher BP than veins and as a result are surrounded by a thicker layer of SMCs that allow for support as well as adaptation to changes in BP, by initiating either vaso-dilation or -constriction [226]. To determine the effects of vasodilation and vasoconstriction on the DKO mice, Captopril and L-NAME were administered respectively. Captopril intake resulted in a further drop in the BP of DKO animals, due to a dilative

environment already, as well as the controls. L-NAME treatment in the control mice increased BP and reduced HR, as a rise in BP coincides with a reduction in HR, so as not to stress and damage the heart [227]. The DKO mice however responded with a slight increase in BP and a slight decrease in HR. This lack of response to vasoconstriction was due to the reduced number and coverage of SMCs in the DKO animals, which are vital in regulating vascular tone [228]. Taken together these results suggest that changes in the vascular structure, i.e. an increase in vessel dilation, leads to changes in blood volume, which increases the force exerted on the heart during filling, causing the heart to increase in size. As previously reported in other studies, the DKO mice display increases in blood volume and vascular dilation with reduced vascular resistance and BP, allowing an increase in BF and BV to ensure enough blood is pumped around the system [227]. Loss of SMCs that result in hypotension and cardiac hypertrophy have been previously described by Schreier *et al.* [229]. Mice lacking vSMC *Egfr* display similar vascular and cardiac defects compared with the BMP9 and BMP10 DKO mice; increased cardiac hypertrophy, no fibrosis, reduced BP and reduced SMC coverage [229]. They too hypothesise that loss of *Egfr* in SMCs results in a destabilisation of the vascular system which results in altered vascular function that ends in the loss of tissue homeostasis [229].

To understand potential downstream targets that could affect primarily the vasculature as well as the cardiac system, *ex vivo* retina assays were performed to determine events during vascularisation without BMP9 and BMP10 while gene arrays for DKO hearts and *in vitro* stimulated HUVECs were used to determine global transcriptional changes. During angiogenesis an important balance between tip cell migration and stalk cell proliferation is needed for the correct development of the sprouting vascular network. As discussed previously it is known that Notch, BMP, VEGF and NRP signalling plays a major role in tip/ stalk cell selection. Gene array data from HUVECs stimulated with BMP9 and BMP10 show a downregulation of *DLL4* and a major upregulation of genes involved in stalk cell behaviour such as *JAG1*, *HEY1*, *HEY2* and *ID1* which had also been reported previously [120,230,231]. Although not all genes were detected in the DKO heart array, *Hey1* and *Hey2* were downregulated and *Apln*, known to be more highly expressed in tip cells and induce EC proliferation, was upregulated indicating a more tip cell environment [62,231,232]. It is essential to stabilize and mature a new vascular network to allow for recruitment of mural cells, therefore having a more sprouting and active network means there is interference with coordinated sprouting which results in hyperplasia and vessel enlargement [231,233]. Quantification showed a denser network in PECAM levels of the DKO and SKO retinas with a reduction in SMC coverage at both early and late stages of vascularisation. One explanation could be VEGF, which is a known player in this process and its availability in the vascular plexus determines

the rate of cellular division [234]. In a normal retina, where VEGF is limited to the periphery of the vascular plexus there is a significant proliferation rate in ECs directly behind the sprouting front where administration of VEGF results in widespread proliferation throughout the whole vascular plexus [234]. Within the growing plexus, levels of VEGF differ according to location and vessel type. In the avascular region of the retinas it is considered a hypoxic environment where VEGF levels are higher than in the vascular plexus where O_2 levels are normal and therefore has lower VEGF signalling [234]. The vein is also considered hypoxic, with high VEGF, and arteries normoxic, with lower VEGF, leading to lower levels of migration and more stalk cell proliferation or an increase in migration and less proliferation, respectively [234]. Taken together these data would suggest that VEGF has a dual role and can act as a mitogen and chemotactic factor on ECs *in vivo*, where they have to choose to either proliferate or migrate in the presence of VEGF. Results suggest if VEGF levels are high around an actively growing vessel, then ECs seem to react by proliferating to increase the vessel calibre, while if VEGF is lower at the cell but higher at a distance, then ECs polarize and extend filopodia to migrate towards the VEGF source [235]. Changes in O_2 levels are also known to affect other factors such as vasodilation and SMC differentiation where hypoxic conditions were shown to create a less dense and patchier SMC coverage in arteries at P6 [236]. Although it was not fully proven that the DKO mice suffer from an increase in VEGF expression or hypoxic environment, it is clear that at P5 loss of BMP9 and BMP10 leads to a reduction in network extension and SMC coverage and an increase in PECAM density, proliferating ECs, protruding filopodia and branch points. These findings support the theory that ECs do not undergo quiescence resulting in a lack of SMC coverage, weakening the vessel and creating are environment for developing vascular abnormalities.

AVM's can form *de novo* under certain conditions, such as wounding or during angiogenesis, and have been suggested to develop due to a lack a vascular identity and vascular dilation [134,141]. This could explain why AVM's are not seen as early as P5 in DKO mice, but need time to develop, and are formed during active angiogenesis in the post-natal retina and are therefore seen at P21 in the DKOs, when regression and blood flow is established. As well as the presence of AVMs in the DKOs at P21, highly tortuous vascular beds and the overlay of veins and arteries, where the normal spacing between the two was lost, were also observed. Previous studies showed that hypoxia can lead to an increase in overall APLNR expression throughout the network, where normally it is an early and specific venous marker, which resulted in expansion of venous capillaries while the spatial distance between arterial and venous networks was compromised [236,237]. These results can be explained by the fact that loss of BMP9 and BMP10 leads to an increase in APLNR expression, indicating towards an increase in APLN signalling and potentially a hypoxic

environment. Along with the known fact that loss of *Alk1* and *Eng* leads to AVMs, tortuous vascular beds and loss of distance between arteries and veins, the retina assay clearly showed the presence of these vascular abnormalities in the DKO retinas, although at a lower rate that the receptors KO mice, confirming BMP9 and BMP10 are important to preventing the development of these vascular abnormalities.

Once it had been determined that within the retinas there were changes in PECAM and αSMA expression, qRT-PCR of heart samples at different time points was performed. In conjunction with the retinas results, αSMA levels showed a significant reduction in expression at both 1 and 2 months while PECAM levels were only slightly elevated at 1 month of age in the DKO hearts. These results confirmed that the vascular phenotype was a global problem that displays it's most significant phenotype not long after birth where other mechanisms appear to compensate for the loss of BMP9 and BMP10 and maintain a functioning system throughout adult life. As mentioned previously when the DKO animals had been challenged with L-NAME and there was only a slight change in vasoconstriction, EM imaging gave an insight into the possible explanation for this response. EM images showed that large vessels in the DKO samples had fewer SMCs and these few SMCs were stretched tightly around the vessel for support. These SMCs in the DKO mice had lost their shape and volume as a result of the SMCs being stretched around the vessel, resulting in a thinner SMC layer. GSEA analysis of DKO aortas versus control aortas showed an upregulation of genes involved in respiration, which could be due to the loss of SMCs as a way to maintain normal function. Not much is currently known about mitochondria in smooth muscle cells although some studies have shown mitochondrial function to be involved in maintaining vascular tone, transport and vascular energy production [238]. Interestingly genes downregulated in the DKO aortas were related to cell division and maturation, meaning SMCs absent of BMP9 and BMP10 are not recruited properly or do not mature efficiently. EFNB2, a marker for defining arteries, has been shown to be dramatically reduced in *Alk1* KO mice and that BMP9 is able to induce EFNB2 expression in ECs [134,239]. Interestingly in the DKO aortas, EFNB2 expression was significantly upregulated, although BMP9 is absent, but is explained by the discovery that Notch signalling is able to compensate for this loss [239]. Overall it is important to comprehend the direct effects BMP9 and BMP10 have on ECs and SMCs as well as cross talk signalling pathways between the two and results here would suggest a possible direct interaction with BMP9 and BMP10 with SMCs but that secreted factors play a role with other signalling pathways being involved too.

The role BMP9, BMP10 and TGFβ have in the vasculature and how they work in concert or in opposition to each other is still highly controversial [140,208]. It is well understood that TGFβ signals via TGFBR2 and ALK5 while BMP9 and BMP10 signal via BMPR2 and

ALK1, however what is not well understood is the balance these two signalling pathways manage and how alterations in either of these signals can change vascular homeostasis. Singularly BMP9 and BMP10 are able to inhibit HUVEC proliferation and have a more dramatic effect when combined, reiterating their quiescent potential. Under these conditions TGFβ does not inhibit proliferation as strongly as BMP9 and BMP10, possibly due to the fact that ALK5 is not expressed on ECs [140,240,241]. However when all three compounds are added together, TGFβ is able to alleviate the degree of cellular inhibition that BMP9 and BMP10 oppose suggesting a crosstalk between these two signalling cascades. The differences in results could be due to different cell culture setups, different cell lines or the type of ligand competitive environment. One publication showed that loss of EC *Smad1* and complete *Smad5* in the embryo lead to a reduction in pericytes coverage resulting in the fusion of vessels into large cavities [183]. These embryos also addressed the question of SMAD 1/5/ - Notch signalling crosstalk, where the absence of SMAD 1/5 in ECs showed alterations in Notch signalling that resulted in an increase in protruding filopodia and a reduction in stalk cell markers, such as HEY1 [183]. This was clearing shown in the BMP9 and BMP10 DKO retinas where reduced SMAD 1/5/8 saw an increase in ERG positive cells at the angiogenic front. Therefore stimulation of HUVECS with BMP9 and BMP10 that result in a significant increase in stalk cell markers like HEY1, mentioned previously, shows that these two BMPs are important in the tip cell-stalk cell switch that regulates cellular proliferation and vessel maturation. GO analysis of these stimulated HUVECs confirmed these findings where genes highly involved in blood vessel morphogenesis and cellular differentiation were the most upregulated biological processes in the presence of BMP9 and BMP10. In line with other publications, GO analysis showed the genes involved in cell division and cell cycle were most downregulated when stimulated with BMP9 and BMP10 [119,120]. Under normal conditions vascular quiescence is achieved by the reduction of sprouting tip cells, the presence of stalk cells and the coverage of the vessel with SMCs [242].Taken together BMP9 and BMP10 could induce vascular quiescence by increasing the expression of stalk cell markers while reducing proliferation of tip cells, which would then allow for the proper recruit of SMCs and induce vascular quiescence and stability.

Till now it has not been discovered as to whether BMP9 and BMP10 are able to recruit SMCs directly or whether they control the release of signalling cues from quiescence ECs, like Apelin, that in turn recruit SMCs. To address the question of the direct effects BMP9 and BMP10 have on mSMCs, SMCs were isolated from rat and mouse aortas and directly stimulated with BMP9, BMP10 and Apelin-13. To answer the question *in vivo*, an *Alk1*$^{-/-}$ specific for SMCs needs to be generated. *In vitro* stimulation of mSMCs with BMP9 and BMP10, both individually as well as combined, saw a stark re-expression of αSMA with a

higher expression level in double stimulated cells both via immunofluorescence and qRT-PCR. Under normal culture conditions SMCs loss their contractile markers and express synthetic markers [193]. Therefore re-expression of αSMA in mSMCs would suggest that BMP9 and BMP10 can have a direct effect on SMCs and help them maintain their contractile state as well as proliferation and migration. To determine the potency of these two factors, heterozygous mice for mir143 and mir145 (*mir143*$^{+/-}$*, mir145*$^{+/-}$) were used and mSMCs were isolated. These mice were used because loss of mir143 and mir145 results in loss of contractility markers in SMCs where they are unable to re-express them [194]. Although not as dramatic as stimulation of WT mSMCs, stimulation of *mir143*$^{+/-}$*, mir145*$^{+/-}$ SMCs with BMP9 and BMP10 together resulted in an increase in αSMA showing their potency as SMC phenotypic modulators. Direct stimulation of mSMCs with BMP9 and BMP10 also showed a downregulation of *Apln* and *Aplnr*, the same result seen in HUVECs, strengthening the theory that BMP9 and BMP10 are able to target the Apelin signalling pathway. As well as direct inhibition of APLN expression, when in combination BMP9 and BMP10 are able to reduce the proliferative effects of apelin-13in in HUVECs again arguing for their ability to repress APLN expression and function. Loss of *Pdgfβ* and its receptor leads to embryonic lethality in mice due to defective SMC recruitment and are well known growth factors that are secreted from ECs and effect SMC migration and recruitment, however in our stimulated HUVEC array they are unchanged [195,243,244]. HB-EGF, also implicated in EC-SMC communication, is expressed by HUVEC's and stimulates migration in numerous SMC lines [244]. *In vitro* array data of BMP9 and BMP10 stimulated HUVECs showed increased HB-EGF's secretion meaning these BMPs are involved in EC-SMC communication. Many factors are secreted from ECs and loss of factors or higher secretion of factors may be the cause of the problems for the SMCs, therefore co-culture experiments were performed. Results were similar for APLN and αSMA, though not as dramatic, when HUVECs were stimulated with BMP9 and BMP10 and this media was added to SMCs concluding that factors secreted from ECs, or inhibition of factors, can directly affect SMC maturation and contractile phenotype. These results suggest that factors secreted from ECs, such as APLN, can effect phenotypic modulation of SMCs but that direct stimulation with BMP9 and BMP10 has a more dramatic effect.

Since the APLNR is known to be expressed on EC, SMCs and CMs eliciting various effects on them, it was hypothesised that Apelin signalling could account for the phenotypes seen in the DKO mice, where all these cell types are effected [245–247]. Upon direct stimulation of HUVECs and mSMCs with BMP9 and BMP10, *Apln* and *Aplnr*, were dramatically downregulated while loss of BMP9 and BMP10 in the heart saw an increase in both, making this a candidate gene of interest [247]. This lead to the theory that reduction of APLN levels in

our DKO mice could restore SMC coverage and reduce the hypertrophic response. *Apln*$^{-/-}$ mice were then bred with the DKO mice to generate a TKO mouse line, where loss of *Apln* was confirmed by qRT-PCR. Three criteria were used to determine if these TKO mice were a rescue; reduced cardiac hypertrophy, reduced vascular dilation and the return of proper SMC coverage. At 2 months of age these mice still had a high heart:tibia ratio, increase in aorta diameter, reduced aortic wall thickness and a lower expression of αSMA compared to WT mice. Taken together the loss of APLN in the DKO background does not rescue these animals but still displays the same phenotype.

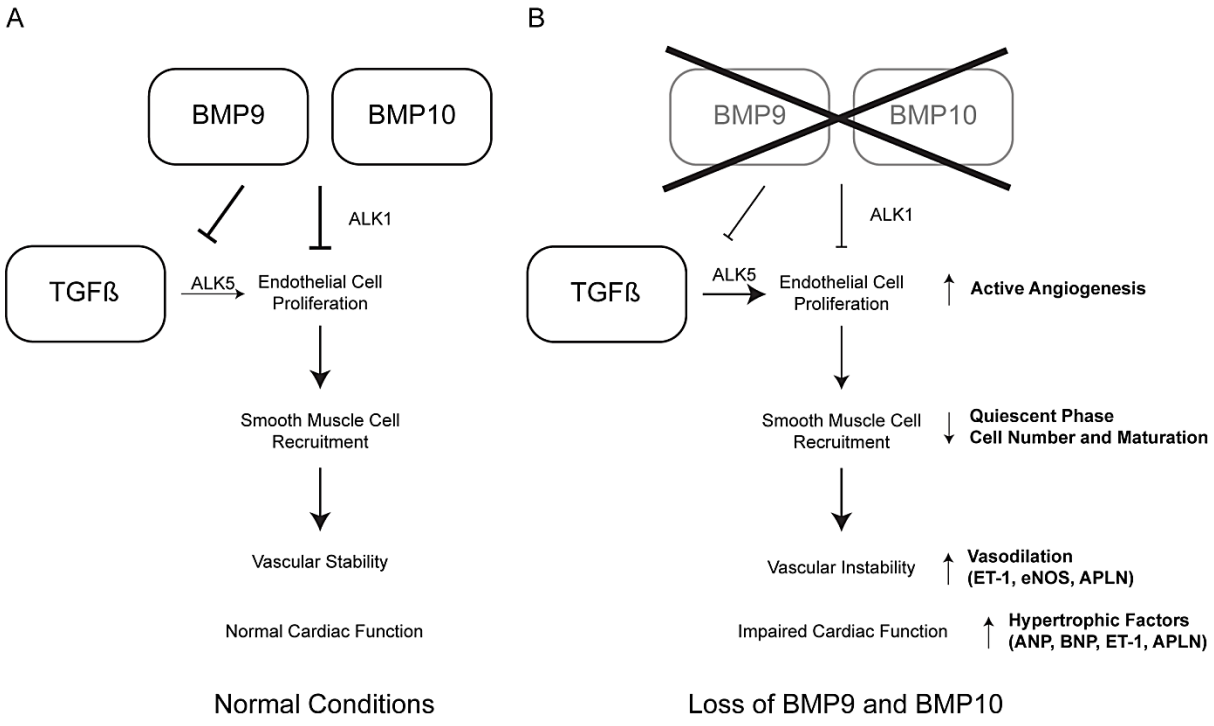

Figure 24: General overview of the role of BMP9 and BMP10 in cardiovascular homeostasis

(A) Under normal conditions BMP9 and BMP10 block EC proliferation via ALK1. BMP9 and BMP10 can work in opposition to TGFβ that also reduces signals inducing EC proliferation. This allows for the quiescence of a vessel that recruits SMCs to stabilize the network. Once vascular stability is achieved pathological stresses are not put on the heart allowing for normal cardiac function. (B) Loss of BMP9 and BMP10 does not lead to lethality like the ALK1 receptor which may be explained by other factors singling via or in conjunction with ALK1, like TGFβ. Loss of BMP9 and BMP10 results in an increase in EC proliferation, causing an active angiogenic and immature state. This results in the loss of a quiescent phase where SMCs are not recruited or proliferate and those that are present loss their contractile, mature phenotype. Losing SMCs ends in vascular instability where vasodilation occurs. This can be due to upregulation of numerous factors such as ET-1, eNOS and APLN. Vascular instability puts pressure on the heart which must remodel to deal with these stresses and it results in cardiac hypertrophy and various hemodynamic changes. Vessels themselves are able to secrete factors that cause the heart to hypertrophy such as ANP, BNP, ET-1 and APLN.

9.2 BMP9 and BMP10 as potential therapeutic targets for cardiac and vascular diseases

Pulmonary hypertension (PH) occurs when BF through the pulmonary vasculature is restricted and results in increased pressure. Increased pressure then causes a rise in right ventricle (RV) afterload, initiating an adaptive response, followed by maladaptive RV hypertrophy (RVH) because the right side of the heart must force blood through small arteries and arterioles of the lung to compensate. This condition is characterized by an imbalance in vascular tone, due to an increase in proliferation of SMCs, adventitial fibroblasts and ECs [248]. Maladaptive remodelling leads to changes in gene transcription in the right ventricle inflicting regional ischemia upon the heart where dedifferentiation of CMs then occurs alongside the accumulation of inflammatory cells all which contribute to the further decline in RV function [249–251]. However to date the mechanisms underlying PH are still not well understood due to the heterogeneous conditions this disease presents. In healthy individuals the endothelium releases numerous different growth factors and vasoactive mediators, which keep a balance between the different responses of these factors to maintain a low basal vascular tone and vascular homeostasis via vascular cell contractility and growth [248]. Currently it is thought that EC dysfunction results in a change in this important balance, where endothelium-derived vasodilators are decreased and vasoconstrictors are upregulated, which leads to severe vasoconstriction seen in patients with PH and also contributes to SMC and adventitial hypertrophy [194].

Patients with heritable forms of PH have mutations in genes encoding receptors of the TGF receptor superfamily, the majority of cases having mutations in BMPR2 but other cases also having them in the receptors for ALK1 and ENG although less frequently [252]. Patients who suffer from HHT due to mutations in *Alk1* also have an increased likelihood of displaying associated PH [253]. Patients who are haploinsufficent for BMPR2 develop PH and mice models also recapitulate this condition where *Bmpr2*$^{+/-}$ mice show an increase in pulmonary arterial pressure and vascular resistance along with an increase in wall thickness of muscularised arteries and under hypoxic conditions were not able to remodel [254]. A link between PH and HHT has been discovered by Rigelsky *et al.* where a patient who was diagnosed with PH was then later diagnosed with HHT after multiple pulmonary AVMs although they did not have any mutations in any of the HHT associated genes, *Alk1*, *Eng*, and *Smad4* [131]. Mouse models for both ALK1 and ENG show a development of PH, where there are signs of increased RVSP, RVH and a decrease in pulmonary density in adult mice over time due to oxidative stress [255,256]. Taken together these results show the importance this signalling pathway and the TGFβ receptors have in the development of PH and therefore one could speculate that BMP9 and BMP10 could play an important role in PH.

Recently a publication from Long *et al.* suggest conflicting results with this hypothesis where they demonstrated a beneficial role of enhanced BMP9 signalling during vascular remodelling in a new mouse model. This model shows mice with a heterozygous knock-in allele of a human *BMPR2* mutation (*Bmpr2*$^{+/R899X}$) which spontaneously developed PH, and injection of BMP9 can prevent apoptosis and enhance EC layer integrity having therefore a beneficial role in preventing adverse vascular remodelling during PH [257].

Our preliminary data showed that the loss of both BMP9 and BMP10 leads to dramatic changes in blood vessel integrity where EC number is slightly increased but SMC coverage is significantly reduced leading to an increased vessel diameter. BP measurements also showed the DKO mice had a lower basal BP and administration of L-NAME failed to increase BP in these mice suggesting impaired vasoconstriction. These findings are interesting as current therapies for PH mainly target drugs with vasodilative properties and our results would suggest that antagonizing BMP9 and BMP10 may represent a therapeutic approach to treat PH patients. Gene array data from the DKO mice or stimulated HUVECs revealed the changes in gene expression of key factors, including *eNOS*, *KDR*, *EDN1*, thrombospondin1 (*THBS1*) and *APLN* which are regulated by TGFβ signalling, that regulate angiogenesis, inflammation and SMC proliferation; all of which are known to be involved in the development of PH. Since ALK1 was shown to antagonize the activities of TGFβ by controlling of EC function and ALK5 mediates proliferation of SMCs from patients with PH this raises the possibility that BMP9 and BMP10 induces vascular quiescence by antagonizing TGFβ signalling via cross-talk between ALK1 and ALK5 receptors [66]. An explanation of these controversial and opposing results might be due to the differences in the mouse models used or the differences in time where we use a model with persistent loss of BMP9 and BMP10 and where they administer BMP9 over a short space of time. Taken together it is known that BMP9 and BMP10, via ALK1, are critical for vascular development and that changes in this signalling pathway leads to changes in vascular homeostasis and in some cases could be involved in the vascular pathogenesis of PH while could also be new potential therapeutic targets for the treatment of PH.

During HF or MI, CMs undergo cell death due to lack of blood flow in a certain region of the heart resulting in an acute imbalance between oxygen supply and demand causing damage to the heart muscle [258]. As mentioned previously MIs normally occur due to coronary artery disease where a blockage of a coronary artery could be a result of a ruptured atherosclerotic plaque or due to other obstructions. Numerous risk factors are involved which can include elevated BP, high blood cholesterol, side effect of diabetes, or life style choices like smoking, lack of exercise, obesity, poor diet, and excessive alcohol consumption [259]. After MI, reperfusion is performed as an attempt to re-establish blood flow

to the damaged area, although during the early phase this may cause further injury as the recruitment and activation of inflammatory cells is needed for cardiac healing [251]. The extent of post infarction remodelling depends largely on the size of the initial infarct and the quality of cardiac repair. A major issue to overcome after MI is the fact that CMs have a low regenerative capacity and after MI there is a loss of a large number of CMs, hence why scar formation is essential. The cardiac repair program is needed to clear the wound of dead cells and ECM debris, as well as providing molecular signals for activation of reparative cells [260]. Incorrect timing or too long a duration can have fatal effects; while an increase in early inflammation can lead to ECM degradation resulting in cardiac rupturing, prolonged inflammation can impair collagen deposition leading to weak scar formation resulting in chamber dilation. Enhanced severe inflammation activates proapoptotic signalling increasing the loss of CMs and lastly defective containment of the inflammation response results in an expansion into the non-infarcted area which enhances fibrosis and decreases cardiac performance [260]. Numerous different cell groups are vital for the initial response however evidence also supports the theory that other cells, such as neutrophils, mononuclear cells, ECs, and pericytes, also contribute to the suppression and resolution phase of the inflammatory reaction [260]. Here the importance of vascular cells, ECs and SMCs, and the role the vasculature is seen where ECs synthesize and present chemokines and adhesion molecules to allow for adhesion of inflammatory cells. An increase in angiogenesis is necessary to provide oxygen and nutrients to areas of damage to allow for healing and a reduction in infarct size and it has been shown that there is a high increase in EC number a few hours after infarction as these new vessels are highly permeable due to the lack of SMC coverage [261]. Work by Ren *et al.* demonstrates that maturation of scar formation depends on the recruitment of mural cells which give stability to the scar and are also able to promote resolution as they repress granulation tissue formation [262].

To date extensive work on the role of ALK1 has not been carried out although there is some evidence for its potential role in cardiac remodelling after MI. The main argument for this hypothesis is the known role that ALK1 plays in ECM expression and production in various cell types, such as myoblasts, fibroblasts and ECs, although ALK1's role and effect is context dependent [263–265]. No studies have been performed to understand the role of ALK1 on cardiac fibroblasts and MI. However the role of ENG during cardiac remodelling has been studied. Mice heterozygous for *Eng* (*Eng*$^{+/-}$) underwent thoracic aortic constriction (TAC), where a knot is tied around the transverse aorta to induce pressure overload HF, and were shown to have reduced cardiac fibrosis [266,267]. Knowing that ALK1 and ENG work closely together to regulate gene expression indicates ALK1 could also regulate cardiac fibrosis. Again not much is known about ALK1 and the immune response but it has been shown that

ALK1 is expressed by macrophages and monocytes [268,269]. *Eng*$^{+/-}$ mice that underwent renal ischaemia–reperfusion showed less signs of injury concluding that these mice may be protected from injury due to reduced endothelial activation and macrophage maturation [270]. Recent reports have suggested the BMP9 plays a role in fibrosis *in vitro* where they demonstrated that BMP9 is a profibrotic factor in fibroblasts by promoting ECM protein expression through both, ALK1 and ALK5 receptors [172]. Although in depths studies into BMP10 and its fibrotic potential have not been carried out, overexpression of BMP10 in a murine model was not associated with cardiac fibrosis but disrupted post-natal hypertrophic growth [189].

After the initial response of ECM deposit and immune cell infiltration to ensure the least amount of damage, angiogenesis is needed in the damage area to ensure survival of the tissue. As a model of MI normally a permanent ligation of the left anterior descending artery (LAD) is carried out. The LAD is ligated with one single stitch, forming an ischemia that can be seen almost immediately. By closing the LAD, no further blood flow is permitted in that area, while the surrounding myocardial tissue is nearly not affected [271]. Reperfusion of the ischemic area is essential in salvaging damaged tissue; therefore angiogenesis plays a major role in this process. There are a number of important signalling pathways that are involved in myocardial angiogenesis after an infarction has occurred. One pathway involved is HIF1α that is activated under hypoxic conditions and can activate a number of target genes such as *Vegf* or *Cxcl12*, which are important for the angiogenic response and chemokine response of progenitor cells respectively [272]. Two HIF isoforms, HIF1α and HIF2α, have been shown to be expressed in the early stages after MI in ECs, CMs and inflammatory cells, where mice that constantly express HIF1α in CMs have an improved cardiac performance which has been correlated to increased levels of VEGF and angiogenesis [273,274]. Data from the gene array of stimulated HUVECs with BMP9 and BMP10 showed that there was an increase in *HIF1α* expression while the gene array of the DKO hearts showed with a slight reduction in *HIF1α* levels. Studies in different cell culture conditions, such as mesenchymal stromal progenitor cells, have shown that BMP9 is able to induce *HIF1α* expression via SMAD1/5/8 and is important for angiogenic signalling [275]. CXCR4, the receptor for CXCL12, was shown to protect mice after MI where *Cxcr4* $^{+/-}$ mice had a smaller but more fibrotic scar that underwent an acute inflammatory response and an improved adaptation of cardiomyocytes [276]. This response in these mice however was counter balanced by an impaired outgrowth of cells, myocardial neovascularization and coronary flow recovery after MI which ultimately resulted in a defective ventricular function [276]. Loss of BMP9 and BMP10 in the heart showed a dramatic decrease in *Cxcl12* expression while stimulated HUVECs saw a 2 fold increase in *CXCL12* expression,

suggesting a role for BMP9 and BMP10 in cardiac remodelling after MI. Taken together these results show the BMP9 and BMP10 are able to regulate target genes important in the angiogenic processes needed after MI.

VEGF family members also play a major role in post MI angiogenesis and are known to be rapidly expressed in the heart of humans and rodents following MI due to the hypoxic environment but also due to mechanical stress [277–279]. Interactions between these family members are essential during different phases as VEGFA is able to initiate the formation of immature vessels but if the signalling is not switched off these vessels become leaky and disorganized as VEGFA can inhibit PDGFB signalling, altering mural cell recruitment, which is essential for vessel maturation [280–282]. Another family member that is able to bind VEGFR1 is Placental Growth Factor (PlGF) which activates angiogenesis after MI [283,284]. Other family members such as VEGFB or VEGFC do not have such a clear role in angiogenesis after MI as other family members do. Rather than having a direct effect and role on angiogenesis VEGF-B could be more responsible for its prosurvival actions that may allow newly formed vessels to survive and mature in the damaged area allowing for the return of blood flow and preventing long term adverse remodelling [285]. In the case of VEGFC it is known to play a role in lymphangiogenesis via VEGFR3 and early findings have suggested it may play a role in promoting angiogenesis in an indirect manner by promoting PDGFB expression which would allow for vessel maturation [285]. Stimulation of HUVECs with BMP9 and BMP10 showed regulation of *VEGFA*, *VEGFB* and *VEGFC*, again implying the cross-talk that occurs between these two signalling pathways and the important role angiogenesis has in reducing damaged tissue after MI [208]. Taken together this data could suggest that BMP9 and BMP10 are involved in the repair response after MI seeing as other members of this super protein family have been reported to also be involved.

Overall these results show the importance of a mature and stable vascular network for systemic vascular homeostasis but also how essential homeostasis is to prevent disease conditions and especially during remodelling and prevention of damage to an already deteriorating area. The role of BMP9 and BMP10 is clear in maintaining vascular quiescence in a normal situation where active angiogenesis is not needed. Loss of these two proteins under basal conditions leads to an increase in vessel dilation due to active ECs and a lack of SMC coverage which results in lower basal BP. This is turn increases blood volume within the vascular system which puts extra pressure on the heart causing the ventricles to increase in size. However under these circumstances the ventricular wall does not dilate and fibrosis does not occur therefore suggesting this is not a pathological response. Hypertrophy is due to the CMs increasing in size in response to the pressure of the extra blood within the system and lethality does not occur as cardiac function still remains with contracting,

functioning CMs. One possible downstream target that could have explained the different changes seen was *Apln*, as *Apln* expression increases when BMP9 and BMP10 are lost and *in vitro* stimulation of HUVECs with BMP9 and BMP10 leads to a drastic decrease in *APLN* levels. APLN has been shown to inhibit apoptosis in ECs which allows for an increase in angiogenic potential along with an increase in eNOS secretion, higher levels of eNOS signal to SMCs to allow for vasodilation but also an increase in APLN in SMCs directly blocks proliferation and recruitment of SMCs. APLN affects CMs by inducing hypertrophy but also keeping them contractile while preventing fibrosis and apoptosis. Taken together this could have explained much of what was seen in these DKO mice. Preliminary data in the TKO mice generated shows that loss of *Apln* in the DKO mice does not rescue them. This could be due to the fact that one gene cannot account for everything because multiple factors and signalling pathways are also known to play important roles in this hypertrophic response. Loss of BMP9 and BMP10 in a disease model may possess beneficial aspects. For example in PH where SMCs are affected and blood vessels are constricted causing elevation in BP and therefore RV hypertrophy and failure loss of these two proteins won't allow for vascular constriction due to loss of SMC coverage and therefore may not develop severe cases of PH. Or even in MI where tissue damage has occurred, CMs may be protected from apoptosis and there hypertrophic response may allow for a reduction in scar formation, seeing as BMP9 has been proposed as a pro-fibrotic factor, but also due to the increase in vascular dilation and increase in angiogenesis allowing for better perfusion and access of nutrients to prevent tissue death.

9.3 Thesis perspective

To date the direct role of BMP9 and BMP10 in maintaining cardiovascular homeostasis has not been addressed. In this thesis the first conditional BMP10 KO mouse and BMP9 and 10 DKO mice were generated and used to answer essential questions regarding the function of BMP9 and BMP10 in angiogenesis and cardiac function as well as their overlapping roles. Loss of BMP9 and BMP10 leads to alterations in vascular structure characterised by an increase in active ECs and a reduction in SMC coverage, resulting in dilation of blood vessels. Changes in the vascular structure also lead to alterations in vascular hemodynamics, with a significantly reduced basal BP and an increased BF and BV. Global gene transcription analysis of DKO hearts and aortas showed an increase in genes involved in angiogenesis and epithelial cell migration while genes governing cell maturation and SMC division were reduced. *In vitro* data demonstrated that HUVECs stimulated with BMP9 and BMP10 resulted in a global upregulation of genes that are essential for vascular morphogenesis and EC differentiation while genes involved in cell cycle regulation and division were downregulated. Overall these results clearly show that BMP9 and BMP10 play an important role in adult vascular morphogenesis and in maintaining vascular stability. Further, it is very likely that this disruption to vascular homeostasis is responsible for the cardiac defects observed in DKO mice, namely; a significant decrease in EF and an increase in SV and LVM. Increased pre-load as a result of higher blood volume and flow leads to an overall hypertrophic response, essentially an adaptation to the changes in vascular hemodynamics.

These results show how BMP9 and BMP10 function to mediate the intrinsic relationship between the cardiovascular system and cardiac remodelling and function. This new DKO model will be extremely useful for understanding the molecular mechanisms responsible for the development of vascular diseases such as HHT, atherosclerosis and vascular calcification as well as other diseases such as in PH or MI. Future development of agonists or antagonists for BMP9 and BMP10 may serve as a novel therapeutic approach to target this group of diseases.

10 References

1. Townsend, N., Nichols, M., Scarborough, P. & Rayner, M. Cardiovascular disease in Europe - epidemiological update 2015. *Eur. Heart J.* **36,** 2696–2705 (2015).
2. Townsend, N., Nichols, M., Scarborough, P. & Rayner, M. Cardiovascular disease in Europe: Epidemiological update. *Eur. Heart J.* **34,** 3028–3034 (2013).
3. Townsend, N., Nichols, M., Scarborough, P. & Rayner, M. Cardiovascular disease in Europe 2014: Epidemiological update. *Eur. Heart J.* **35,** 2950–2959 (2014).
4. Segers, V. F. M. & Lee, R. T. Stem-cell therapy for cardiac disease. *Nature* **451,** 937–942 (2008).
5. Mayo Clinic Staff. Heart Disease. (2014). at <http://www.mayoclinic.org/diseases-conditions/heart-disease/basics/definition/con-20034056>
6. Reinecke, H., Minami, E., Zhu, W.-Z. & Laflamme, M. A. Cardiogenic differentiation and transdifferentiation of progenitor cells. *Circ. Res.* **103,** 1058–71 (2008).
7. Frangogiannis, N. G. The immune system and cardiac repair. *Pharmacol. Res.* **58,** 88–111 (2008).
8. Porrello, E. R. & Olson, E. N. A neonatal blueprint for cardiac regeneration. *Stem Cell Res.* **13,** 556–70 (2014).
9. Kennedy-Lydon, T. & Rosenthal, N. Cardiac regeneration: epicardial mediated repair. *Proc Biol Sci.* **282,** (2015).
10. Hazebroek, M., Dennert, R. & Heymans, S. Idiopathic dilated cardiomyopathy: possible triggers and treatment strategies. *Netherlands Hear. J.* **20,** 332–335 (2012).
11. Kelvinsong - Own work, C. B.-S. 3. . Diagram of blood vessel structures. at <https://commons.wikimedia.org/w/index.php?curid=25165240>
12. Risau, W. *et al.* Vasculogenesis and angiogenesis in embryonic-stem-cell-derived embryoid bodies. *Development* **102,** 471–478 (1988).
13. Bai, H. & Wang, Z. Z. Directing human embryonic stem cells to generate vascular progenitor cells. *Gene Ther.* **15,** 89–95 (2008).
14. Swift, M. R. & Weinstein, B. M. Arterial-venous specification during development. *Circ. Res.* **104,** 576–588 (2009).
15. Eguchi, M., Masuda, H. & Asahara, T. Endothelial progenitor cells for postnatal vasculogenesis. *Clin. Exp. Nephrol.* **11,** 18–25 (2007).
16. Caprioli, a *et al.* Hemangioblast commitment in the avian allantois: cellular and molecular aspects. *Dev. Biol.* **238,** 64–78 (2001).
17. Patel-Hett, S. & D'Amore, P. A. Signal transduction in vasculogenesis and developmental angiogenesis. *Int. J. Dev. Biol.* **55,** 353–363 (2011).
18. Rhee, J. M. & Iannaccone, P. M. Mapping mouse hemangioblast maturation from headfold stages. *Dev. Biol.* **365,** 1–13 (2012).
19. Palis, J. & Yoder, M. C. Yolk-sac hematopoiesis: The first blood cells of mouse and man. *Exp. Hematol.* **29,** 927–936 (2001).
20. Drake, C. J. Embryonic and adult vasculogenesis. *Birth Defects Res. Part C - Embryo Today Rev.* **69,** 73–82 (2003).
21. Reagan, F. Vascularization phenomena in fragments of embryonic bodies completely isolated from yolk-sac blastoderm. *Anat. Rec.* **9,** 329–341 (1915).
22. Sabin, F. Studies on the origin of blood-vessels and of red blood-corpuscles as seen in the living blastoderm of chicks during the second day of incubation. *Contrib Embryol* **36,** 213–259 (1920).
23. Pardanaud, L. & Dieterlen-Lièvre, F. Emergence of endothelial and hemopoietic cells in the avian embryo. *Anat. Embryol. (Berl).* **187,** 107–14 (1993).
24. Potente, M., Gerhardt, H. & Carmeliet, P. Basic and therapeutic aspects of angiogenesis. *Cell* **146,** 873–887 (2011).
25. Risau, W. & Flamme, I. Vasculogenesis. *Annu. Rev. Cell Dev. Biol.* **11,** 73–91 (1995).
26. Lucitti, J. L. *et al.* Vascular remodeling of the mouse yolk sac requires hemodynamic force. *Development* **134,** 3317–3326 (2007).
27. Pardanaud, L., Yassine, F. & Dieterlen-Lievre, F. Relationship between vasculogenesis, angiogenesis and haemopoiesis during avian ontogeny. *Development* **105,** 473–485 (1989).

28. Ribatti, D., Nico, B. & Crivellato, E. Morphological and molecular aspects of physiological vascular morphogenesis. *Angiogenesis* **12,** 101–111 (2009).
29. Cox, C. M. & Poole, T. J. Angioblast differentiation is influenced by the local environment: FGF-2 induces angioblasts and patterns vessel formation in the quail embryo. *Dev. Dyn.* **218,** 371–382 (2000).
30. Dyer, M. a, Farrington, S. M., Mohn, D., Munday, J. R. & Baron, M. H. Indian hedgehog activates hematopoiesis and vasculogenesis and can respecify prospective neurectodermal cell fate in the mouse embryo. *Development* **128,** 1717–1730 (2001).
31. Vokes, S. a *et al.* Hedgehog signaling is essential for endothelial tube formation during vasculogenesis. *Development* **131,** 4371–4380 (2004).
32. Takashima, S. *et al.* Targeting of both mouse neuropilin-1 and neuropilin-2 genes severely impairs developmental yolk sac and embryonic angiogenesis. *Proc. Natl. Acad. Sci. U. S. A.* **99,** 3657–62 (2002).
33. Kawasaki, T. *et al.* A requirement for neuropilin-1 in embryonic vessel formation. *Development* **126,** 4895–4902 (1999).
34. Patan, S. Vasculogenesis and angiogenesis as mechanisms of vascular network formation, growth and remodeling. *J. Neurooncol.* **50,** 1–15 (2000).
35. Choi, K., Kennedy, M., Kazarov, a, Papadimitriou, J. C. & Keller, G. A common precursor for hematopoietic and endothelial cells. *Development* **125,** 725–732 (1998).
36. Yamaguchi, T. P., Dumont, D. J., Conlon, R. a, Breitman, M. L. & Rossant, J. Flk-1, an Flt-Related Receptor Tyrosine Kinase Is an Early Marker for Endothelial Cell Precursors. *Development* **118,** 489–498 (1993).
37. Dickson, M. C. *et al.* Defective haematopoiesis and vasculogenesis in transforming growth factor-beta 1 knock out mice. *Development* **121,** 1845–1854 (1995).
38. Larsson, J. *et al.* Abnormal angiogenesis but intact hematopoietic potential in TGF-β type I receptor-deficient mice. *EMBO J.* **20,** 1663–1673 (2001).
39. Oshima, M., Oshima, H. & Taketo, M. M. TGF-beta receptor type II deficiency results in defects of yolk sac hematopoiesis and vasculogenesis. *Dev. Biol.* **179,** 297–302 (1996).
40. Crosby, C. V *et al.* VE-cadherin is not required for the formation of nascent blood vessels but acts to prevent their disassembly. *Blood* **105,** 2771–2776 (2005).
41. Krüger, O. *et al.* Defective vascular development in connexin 45-deficient mice. *Development* **127,** 4179–4193 (2000).
42. Hirashima, M. Regulation of endothelial cell differentiation and arterial specification by VEGF and Notch signaling. *Anat. Sci. Int.* **84,** 95–101 (2009).
43. Wang, H. U., Chen, Z. F. & Anderson, D. J. Molecular distinction and angiogenic interaction between embryonic arteries and veins revealed by ephrin-B2 and its receptor Eph-B4. *Cell* **93,** 741–753 (1998).
44. Herzog, Y., Kalcheim, C., Kahane, N., Reshef, R. & Neufeld, G. Differential expression of neuropilin-1 and neuropilin-2 in arteries and veins. *Mech. Dev.* **109,** 115–119 (2001).
45. Gerety, S. S., Wang, H. U., Chen, Z. F. & Anderson, D. J. Symmetrical mutant phenotypes of the receptor EphB4 and its specific transmembrane ligand ephrin-B2 in cardiovascular development. *Mol. Cell* **4,** 403–414 (1999).
46. Herzog, Y., Guttmann-Raviv, N. & Neufeld, G. Segregation of arterial and venous markers in subpopulations of blood islands before vessel formation. *Dev. Dyn.* **232,** 1047–55 (2005).
47. Villa, N. *et al.* Vascular expression of Notch pathway receptors and ligands is restricted to arterial vessels. *Mech. Dev.* **108,** 161–164 (2001).
48. Alva, J. A. & Iruela-Arispe, M. L. Notch signaling in vascular morphogenesis. *Curr. Opin. Hematol.* **11,** 278–283 (2004).
49. Duarte, A. *et al.* Dosage-sensitive requirement for mouse Dll4 in artery development. *Genes Dev.* **18,** 2474–2478 (2004).
50. Patan, S. Vasculogenesis and angiogenesis. *Cancer Treat. Res.* **117,** 3–32 (2004).
51. Carmeliet, P. & Jain, R. K. Molecular mechanisms and clinical applications of angiogenesis. *Nature* **473,** 298–307 (2011).
52. Mazzone, M. *et al.* Heterozygous deficiency of PHD2 restores tumor oxygenation and inhibits metastasis via endothelial normalization. *Cell* **136,** 839–851 (2009).
53. Bergers, G. & Song, S. The role of pericytes in blood-vessel formation and maintenance. *Neuro. Oncol.* **7,** 452–464 (2005).
54. Augustin, H. G., Koh, G. Y., Thurston, G. & Alitalo, K. Control of vascular morphogenesis and homeostasis through the angiopoietin-Tie system. *Nat. Rev. Mol. Cell Biol.* **10,** 165–177 (2009).

55. Rundhaug, J. Matrix metalloproteinases and angiogenesis. *J. Cell. Mol. Med.* **9,** 267–285 (2005).
56. Gerhardt, H. *et al.* VEGF guides angiogenic sprouting utilizing endothelial tip cell filopodia. *J. Cell Biol.* **161,** 1163–1177 (2003).
57. Blanco, R. & Gerhardt, H. VEGF and Notch in tip and stalk cell selection. *Cold Spring Harb. Perspect. Med.* **3,** a006569 (2013).
58. Phng, L. K. & Gerhardt, H. Angiogenesis: A Team Effort Coordinated by Notch. *Dev. Cell* **16,** 196–208 (2009).
59. Jakobsson, L. *et al.* Endothelial cells dynamically compete for the tip cell position during angiogenic sprouting. *Nat. Cell Biol.* **12,** 943–953 (2010).
60. Benedito, R. *et al.* The Notch Ligands Dll4 and Jagged1 Have Opposing Effects on Angiogenesis. *Cell* **137,** 1124–1135 (2009).
61. Bali, J. & Bali, R. Pathological ocular angiogenesis in diabetes: A perspective of emerging paradigms and current evidence. *J. Clin. Ophthalmol. Res.* **1,** 3–10 (2013).
62. Aspalter, I. M. *et al.* Alk1 and Alk5 inhibition by Nrp1 controls vascular sprouting downstream of Notch. *Nat. Commun.* **6,** 7264 (2015).
63. Hellström, M. *et al.* Dll4 signalling through Notch1 regulates formation of tip cells during angiogenesis. *Nature* **445,** 776–780 (2007).
64. Siekmann, A. F. & Lawson, N. D. Notch signalling limits angiogenic cell behaviour in developing zebrafish arteries. *Nature* **445,** 781–784 (2007).
65. Tammela, T. *et al.* VEGFR-3 controls tip to stalk conversion at vessel fusion sites by reinforcing Notch signalling. *Nat. Cell Biol.* **13,** 1202–1213 (2011).
66. Goumans, M. J. *et al.* Balancing the activation state of the endothelium via two distinct TGF-β type I receptors. *EMBO J.* **21,** 1743–1753 (2002).
67. Muller, G., Behrens, J., Nussbaumer, U., Bohlen, P. & Birchmeier, W. Inhibitory action of transforming growth factor beta on endothelial cells. *Proc Natl Acad Sci U S A* **84,** 5600–5604 (1987).
68. Ito, C., Akimoto, T., Ioka, T., Kobayashi, T. & Kusano, E. TGF-beta inhibits vascular sprouting through TGF-beta type I receptor in the mouse embryonic aorta. *The Tohoku journal of experimental medicine* **218,** 63–71 (2009).
69. Mallet, C., Vittet, D., Feige, J.-J. & Bailly, S. TGFbeta1 induces vasculogenesis and inhibits angiogenic sprouting in an embryonic stem cell differentiation model: respective contribution of ALK1 and ALK5. *Stem Cells* **24,** 2420–7 (2006).
70. Gerhardt, H. *et al.* Neuropilin-1 is required for endothelial tip cell guidance in the developing central nervous system. *Dev. Dyn.* **231,** 503–509 (2004).
71. Fantin, A. *et al.* NRP1 acts cell autonomously in endothelium to promote tip cell function during sprouting angiogenesis. *Blood* **121,** 2352–2362 (2013).
72. Jones, E. a V, Yuan, L., Breant, C., Watts, R. J. & Eichmann, A. Separating genetic and hemodynamic defects in neuropilin 1 knockout embryos. *Development* **135,** 2479–2488 (2008).
73. Neufeld, G. *et al.* The neuropilins: Multifunctional semaphorin and VEGF receptors that modulate axon guidance and angiogenesis. *Trends in Cardiovascular Medicine* **12,** 13–19 (2002).
74. Glinka, Y. & Prud'homme, G. J. Neuropilin-1 is a receptor for transforming growth factor beta-1, activates its latent form, and promotes regulatory T cell activity. *J. Leukoc. Biol.* **84,** 302–310 (2008).
75. He, Z. & Tessier-Lavigne, M. Neuropilin is a receptor for the axonal chemorepellent semaphorin III. *Cell* **90,** 739–751 (1997).
76. Soker, S., Takashima, S., Miao, H. Q., Neufeld, G. & Klagsbrun, M. Neuropilin-1 is expressed by endothelial and tumor cells as an isoform-specific receptor for vascular endothelial growth factor. *Cell* **92,** 735–745 (1998).
77. Sörensen, I., Adams, R. H. & Gossler, A. DLL1-mediated Notch activation regulates endothelial identity in mouse fetal arteries. *Blood* **113,** 5680–5688 (2009).
78. Korn, C. & Augustin, H. G. Mechanisms of Vessel Pruning and Regression. *Dev. Cell* **34,** 5–17 (2015).
79. Mallat, Z. & Tedgui, a. Apoptosis in the vasculature: mechanisms and functional importance. *Br. J. Pharmacol.* **130,** 947–962 (2000).
80. Pauli, A. *et al.* Toddler: an embryonic signal that promotes cell movement via Apelin receptors. *Science* **343,** 1248636 (2014).
81. Lang, R., Lustig, M., Francois, F., Sellinger, M. & Plesken, H. Apoptosis during macrophage-

dependent ocular tissue remodelling. *Development* **120,** 3395–403 (1994).
82. Mitchell, C. A., Risau, W. & Drexler, H. C. Regression of vessels in the tunica vasculosa lentis is initiated by coordinated endothelial apoptosis: a role for vascular endothelial growth factor as a survival factor for endothelium. *Dev. Dyn.* **213,** 322–33 (1998).
83. Dimmeler, S. & Zeiher, a M. Endothelial cell apoptosis in angiogenesis and vessel regression. *Circ. Res.* **87,** 434–439 (2000).
84. Wietecha, M. S., Cerny, W. L. & DiPietro, L. A. Mechanisms of vessel regression: toward an understanding of the resolution of angiogenesis. *Curr Top Microbiol Immunol* **367,** 3–32 (2013).
85. Franco, C. A. *et al.* Dynamic endothelial cell rearrangements drive developmental vessel regression. *PLoS Biol.* **13,** e1002125 (2015).
86. Paszkowiak, J. J. & Dardik, A. Arterial wall shear stress: observations from the bench to the bedside. *Vasc. Endovascular Surg.* **37,** 47–57 (2003).
87. Dekker, R. J. *et al.* Endothelial KLF2 Links Local Arterial Shear Stress Levels to the Expression of Vascular Tone-Regulating Genes. *Am. J. Pathol.* **167,** 609–618 (2005).
88. Lobov, I. B. *et al.* The DII4/notch pathway controls postangiogenic blood vessel remodeling and regression by modulating vasoconstriction and blood flow. *Blood* **117,** 6728–6737 (2011).
89. Korn, C. *et al.* Endothelial cell-derived non-canonical Wnt ligands control vascular pruning in angiogenesis. *Development* **141,** 1757–1766 (2014).
90. Salvucci, O. *et al.* EphrinB2 controls vessel pruning through STAT1-JNK3 signalling. *Nat. Commun.* **6,** 6576 (2015).
91. Pardali, E., Goumans, M. J. & ten Dijke, P. Signaling by members of the TGF-β family in vascular morphogenesis and disease. *Trends in Cell Biology* **20,** 556–567 (2010).
92. Gaengel, K., Genové, G., Armulik, A. & Betsholtz, C. Endothelial-mural cell signaling in vascular development and angiogenesis. *Arteriosclerosis, Thrombosis, and Vascular Biology* **29,** 630–638 (2009).
93. Huang, H., Bhat, A., Woodnutt, G. & Lappe, R. Targeting the ANGPT-TIE2 pathway in malignancy. *Nat. Rev. Cancer* **10,** 575–585 (2010).
94. Pitulescu, M. E. & Adams, R. H. Eph/ephrin molecules - A hub for signaling and endocytosis. *Genes Dev.* **24,** 2480–2492 (2010).
95. Gridley, T. Notch signaling in the vasculature. *Curr. Top. Dev. Biol.* **92,** 277–309 (2010).
96. Arroyo, A. G. & Iruela-Arispe, M. L. Extracellular matrix, inflammation, and the angiogenic response. *Cardiovasc. Res.* **86,** 226–235 (2010).
97. Blasi, F. & Carmeliet, P. uPAR: a versatile signalling orchestrator. *Nat. Rev. Mol. Cell Biol.* **3,** 932–943 (2002).
98. Davies, P. F. Flow-mediated endothelial mechanotransduction. *Physiol. Rev.* **75,** 519–60 (1995).
99. Hahn, C. & Schwartz, M. A. Mechanotransduction in vascular physiology and atherogenesis. *Nat. Rev. Mol. Cell Biol.* **10,** 53–62 (2009).
100. Osawa, M., Masuda, M., Harada, N., Lopes, R. B. & Fujiwara, K. Tyrosine phosphorylation of platelet endothelial cell adhesion molecule-1 (PECAM-1, CD31) in mechanically stimulated vascular endothelial cells. *Eur. J. Cell Biol.* **72,** 229–237 (1997).
101. Tzima, E. *et al.* A mechanosensory complex that mediates the endothelial cell response to fluid shear stress. *Nature* **437,** 426–431 (2005).
102. Shay-Salit, A. *et al.* VEGF receptor 2 and the adherens junction as a mechanical transducer in vascular endothelial cells. *Proc. Natl. Acad. Sci. U. S. A.* **99,** 9462–9467 (2002).
103. Conway, D. E. & Schwartz, M. a. Flow-dependent cellular mechanotransduction in atherosclerosis. *J. Cell Sci.* **126,** 5101–9 (2013).
104. Nigro, P., Abe, J.-I. & Berk, B. C. Flow shear stress and atherosclerosis: a matter of site specificity. *Antioxid. Redox Signal.* **15,** 1405–14 (2011).
105. Davies, P. & Barbee, K. Endothelial cell surface imaging: insights into hemodynamic force transduction. *Physiology (Bethesda).* 153–157 (1994).
106. Wang, C., Baker, B. M., Chen, C. S. & Schwartz, M. A. Endothelial cell sensing of flow direction. *Arterioscler. Thromb. Vasc. Biol.* **33,** 2130–2136 (2013).
107. Haga, J. H., Li, Y.-S. J. & Chien, S. Molecular basis of the effects of mechanical stretch on vascular smooth muscle cells. *J. Biomech.* **40,** 947–960 (2007).
108. Laughlin, M. H., Newcomer, S. C. & Bender, S. B. Importance of hemodynamic forces as signals for exercise-induced changes in endothelial cell phenotype. *J. Appl. Physiol.* **104,** 588–600 (2008).
109. Weiss, A. & Attisano, L. The TGFbeta superfamily signaling pathway. *Wiley Interdiscip. Rev.*

Dev. Biol. **2,** 47–63 (2013).
110. Tillet, E. & Bailly, S. Emerging roles of BMP9 and BMP10 in hereditary hemorrhagic telangiectasia. *Front. Genet.* **5,** 456 (2014).
111. Susan-Resiga, D. *et al.* Furin is the major processing enzyme of the cardiac-specific growth factor bone morphogenetic protein 10. *J. Biol. Chem.* **286,** 22785–94 (2011).
112. Bidart, M. *et al.* BMP9 is produced by hepatocytes and circulates mainly in an active mature form complexed to its prodomain. *Cell. Mol. life Sci.* **69,** 313–24 (2012).
113. David, L., Mallet, C., Mazerbourg, S., Feige, J. J. & Bailly, S. Identification of BMP9 and BMP10 as functional activators of the orphan activin receptor-like kinase 1 (ALK1) in endothelial cells. *Blood* **109,** 1953–1961 (2007).
114. Chen, H. *et al.* Context-dependent signaling defines roles of BMP9 and BMP10 in embryonic and postnatal development. *Proc. Natl. Acad. Sci. U. S. A.* **110,** 11887–92 (2013).
115. Jiang, H. *et al.* The Prodomain-Bound Form of Bone Morphogenetic Protein 10 is Biologically Active on Endothelial Cells. *JBC* (2015).
116. Miller, A. F., Harvey, S. A., Thies, R. S. & Olson, M. S. Bone morphogenetic protein-9. An autocrine/paracrine cytokine in the liver. *J. Biol. Chem.* **275,** 17937–45 (2000).
117. Neuhaus, H., Rosen, V. & Thies, R. S. Heart specific expression of mouse BMP-10 a novel member of the TGF-beta superfamily. *Mech. Dev.* **80,** 181–4 (1999).
118. Chen, H. *et al.* BMP10 is essential for maintaining cardiac growth during murine cardiogenesis. *Development* **131,** 2219–2231 (2004).
119. David, L. *et al.* Bone morphogenetic protein-9 is a circulating vascular quiescence factor. *Circ. Res.* **102,** 914–922 (2008).
120. Ricard, N. *et al.* BMP9 and BMP10 are critical for postnatal retinal vascular remodeling. *Blood* **119,** 6162–6171 (2012).
121. Scharpfenecker, M. *et al.* BMP-9 signals via ALK1 and inhibits bFGF-induced endothelial cell proliferation and VEGF-stimulated angiogenesis. *J. Cell Sci.* **120,** 964–972 (2007).
122. Shi, Y. & Massagué, J. Mechanisms of TGF-beta signaling from cell membrane to the nucleus. *Cell* **113,** 685–700 (2003).
123. Townson, S. a *et al.* Specificity and structure of a high affinity activin receptor-like kinase 1 (ALK1) signaling complex. *J. Biol. Chem.* **287,** 27313–25 (2012).
124. Castonguay, R. *et al.* Soluble endoglin specifically binds bone morphogenetic proteins 9 and 10 via its orphan domain, inhibits blood vessel formation, and suppresses tumor growth. *J. Biol. Chem.* **286,** 30034–30046 (2011).
125. Itoh, S. & ten Dijke, P. Negative regulation of TGF-beta receptor/Smad signal transduction. *Curr. Opin. Cell Biol.* **19,** 176–84 (2007).
126. Rider, C. C. & Mulloy, B. Bone morphogenetic protein and growth differentiation factor cytokine families and their protein antagonists. *Biochem. J.* **429,** 1–12 (2010).
127. Schmierer, B. & Hill, C. S. TGFbeta-SMAD signal transduction: molecular specificity and functional flexibility. *Nat. Rev. Mol. Cell Biol.* **8,** 970–982 (2007).
128. Garg, N., Khunger, M., Gupta, A. & Kumar, N. Optimal management of hereditary hemorrhagic telangiectasia. *J. Blood Med.* **5,** 191–206 (2014).
129. Storkebaum, E., Quaegebeur, A., Vikkula, M. & Carmeliet, P. Cerebrovascular disorders: molecular insights and therapeutic opportunities. *Nat. Neurosci.* **14,** 1390–1397 (2011).
130. Wooderchak-Donahue, W. L. *et al.* BMP9 Mutations Cause a Vascular-Anomaly Syndrome with Phenotypic Overlap with Hereditary Hemorrhagic Telangiectasia. *Am. J. Hum. Genet.* **93,** 530–537 (2013).
131. Rigelsky, C. M. *et al.* BMPR2 mutation in a patient with pulmonary arterial hypertension and suspected hereditary hemorrhagic telangiectasia. *Am. J. Med. Genet. A* **146A,** 2551–6 (2008).
132. Peacock, H., Caolo, V. & Jones, E. Arteriovenous malformations in Hereditary Haemorrhagic Telangiectasia: looking beyond ALK1-NOTCH interactions. *Cardiovasc. Res.* (2015).
133. Strizhak, A. Arteriovenous Malformations (AVM). (2016). at <https://www.doctorstrizhak.com/Arteriovenous_Malformation.php>
134. Urness, L. D., Sorensen, L. K. & Li, D. Y. Arteriovenous malformations in mice lacking activin receptor-like kinase-1. *Nat. Genet.* **26,** 328–31 (2000).
135. Oh, S. P. *et al.* Activin receptor-like kinase 1 modulates transforming growth factor- beta 1 signaling in the regulation of angiogenesis. *Proc Natl Acad Sci U S A* **97,** 2626–2631 (2000).
136. Tkachuk, V., Stepanova, V., Little, P. J. & Bobik, A. Regulation and role of urokinase plasminogen activator in vascular remodelling. *Clin Exp Pharmacol Physiol* **23,** 759–765 (1996).
137. Pepper, M. S., Vassalli, J. D., Montesano, R. & Orci, L. Urokinase-type plasminogen activator

is induced in migrating capillary endothelial cells. *J Cell Biol* **105,** 2535–2541 (1987).
138. Bacharach, E., Itin, A. & Keshet, E. In vivo patterns of expression of urokinase and its inhibitor PAI-1 suggest a concerted role in regulating physiological angiogenesis. *Proc Natl Acad Sci U S A* **89,** 10686–90 (1992).
139. Mandriota, S. J. *et al.* Vascular endothelial growth factor increases urokinase receptor expression in vascular endothelial cells. *J. Biol. Chem.* **270,** 9709–9716 (1995).
140. Park, S. O. *et al.* ALK5- and TGFBR2-independent role of ALK1 in the pathogenesis of hereditary hemorrhagic telangiectasia type 2. *Blood* **111,** 633–642 (2008).
141. Park, S. O. *et al.* Real-time imaging of de novo arteriovenous malformation in a mouse model of hereditary hemorrhagic telangiectasia. *J. Clin. Invest.* **119,** 3487–96 (2009).
142. McAllister, K. *et al.* Endoglin, a TGF-beta binding protein of endothelial cells, is the gene for hereditary haemorrhagic telangiectasia type 1. *Nat. Genet.* **8,** 345–351 (1994).
143. Li, D. Y. *et al.* Defective angiogenesis in mice lacking endoglin. *Science* **284,** 1534–1537 (1999).
144. Bourdeau, A., Dumont, D. J. & Letarte, M. A murine model of hereditary hemorrhagic telangiectasia. *J. Clin. Invest.* **104,** 1343–51 (1999).
145. Mahmoud, M. *et al.* Pathogenesis of arteriovenous malformations in the absence of endoglin. *Circ. Res.* **106,** 1425–1433 (2010).
146. Gallione, C. J. *et al.* SMAD4 mutations found in unselected HHT patients. *J. Med. Genet.* **43,** 793–7 (2006).
147. Gallione, C. J. *et al.* A combined syndrome of juvenile polyposis and hereditary haemorrhagic telangiectasia associated with mutations in MADH4 (SMAD4). *Lancet* **363,** 852–859 (2004).
148. Beppu, H. *et al.* BMP type II receptor is required for gastrulation and early development of mouse embryos. *Dev. Biol.* **221,** 249–258 (2000).
149. Liu, D. *et al.* Dosage-dependent requirement of BMP type II receptor for maintenance of vascular integrity. *Blood* **110,** 1502–10 (2007).
150. Sirard, C. *et al.* The tumor suppressor gene Smad4/Dpc4 is required for gastrulation and later for anterior development of the mouse embryo. *Genes Dev.* **12,** 107–119 (1998).
151. Gallione, C. *et al.* Overlapping spectra of SMAD4 mutations in juvenile polyposis (JP) and JP-HHT syndrome. *Am. J. Med. Genet. A* **152A,** 333–9 (2010).
152. Jane, J. a *et al.* Ectopic osteogenesis using adenoviral bone morphogenetic protein (BMP)-4 and BMP-6 gene transfer. *Mol. Ther.* **6,** 464–470 (2002).
153. Sharff, K. a *et al.* Hey1 basic helix-loop-helix protein plays an important role in mediating BMP9-induced osteogenic differentiation of mesenchymal progenitor cells. *J. Biol. Chem.* **284,** 649–59 (2009).
154. López-Coviella, I., Berse, B., Krauss, R., Thies, R. S. & Blusztajn, J. K. Induction and maintenance of the neuronal cholinergic phenotype in the central nervous system by BMP-9. *Science* **289,** 313–316 (2000).
155. Upton, P. D., Davies, R. J., Trembath, R. C. & Morrell, N. W. Bone morphogenetic protein (BMP) and activin type II receptors balance BMP9 signals mediated by activin receptor-like kinase-1 in human pulmonary artery endothelial cells. *J. Biol. Chem.* **284,** 15794–804 (2009).
156. Laux, D. W. *et al.* Circulating Bmp10 acts through endothelial Alk1 to mediate flow-dependent arterial quiescence. *Development* **140,** 3403–12 (2013).
157. Shou, W. *et al.* Cardiac defects and altered ryanodine receptor function in mice lacking FKBP12. *Nature* **391,** 489–492 (1998).
158. Schierling, W. *et al.* Increased intravascular flow rate triggers cerebral arteriogenesis. *J. Cereb. Blood Flow Metab.* **29,** 726–737 (2009).
159. Schürmann, C., Gremse, F., Jo, H., Kiessling, F. & Brandes, R. Micro-CT Technique Is Well Suited for Documentation of Remodeling Processes in Murine Carotid Arteries. *PLoS One* **10,** (2015).
160. Stahl, A. *et al.* The mouse retina as an angiogenesis model. *Investigative Ophthalmology and Visual Science* **51,** 2813–2826 (2010).
161. O'Connell, T. D., Rodrigo, M. C. & Simpson, P. C. Isolation and culture of adult mouse cardiac myocytes. *Methods Mol. Biol.* **357,** 271–296 (2007).
162. Owens, G. K., Rabinovitch, P. S. & Schwartz, S. M. Smooth muscle cell hypertrophy versus hyperplasia in hypertension. *Proc. Natl. Acad. Sci.* **78,** 7759–7763 (1981).
163. Eden, E., Navon, R., Steinfeld, I., Lipson, D. & Yakhini, Z. GOrilla: a tool for discovery and visualization of enriched GO terms in ranked gene lists. *BMC Bioinformatics* **10,** 48 (2009).
164. Mootha, V. K. *et al.* PGC-1alpha-responsive genes involved in oxidative phosphorylation are coordinately downregulated in human diabetes. *Nat. Genet.* **34,** 267–273 (2003).

165. Subramanian, A. *et al.* Gene set enrichment analysis: a knowledge-based approach for interpreting genome-wide expression profiles. *Proc. Natl. Acad. Sci. U. S. A.* **102,** 15545–50 (2005).
166. Van de Peer, Y. Calculate and draw custom Venn diagrams. at <http://bioinformatics.psb.ugent.be/webtools/Venn/>
167. Bücker, S. BMP und SMAD signale im kardiovaskulären system. (JUSTUS-LIEBIG-UNIVERSITÄT, GIESSEN, 2011).
168. De Lange, F. J., Moorman, A. F. M. & Christoffels, V. M. Atrial cardiomyocyte-specific expression of Cre recombinase driven by an Nppa gene fragment. *Genesis* **37,** 1–4 (2003).
169. Kuba, K. *et al.* Impaired heart contractility in Apelin gene-deficient mice associated with aging and pressure overload. *Circ. Res.* **101,** (2007).
170. Hershberger, R. E., Hedges, D. J. & Morales, A. Dilated cardiomyopathy: the complexity of a diverse genetic architecture. *Nat. Rev. Cardiol.* **10,** 531–47 (2013).
171. Conrad, C. H. *et al.* Myocardial fibrosis and stiffness with hypertrophy and heart failure in the spontaneously hypertensive rat. *Circulation* **91,** 161–170 (1995).
172. Muñoz-Félix JM *et al.* Identification of bone morphogenetic protein 9 (BMP9) as a novel profibrotic factor in vitro. *Cell Signal* **28,** 1252–61 (2016).
173. Frey, N., Katus, H. A., Olson, E. N. & Hill, J. A. Hypertrophy of the Heart: A New Therapeutic Target? *Circulation* **109,** 1580–1589 (2004).
174. Razeghi, P. *et al.* Metabolic gene expression in fetal and failing human heart. *Circulation* **104,** 2923–2931 (2001).
175. Sato, Y. Role of ETS family transcription factors in vascular development and angiogenesis. *Cell Struct. Funct.* **26,** 19–24 (2001).
176. Ola, R. *et al.* PI3 kinase inhibition improves vascular malformations in mouse models of hereditary haemorrhagic telangiectasia. *Nat Commun.* **7,** (2016).
177. Ruiz, S. *et al.* A mouse model of hereditary hemorrhagic telangiectasia generated by transmammary-delivered immunoblocking of BMP9 and BMP10. *Sci. Rep.* (2016). doi:10.1038/srep37366
178. Daly, A., Randall, R. & Hill, C. Transforming Growth Factor β-Induced Smad1/5 Phosphorylation in Epithelial Cells Is Mediated by Novel Receptor Complexes and Is Essential for Anchorage-Independent Growth. *Mol. Cell. Biol* **28,** 6889–6902 (2008).
179. Fischer, A., Schumacher, N., Maier, M., Sendtner, M. & Gessler, M. The Notch target genes Hey1 and Hey2 are required for embryonic vascular development. *Genes Dev.* **18,** 901–911 (2004).
180. Sidney, L. E., Branch, M. J., Dunphy, S. E., Dua, H. S. & Hopkinson, A. Concise review: Evidence for CD34 as a common marker for diverse progenitors. *Stem Cells* **32,** 1380–1389 (2014).
181. Kasai, A. *et al.* Inhibition of apelin expression switches endothelial cells from proliferative to mature state in pathological retinal angiogenesis. *Angiogenesis* **16,** 723–734 (2013).
182. Goumans, M.-J., Liu, Z., ten Dijke, P. & Dijke, P. TGF-beta signaling in vascular biology and dysfunction. *Cell Res.* **19,** 116–27 (2009).
183. Moya, I. M. *et al.* Stalk Cell Phenotype Depends on Integration of Notch and Smad1/5 Signaling Cascades. *Dev. Cell* **22,** 501–514 (2012).
184. Somekawa, S. *et al.* Tmem100, an ALK1 receptor signaling-dependent gene essential for arterial endothelium differentiation and vascular morphogenesis. *Proc. Natl. Acad. Sci. U. S. A.* **109,** 12064–9 (2012).
185. Gerthoffer, W. T. Mechanisms of vascular smooth muscle cell migration. *Circulation Research* **100,** 607–621 (2007).
186. Louis, S. F. & Zahradka, P. Vascular smooth muscle cell motility: From migration to invasion. *Experimental and Clinical Cardiology* **15,** (2010).
187. Stow, L. R., Jacobs, M. E., Wingo, C. S. & Cain, B. D. Endothelin-1 gene regulation. *FASEB J.* **25,** 16–28 (2011).
188. Kardami, E. *et al.* Fibroblast growth factor 2 isoforms and cardiac hypertrophy. *Cardiovasc. Res.* **63,** 458–466 (2004).
189. Chen, H. *et al.* Overexpression of bone morphogenetic protein 10 in myocardium disrupts cardiac postnatal hypertrophic growth. *J. Biol. Chem.* **281,** 27481–27491 (2006).
190. Xie, F., Lv, D. & Chen, L. ELABELA: a novel hormone in cardiac development acting as a new endogenous ligand for the APJ receptor. *Acta Biochim Biophys Sin* **46,** 620–622 (2014).
191. Chng, S., Ho, L., Tian, J. & Reversade, B. ELABELA: A hormone essential for heart development signals via the apelin receptor. *Dev. Cell* **27,** 672–680 (2013).

192. González-Núñez, M., Muñoz-Félix, J. M. & López-Novoa, J. M. The ALK-1/Smad1 pathway in cardiovascular physiopathology. A new target for therapy? *Biochimica et Biophysica Acta - Molecular Basis of Disease* **1832,** 1492–1510 (2013).
193. Halayko, A. J., Salari, H., Ma, X. & Stephens, N. L. Markers of airway smooth muscle cell phenotype. *Am.J.Physiol* **270,** L1040--L1051 (1996).
194. Boettger, T. *et al.* Acquistion of the contractile phenotype by murine arterial smooth muscle cells depends on the miR-143/145 gene cluster. *J. Clin. Invest.* **119,** 2634–2647 (2009).
195. Lindahl, P. Pericyte Loss and Microaneurysm Formation in PDGF-B-Deficient Mice. *Science* **277,** 242–245 (1997).
196. Soriano, P. Abnormal kidney development and hematological disorders in PDGF beta-receptor mutant mice. *Genes Dev.* **8,** 1888–1896 (1994).
197. Zhang, H. *et al.* Apelin inhibits the proliferation and migration of rat PASMCs via the activation of PI3K/Akt/mTOR signal and the inhibition of autophagy under hypoxia. *J. Cell. Mol. Med.* **18,** 542–553 (2014).
198. Wang, C. *et al.* Apelin induces vascular smooth muscle cells migration via a PI3K/Akt/FoxO3a/MMP-2 pathway. *Int. J. Biochem. Cell Biol.* **69,** 173–182 (2015).
199. England, J. & Loughna, S. Heavy and light roles: Myosin in the morphogenesis of the heart. *Cellular and Molecular Life Sciences* **70,** 1221–1239 (2013).
200. Guo, X. & Chen, S.-Y. Transforming growth factor-β and smooth muscle differentiation. *World J. Biol. Chem.* **3,** 41–52 (2012).
201. Kim, Y. M. *et al.* Proteomic identification of adam12 as a regulator for tgf-β1-induced differentiation of human mesenchymal stem cells to smooth muscle cells. *PLoS One* **7,** (2012).
202. Sciences, M. *et al.* Epiregulin is a potent vascular smooth muscle cell-derived mitogen induced by angiotensin II, endothelin-1, and thrombin. *Proc. Natl. Acad. Sci. U. S. A.* **96,** 1633–1638 (1999).
203. Gordon, K. J. & Blobe, G. C. Role of transforming growth factor-β superfamily signaling pathways in human disease. *Biochim. Biophys. Acta - Mol. Basis Dis.* **1782,** 197–228 (2008).
204. Akhurst, R. J. & Hata, A. Targeting the TGFβ signalling pathway in disease. *Nat. Rev. Drug Discov.* **11,** 790–811 (2012).
205. Wang, R. N. *et al.* Bone Morphogenetic Protein (BMP) signaling in development and human diseases. *Genes Dis.* **1,** 87–105 (2014).
206. Guo, X. & Wang, X.-F. Signaling cross-talk between TGF-beta/BMP and other pathways. *Cell Res.* **19,** 71–88 (2009).
207. Li, D. Y., Urness, L. D. & Sorensen, L. K. Arteriovenous malformations in mice lacking activin receptor-like kinase-1. *Nat. Genet.* **26,** 328–331 (2000).
208. Cunha, S. I. & Pietras, K. ALK1 as an emerging target for antiangiogenic therapy of cancer. *Blood* **117,** 6999–7006 (2011).
209. College, M. T. The Cardiovascular System: Blood Vessels. (2012). at <http://classes.midlandstech.edu/carterp/Courses/bio211/chap19/chap19.html>
210. Klabunde, R. Regulation of Stroke Volume. *Cardiovascular Physiology Concepts* (2015). at <http://www.cvphysiology.com/Cardiac Function/CF002.htm>
211. Klabunde, R. Frank-Starling Mechanism. *Cardiovascular Physiology Concepts* (2015). at <http://www.cvphysiology.com/Cardiac Function/CF003.htm>
212. Wilcox, J. E. *et al.* 'Targeting the Heart' in Heart Failure: Myocardial Recovery in Heart Failure With Reduced Ejection Fraction. *JACC: Heart Failure* **3,** 661–669 (2015).
213. Cioffi, G., de Simone, G., Mureddu, G., Tarantini, L. & Stefenelli, C. Right atrial size and function in patients with pulmonary hypertension associated with disorders of respiratory system or hypoxemia. *Eur J Echocardiogr.* **8,** 322–331 (2007).
214. Creemers, E. E. & Pinto, Y. M. Molecular mechanisms that control interstitial fibrosis in the pressure-overloaded heart. *Cardiovasc. Res.* **89,** 265–272 (2011).
215. Ho, C. Y. *et al.* Myocardial Fibrosis as an Early Manifestation of Hypertrophic Cardiomyopathy. *N. Engl. J. Med.* **363,** 552–563 (2010).
216. Mihl, C., Dassen, W. R. . & Kuipers, H. Cardiac remodelling: concentric versus eccentric hypertrophy in strength and endurance athletes. *Neth Hear. J* **16,** 129–133 (2008).
217. Senyo, S. E., Lee, R. T. & Kühn, B. Cardiac regeneration based on mechanisms of cardiomyocyte proliferation and differentiation. *Stem Cell Research* **13,** 532–541 (2014).
218. Cameron, V. & Ellmers, L. Mini review: natriuretic peptides during development of the fetal heart and circulation. *Endocrinology* **144,** 2191–2194 (2003).
219. Dietz, J. Mechanisms of atrial natriuretic peptide secretion from the atrium. *Cardiovasc Res* **68,** 8–17 (2005).

220. Cox, E. J. & Marsh, S. A. A systematic review of fetal genes as biomarkers of cardiac hypertrophy in rodent models of diabetes. *PLoS ONE* **9,** (2014).
221. Rosenkranz, A. C., Hood, S. G., Woods, R. L., Dusting, G. J. & Ritchie, R. H. B-type natriuretic peptide prevents acute hypertrophic responses in the diabetic rat heart: Importance of cyclic GMP. *Diabetes* **52,** 2389–2395 (2003).
222. Franco, V. *et al.* Atrial natriuretic peptide dose-dependently inhibits pressure overload-induced cardiac remodeling. *Hypertension* **44,** 746–750 (2004).
223. Wang, D. *et al.* Effects of pressure overload on extracellular matrix expression in the heart of the atrial natriuretic peptide-null mouse. *Hypertension* **42,** 88–95 (2003).
224. Corti, P. *et al.* Interaction between alk1 and blood flow in the development of arteriovenous malformations. *Development* **138,** 1573–1582 (2011).
225. Roman, B. L. *et al.* Disruption of acvrl1 increases endothelial cell number in zebrafish cranial vessels. *Development* **129,** 3009–3019 (2002).
226. Lacolley, P., Regnault, V., Nicoletti, A., Li, Z. & Michel, J. B. The vascular smooth muscle cell in arterial pathology: A cell that can take on multiple roles. *Cardiovascular Research* **95,** 194–204 (2012).
227. Siddiqui, A. Effects of Vasodilation and Arterial Resistance on Cardiac Output. *J. Clin. Exp. Cardiolog.* **2,** 170 (2011).
228. Jackson, W. Ion Channels and Vascular Tone. *Hypertension* **35,** 173–178 (2000).
229. Schreier, B. *et al.* Loss of epidermal growth factor receptor in vascular smooth muscle cells and cardiomyocytes causes arterial hypotension and cardiac hypertrophy. *Hypertension* **61,** 333–340 (2013).
230. Wöltje, K., Jabs, M. & Fischer, A. Serum Induces transcription of Hey1 and Hey2 genes by Alk1 but not notch signaling in endothelial cells. *PLoS One* **10,** (2015).
231. Herbert, S. P. & Stainier, D. Y. Molecular control of endothelial cell behaviour during blood vessel morphogenesis. *Nat Rev Mol Cell Biol* **12,** 551–564 (2011).
232. Del Toro, R. *et al.* Identification and functional analysis of endothelial tip cell-enriched genes. *Blood* **116,** 4025–4033 (2010).
233. Wilhelm, K. *et al.* FOXO1 couples metabolic activity and growth state in the vascular endothelium. *Nature* **529,** 1–18 (2016).
234. Gerhardt, H. VEGF and endothelial guidance in angiogenic sprouting. *Organogenesis* **4,** 241–246 (2008).
235. Ruhrberg, C. Growing and shaping the vascular tree: Multiple roles for VEGF. *BioEssays* **25,** 1052–1060 (2003).
236. Claxton, S. & Fruttiger, M. Oxygen modifies artery differentiation and network morphogenesis in the retinal vasculature. *Dev. Dyn.* **233,** 822–828 (2005).
237. Saint-Geniez, M., Argence, C. B., Knibiehler, B. & Audigier, Y. The msr/apj gene encoding the apelin receptor is an early and specific marker of the venous phenotype in the retinal vasculature. *Gene Expr. Patterns* **3,** 467–472 (2003).
238. Park, S. *et al.* Cardiac, skeletal, and smooth muscle mitochondrial respiration: are all mitochondria created equal? *Am J Physiol Hear. Circ Physiol* **307,** H346–H352 (2014).
239. Kim, J. H., Peacock, M. R., George, S. C. & Hughes, C. C. W. BMP9 induces EphrinB2 expression in endothelial cells through an Alk1-BMPRII/ActRII-ID1/ID3-dependent pathway: Implications for hereditary hemorrhagic telangiectasia type II. *Angiogenesis* **15,** 497–509 (2012).
240. Fràter-Schröder, M., Müller, G., Birchmeier, W. & Böhlen, P. Transforming growth factor-beta inhibits endothelial cell proliferation. *Biochem. Biophys. Res. Commun.* **137,** 295–302 (1986).
241. Seki, T., Hong, K.-H. & Oh, S. P. Nonoverlapping expression patterns of ALK1 and ALK5 reveal distinct roles of each receptor in vascular development. *Lab. Invest.* **86,** 116–29 (2006).
242. Geudens, I. & Gerhardt, H. Coordinating cell behaviour during blood vessel formation. *Development* **138,** 4569–4583 (2011).
243. Hellström, M., Kalén, M., Lindahl, P., Abramsson, A. & Betsholtz, C. Role of PDGF-B and PDGFR-β in recruitment of vascular smooth muscle cells and pericytes during embryonic blood vessel formation in the mouse. *Development* **126,** 3047–3055 (1999).
244. Iivanainen, E. *et al.* Angiopoietin-regulated recruitment of vascular smooth muscle cells by endothelial-derived heparin binding EGF-like growth factor. *FASEB J.* **17,** 1609–21 (2003).
245. Andersen, C. U., Hilberg, O., Mellemkjær, S., Nielsen-Kudsk, J. E. & Simonsen, U. Apelin and pulmonary hypertension. *Pulm. Circ.* **1,** 334–46 (2013).
246. O'Carroll, A. M., Lolait, S. J., Harris, L. E. & Pope, G. R. The apelin receptor APJ: journey from an orphan to a multifaceted regulator of homeostasis. *J Endocrinol* **219,** (2013).

247. Tirziu, D., Giordano, F. & Simons, M. Cell Communications in the Heart. *Circulation* **122,** 928–937 (2010).
248. Budhiraja, R., Tuder, R. M. & Hassoun, P. M. Endothelial dysfunction in pulmonary hypertension. *Am. Hear. Assoc.* **109,** 159–65 (2004).
249. Kreymborg, K. grosse *et al.* Identification of right heart-enriched genes in a murine model of chronic outflow tract obstruction. *J. Mol. Cell. Cardiol.* **49,** 598–605 (2010).
250. Kubin, T. *et al.* Oncostatin M is a major mediator of cardiomyocyte dedifferentiation and remodeling. *Cell Stem Cell* **9,** 420–432 (2011).
251. Lörchner, H. *et al.* Myocardial healing requires Reg3β-dependent accumulation of macrophages in the ischemic heart. *Nat. Med.* **21,** 1–21 (2015).
252. Gore, B. *et al.* Key role of the endothelial TGF-β/ALK1/endoglin signaling pathway in humans and rodents pulmonary hypertension. *PLoS One* **9,** (2014).
253. Soubrier, F. *et al.* Genetics and genomics of pulmonary arterial hypertension. in *Journal of the American College of Cardiology* **62,** (2013).
254. Beppu, H. *et al.* BMPR-II heterozygous mice have mild pulmonary hypertension and an impaired pulmonary vascular remodeling response to prolonged hypoxia. *Am. J. Physiol. Lung Cell. Mol. Physiol.* **287,** L1241–L1247 (2004).
255. Jerkic, M. *et al.* Pulmonary hypertension in adult Alk1 heterozygous mice due to oxidative stress. *Cardiovasc. Res.* **92,** 375–384 (2011).
256. Toporsian, M. *et al.* Spontaneous adult-onset pulmonary arterial hypertension attributable to increased endothelial oxidative stress in a murine model of hereditary hemorrhagic telangiectasia. *Arterioscler. Thromb. Vasc. Biol.* **30,** 509–517 (2010).
257. Long, L. *et al.* Selective enhancement of endothelial BMPR-II with BMP9 reverses pulmonary arterial hypertension. *Nat. Med.* **21,** 777–85 (2015).
258. Montecucco, F., Carbone, F. & Schindler, T. H. Pathophysiology of ST-segment elevation myocardial infarction: novel mechanisms and treatments. *Eur. Heart J.* ehv592 (2015). doi:10.1093/eurheartj/ehv592
259. Mendis, S., Puska, P. & Norrving, B. Global atlas on cardiovascular disease prevention and control. *World Heal. Organ.* 2–14 (2011). doi:NLM classification: WG 120
260. Frangogiannis, N. G. Regulation of the inflammatory response in cardiac repair. *Circulation Research* **110,** 159–173 (2012).
261. Li, J. *et al.* VEGF, flk-1, and flt-1 expression in a rat myocardial infarction model of angiogenesis. *Am. J. Physiol.* **270,** H1803-11 (1996).
262. Ren, G., Michael, L. H., Entman, M. L. & Frangogiannis, N. G. Morphological Characteristics of the Microvasculature in Healing Myocardial Infarcts. *J. Histochem. Cytochem.* **50,** 71–79 (2002).
263. Velasco, S. *et al.* L- and S-endoglin differentially modulate TGFbeta1 signaling mediated by ALK1 and ALK5 in L6E9 myoblasts. *J. Cell Sci.* **121,** 913–9 (2008).
264. Morris, E. *et al.* Endoglin promotes TGF-??/Smad1 signaling in scleroderma fibroblasts. *J. Cell. Physiol.* **226,** 3340–3348 (2011).
265. Goumans, M. J. *et al.* Activin receptor-like kinase (ALK)1 is an antagonistic mediator of lateral TGFβ/ALK5 signaling. *Mol. Cell* **12,** 817–828 (2003).
266. DeAlmeida, A., van Oort, R. & Wehrens, X. Transverse Aortic Constriction in Mice. *J Vis Exp.* **3,** 1729 (2010).
267. Kapur, N. *et al.* Reduced endoglin activity limits cardiac fibrosis and improves survival in heart failure. *Circulation* **125,** 2728–2738 (2012).
268. Fernandez, A. *et al.* Mutation study of Spanish patients with hereditary hemorrhagic telangiectasia and expression analysis of Endoglin and ALK1. *Hum.Mutat.* **27,** 295 (2006).
269. Panchenko, M., Williams, M., Brody, K. & Yu, Q. Type I receptor serine–threonine kinase preferentially expressed in pulmonary blood vessels. *Am. J. Physiol.* **270,** L547–L558 (1996).
270. Docherty, N. G. *et al.* Endoglin regulates renal ischaemia-reperfusion injury. *Nephrol. Dial. Transplant.* **21,** 2106–2119 (2006).
271. Kolk, M. V. V *et al.* LAD-ligation: a murine model of myocardial infarction. *J. Vis. Exp.* e1438 (2009). doi:10.3791/1438
272. Pugh, C. W. & Ratcliffe, P. J. Regulation of angiogenesis by hypoxia: role of the HIF system. *Nat. Med.* **9,** 677–684 (2003).
273. Jürgensen, J. S. *et al.* Persistent induction of HIF-1alpha and -2alpha in cardiomyocytes and stromal cells of ischemic myocardium. *FASEB J.* **18,** 1415–7 (2004).
274. Kido, M. *et al.* Hypoxia-inducible factor 1-alpha reduces infarction and attenuates progression of cardiac dysfunction after myocardial infarction in the mouse. *J. Am. Coll. Cardiol.* **46,** 2116–

2124 (2005).
275. Hu, N. *et al.* BMP9-regulated angiogenic signaling plays an important role in the osteogenic differentiation of mesenchymal progenitor cells. *J Cell Sci* (2012). doi:jcs.114231 [pii]\r10.1242/jcs.114231
276. Liehn, E. A. *et al.* Double-edged role of the CXCL12/CXCR4 axis in experimental myocardial infarction. *J. Am. Coll. Cardiol.* **58,** 2415–2423 (2011).
277. Hashimoto, E. *et al.* Rapid induction of vascular endothelial growth factor expression by transient ischemia in rat heart. *Am J Physiol* **267,** H1948-54 (1994).
278. Lee, S. H. *et al.* Early expression of angiogenesis factors in acute myocardial ischemia and infarction. *N. Engl. J. Med.* **342,** 626–33 (2000).
279. Li, J., Hampton, T., Morgan, J. P. & Simons, M. Stretch-induced VEGF expression in the heart. *J. Clin. Invest.* **100,** 18–24 (1997).
280. Cao, R. *et al.* Comparative Evaluation of FGF-2-, VEGF-A-, and VEGF-C-Induced Angiogenesis Lymphangiogenesis, Vascular Fenestrations, and Permeability. *Circ. Res.* **94,** 664–670 (2004).
281. Greenberg, J. I. *et al.* A role for VEGF as a negative regulator of pericyte function and vessel maturation. *Nature* **456,** 809–13 (2008).
282. Zhao, T., Zhao, W., Chen, Y., Ahokas, R. A. & Sun, Y. Vascular endothelial growth factor (VEGF)-A: Role on cardiac angiogenesis following myocardial infarction. *Microvasc. Res.* **80,** 188–194 (2010).
283. Autiero, M. *et al.* Role of PlGF in the intra- and intermolecular cross talk between the VEGF receptors Flt1 and Flk1. *Nat. Med.* **9,** 936–943 (2003).
284. Iwasaki, H. *et al.* PLGF repairs myocardial ischemia through mechanisms of angiogenesis, cardioprotection and recruitment of myo-angiogenic competent marrow progenitors. *PLoS One* **6,** (2011).
285. Cochain, C., Channon, K. M. & Silvestre, J.-S. Angiogenesis in the Infarcted Myocardium. *Antioxid. Redox Signal.* **18,** 1100–1113 (2012).

11 Supplementary Figures

11.1 Biological processes upregulated in stimulated HUVECs

A

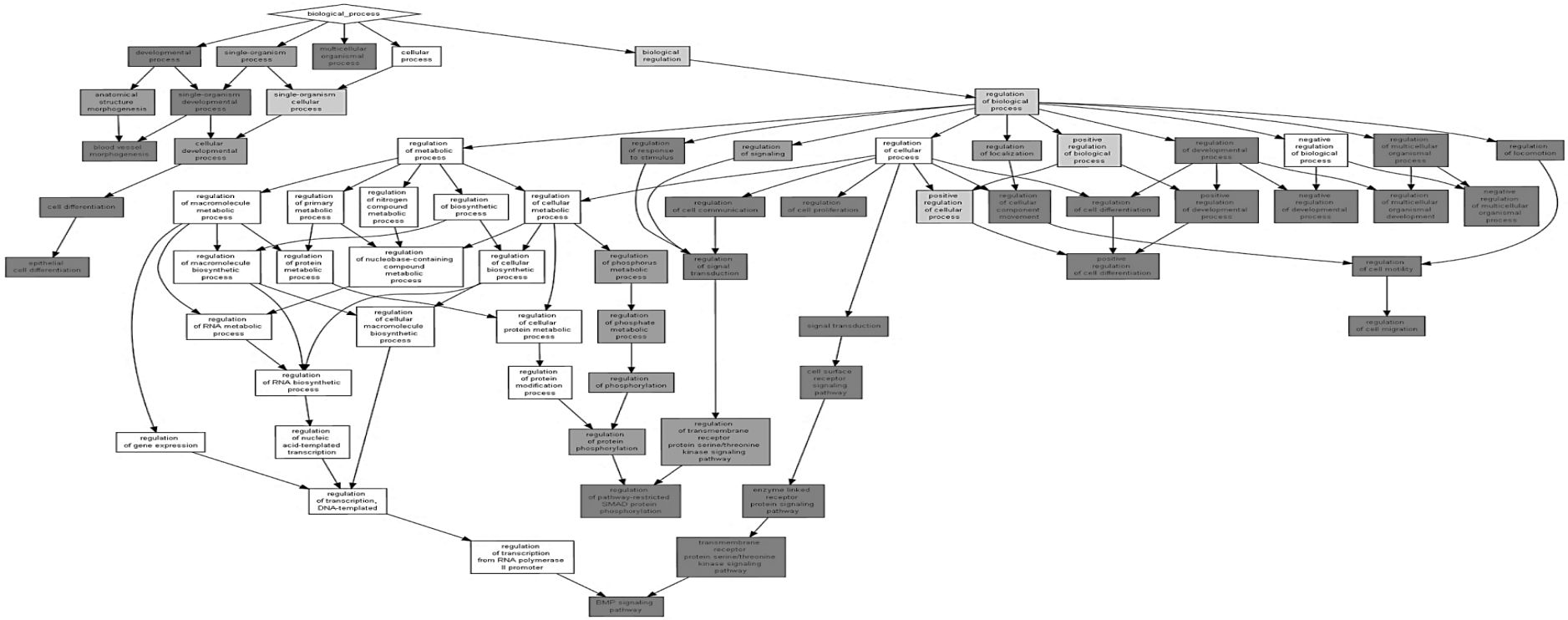

(A) GO analysis for biological processes upregulated in HUVECs stimulated with BMP9 and BMP10 have changes in blood vessel morphogenesis, SMAD signalling and cell differentiation.

11.2 Biological processes downregulated in stimulated HUVECs

B

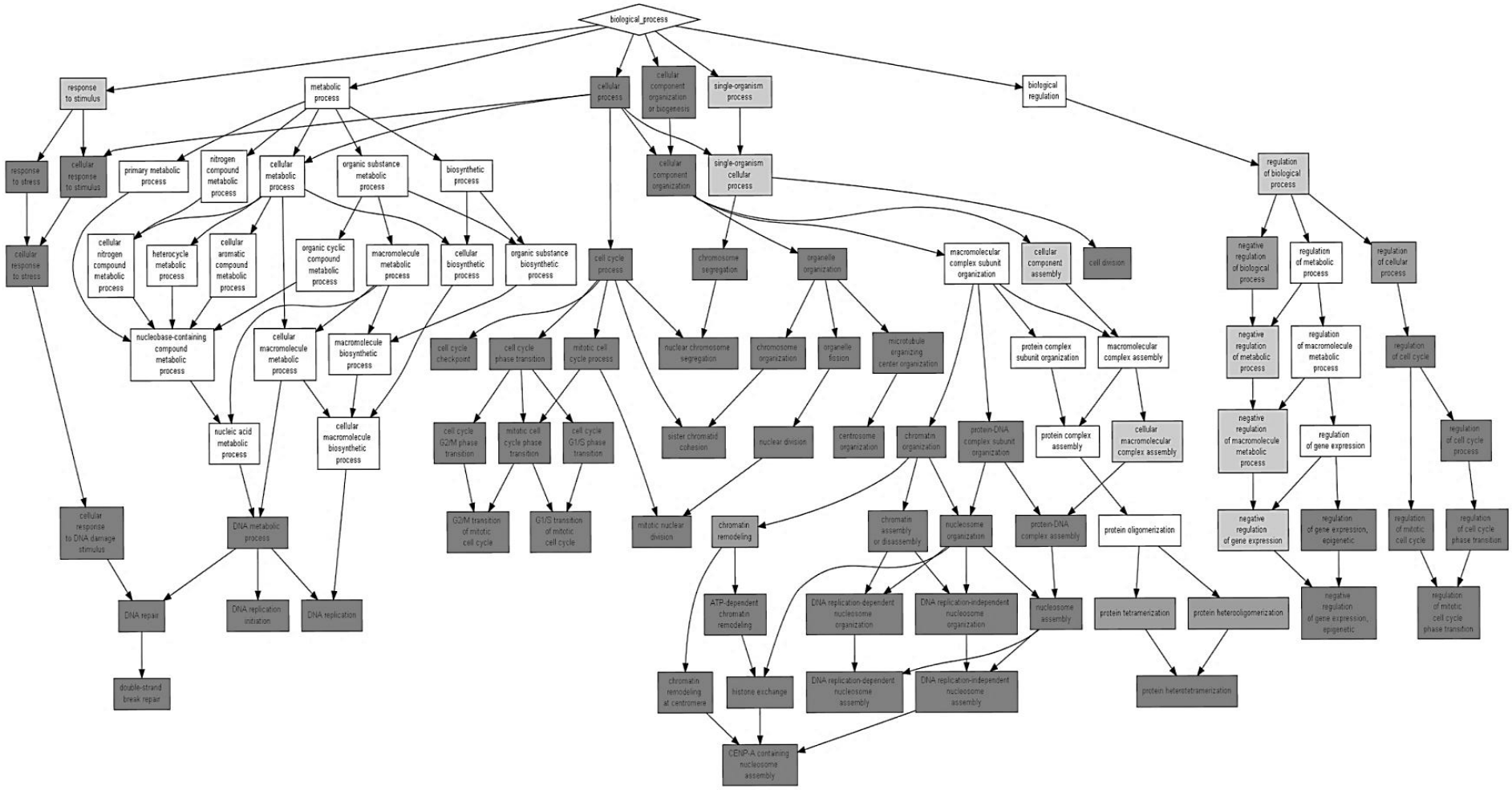

(B) GO analysis for biological processes downregulated in HUVECs stimulated with BMP9 and BMP10 included regulation of cell cycle and cell division.

11.3 Biological processes upregulated in DKO hearts

C

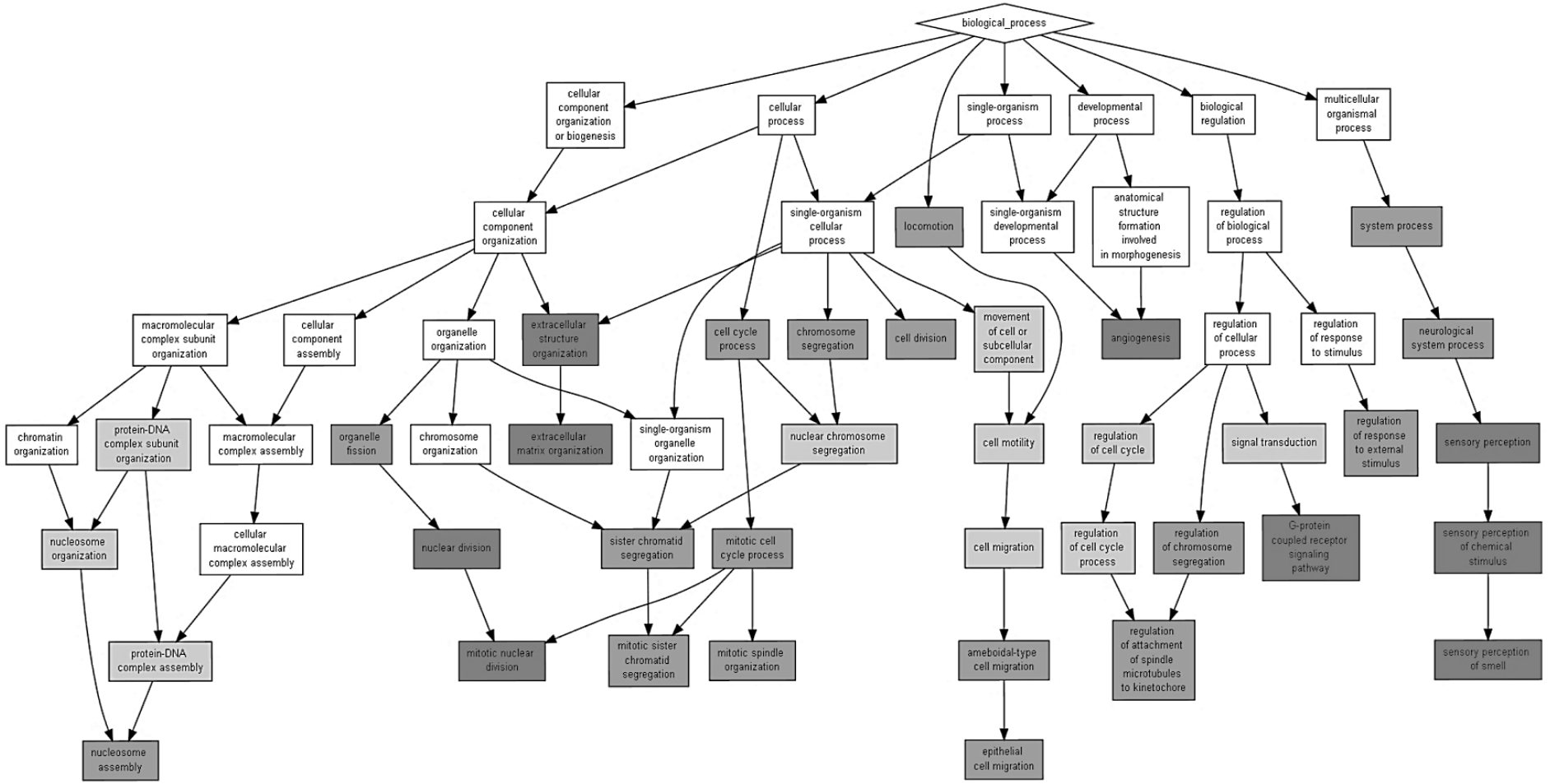

(C) GO analysis for biological processes upregulated in DKO hearts compared to WT at 2 months of age, where genes involved in GPCR signalling, angiogenesis and epithelial cell migration were upregulated.

11.4 Biological processes upregulated in DKO hearts and downregulated in stimulated HUVECs

D

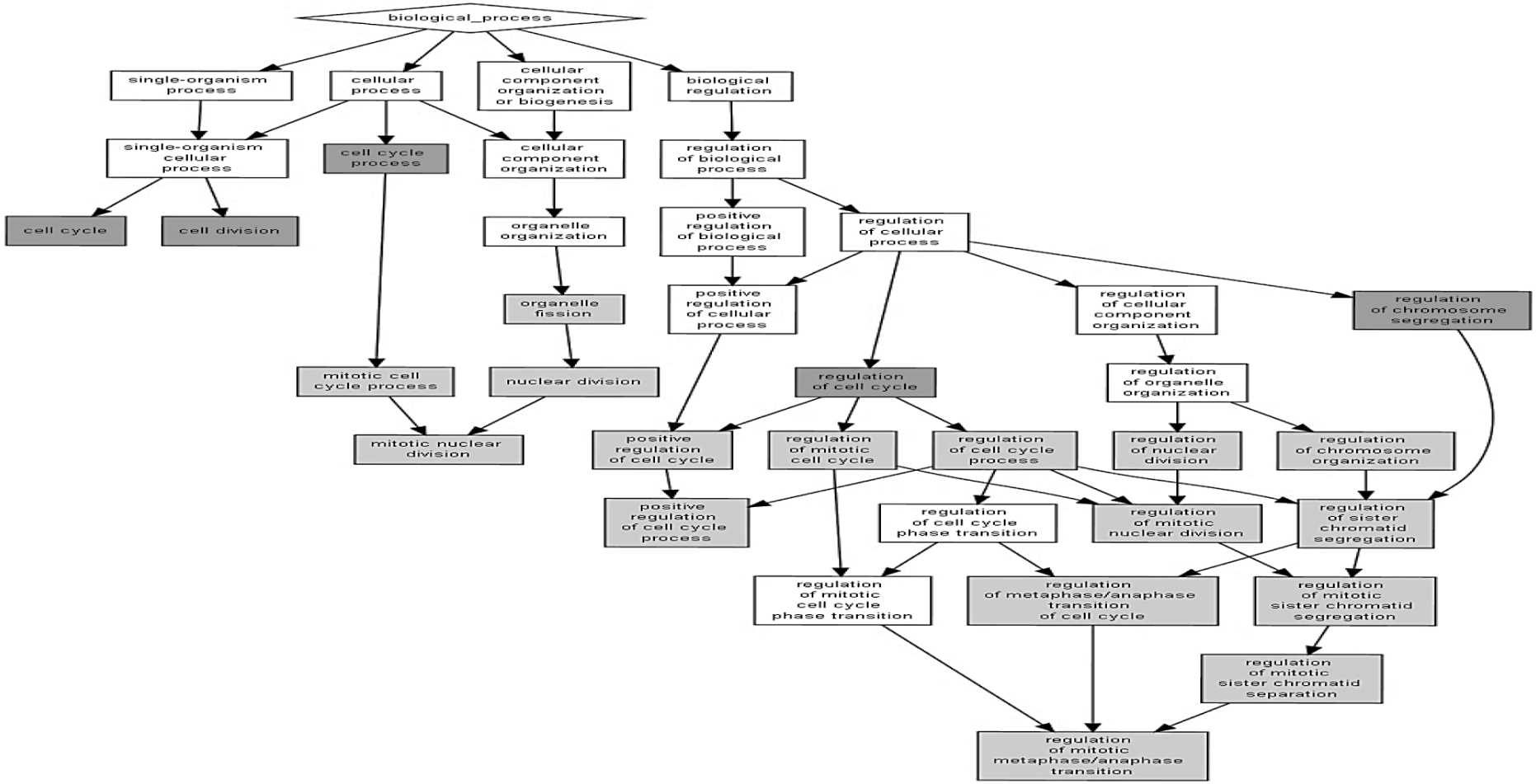

(D) GO analysis of genes highly expressed in DKO hearts but have low expression in stimulated HUVECs shows changes in genes mainly involved in cell division and cycle.

12 Acknowledgements

Ar scáth a chéile a mhaireann na daoine

(Under the shelter of each other, people survive)

An té a bhíónn siúlach, bíonn scéalach

(He who travels has stories to tell)

13 Curriculum vitae